NONLINEAR VIBRATION ANALYSIS OF FUNCTIONALLY GRADED BEAMS

A THESIS SUBMITTED TO
THE GRADUATE SCHOOL OF NATURAL AND APPLIED SCIENCES
OF
MIDDLE EAST TECHNICAL UNIVERSITY

BY

DEMİR DEDEKÖY

IN PARTIAL FULFILLMENT OF THE REQUIREMENTS
FOR
THE DEGREE OF MASTER OF SCIENCE
IN
MECHANICAL ENGINEERING

AUGUST 2022

Approval of the thesis:

NONLINEAR VIBRATION ANALYSIS OF FUNCTIONALLY GRADED BEAMS

submitted by **DEMİR DEDEKÖY** in partial fulfillment of the requirements for the degree of **Master of Science** i**n Mechanical Engineering, Middle East Technical University** by,

Prof. Dr. Halil Kalıpçılar
Dean, Graduate School of **Natural and Applied Sciences** _____

Prof. Dr. M.A. Sahir Arıkan
Head of the Department, **Mechanical Engineering** _____

Prof. Dr. Ender Ciğeroğlu
Supervisor, **Mechanical Engineering, METU** _____

Asst. Prof. Dr. Bekir Bediz
Co-Supervisor, **Mechatronics Engineering, Sabancı University** _____

Examining Committee Members:

Prof. Dr. Suat Kadıoğlu
Mechanical Engineering, METU _____

Prof. Dr. Ender Ciğeroğlu
Mechanical Engineering, METU _____

Prof. Dr. Yiğit Yazıcıoğlu
Mechanical Engineering, METU _____

Assoc. Prof. Dr. Mehmet Bülent Özer
Mechanical Engineering, METU _____

Assoc. Prof. Dr. Barış Sabuncuoğlu
Mechanical Engineering, Hacettepe University _____

Date: 29.08.2022

I hereby declare that all information in this document has been obtained and presented in accordance with academic rules and ethical conduct. I also declare that, as required by these rules and conduct, I have fully cited and referenced all material and results that are not original to this work.

Name Last name :Demir Dedeköy

Signature :

ABSTRACT

NONLINEAR VIBRATION ANALYSIS OF FUNCTIONALLY GRADED BEAMS

Dedeköy, Demir
Master of Science, Mechanical Engineering
Supervisor : Prof. Dr. Ender Ciğeroğlu
Co-Supervisor: Asst. Prof. Dr. Bekir Bediz

August 2022, 98 pages

In this thesis, nonlinear forced vibrations of functionally graded (FG) Euler-Bernoulli Beams are studied. Two types of nonlinearities, large deformation nonlinearity and nonlinearities resulting from rotating beam dynamics, are considered. The Spectral Chebyshev Technique (SCT) is employed for solving governing equations of the spectral-temporal boundary value problems of beam vibrations, which do not always have closed-form analytical solutions. The SCT is combined with Galerkin's method to obtain spatially discretized nonlinear differential equations of motion. Those equations of motion are then converted into nonlinear algebraic equations with the Harmonic Balance Method (HBM), which are solved with the help of Newton's method with arc-length continuation. First, natural frequencies and mode shapes of the uniform and functionally graded beams are obtained with respect to different case scenarios of material distribution properties. A convergence analysis is performed to obtain the minimum number of Chebyshev polynomials required to obtain precise results. Afterward, frequency responses of the nonlinear beams subjected to different boundary conditions are studied.

Keywords: Nonlinear Vibrations, Composite Beams, Forced Response, Spectral Chebyshev Technique, Harmonic Balance Method

ÖZ

FONKSİYONEL OLARAK DERECELENDİRİLMİŞ KİRİŞLERİN DOĞRUSAL OLMAYAN TİTREŞİM ANALİZİ

Dedeköy, Demir
Yüksek Lisans, Makina Mühendisliği
Tez Yöneticisi: Prof. Dr. Ender Ciğeroğlu
Ortak Tez Yöneticisi: Yrd. Doç. Dr. Bekir Bediz

Ağustos 2022, 98 sayfa

Bu çalışmada doğrusal olmayan, fonksiyonel olarak derecelendirilmiş (FOD) Euler-Bernoulli kirişlerinin, kuvvete dayalı lineer olmayan titreşimleri çalışılmaktadır. Problemi lineer olmaktan çıkartan yüksek deformasyon durumu ve dönmeye bağlı oluşan kuvvetler göz önüne alınmıştır. Kirişin görüngesel-zamansal problemini sonlu elemanlarına ayırmak için Chebyshev polinomlarını kullanan Görüngesel Chebyshev Tekniği kullanılmıştır. Bu teknik Galerkin methodu ile birleştirilerek, görüngesel olarak ayrıştırılmış lineer olmayan diferansiyel denklemler elde edilmiştir. Harmonik denge methodu kullanılarak, bu denklemler linear olmayan cebirsel denklemere çevrilmiştir. Denklemlerin çözümü için Newton methodunun yay boyu devam tekniği kullanılmıştır. İlk olarak, doğal frekanslar, farklı materyal dağılımlarını kapsayan senaryolara göre bulunmuştur. Sonrasında kaç polinom kullanılarak hassas sonuçlar elde edilebileceğini gösteren bir yakınsama analizi yapılmıştır. Son olarak da, çalışmada incelenen kiriş yapılarının kuvvete dayalı lineer olmayan frekans tepkileri incelenmiştir.

Anahtar Kelimeler: Lineer Olmayan Titreşimler, Kompozit Kirişler, Kuvvete Dayalı Tepki, Görüngesel Chebyshev Tekniği, Harmonik Denge Metodu

To my family

ACKNOWLEDGMENTS

I would like to thank my advisors Prof. Dr. Ender Ciğeroğlu and Asst. Prof. Dr. Bekir Bediz for their support during my master of science and guidance throughout this thesis.

I would also like to thank Asst. Prof. Dr. Saeed Lotfan for his guidance and helpfulness during my studies.

I also would like to thank Meteksan Savunma Sanayii A.Ş. for their support of graduate education.

TABLE OF CONTENTS

LIST OF TABLES

TABLES

LIST OF FIGURES

FIGURES

LIST OF ABBREVIATIONS

ABBREVIATIONS

SCT	Spectral Chebyshev Technique
HBM	Harmonic Balance Method
FG	Functionally Graded
FGM	Functionally Graded Material
BCs	Boundary Conditions
LCV	Logarithmic Convergence Value
IBVP	Integral Boundary Value Problem
CNT	Carbon-Nanotube
DQM	Differential Quadrature Method
DICF	Direct Integration of Centrifugal Forces
SSED	Steady State Equiblirium Deformations
SACF	Static Analysis under Centrifugal Forces
DOF	Degree of Freedom
DSM	Dynamic Stiffness Matrix

LIST OF SYMBOLS

SYMBOLS

L	Beam length
E	Young modulus
ρ	Density
A	Area
w_t	Width
h_t	Thickness
I	Area Moment of inertia
$\mathbf{Q}_n$	n^{th} order derivative matrix
$\mathbf{v}$	Definite integral vector
$\mathbf{V}$	Inner product matrix
$\mathbf{P}$, $\mathbf{R}$	Boundary projection matrices
m, $\mathbf{M}$	Single mass, mass matrix
k, $\mathbf{K}$	Single stiffness, stiffness matrix
c, $\mathbf{C}$	Viscous damping, viscous damping matrix
α	Slenderness ratio/ Ch5, temporal part of BCs/ Ch4
r_t	Hub radius
δ	Hub radius ratio
ζ	Damping ratio
Ω	Rotation Speed
γ	Dimensionless Excitation Frequency

CHAPTER 1

INTRODUCTION

1.1 Nonlinear Vibrations in the Frequency Domain

With the increasing demand for highly functional and durable engineering materials, the importance of nonlinear vibration analysis has become evident. The linear vibration analysis lacks understanding and pre-determining some of the aspects of dynamic properties. Some failure points of the structures can not be observed with a linear approach due to linear modeling stiffness and boundary conditions. For instance, the structure can have a nonlinear boundary condition that has a piece-wise effect on the system, such as boundaries with gaps. The materials under such boundary conditions behave strictly nonlinear, making it impossible to get accurate results with linear modeling. Moreover, dry friction force and stiffness behavior that material exhibits (such as quadratic or cubic stiffness characteristics) can also induce nonlinearity in the system. Lastly, the problem itself may contain nonlinearity depending on the physical system. For example, finite deformations affect the vibration behavior of structures and introduce nonlinear characteristics to the model.

Fewer studies are conducted to solve nonlinear vibrations than linear vibrations due to their complex form. The nonlinear vibration studies contain different cases from various engineering systems. However, a vast amount of studies focus on free vibrations, and few studies are concentrated on forced vibrations, most of which are based on time-domain solutions. Nevertheless, frequency-domain approaches provide computationally more time and cost-effective solutions than time-domain ones. Therefore, they can be utilized in the design procedure of engineering systems to determine the failure points resulting from nonlinear vibration analysis without the need for costly analysis models.

1.2 Linear and Nonlinear Vibrations of Composite Beams

In recent years, there have been many developments in material technologies. Many new composite materials, such as laminated composites, functionally graded materials, and carbon nano-tube reinforced structures, are used widely in engineering systems. As a result, dynamic aspects of related materials drew the interest of many researchers. Composite beams have become the most commonly studied structures since they can exhibit fundamental physical properties of any form and can be a basis for developing models of more complicated geometries. Therefore, many researchers studied the transverse vibrations of the classical or higher-order composite beam/plate models for linear and nonlinear vibration problems.

Linear vibration problems of composite beams are classified into spectral-temporal boundary problems. The problem does not have a closed-form analytical solution when the system has distributed parameters which is the main case for composite structures. Hence, many different numerical techniques are used to solve those problems, which consist of discretization of the spectral part and the selected solution method. When nonlinear vibrations of these structures are considered, there is also a need to employ a nonlinear solution method. The various approximation, discretization, and nonlinear solution methods are discussed in the Literature Search section.

The main nonlinearity source for the beam problems in the literature is the large deformation of structures. Large deformation nonlinearity, also known as geometric nonlinearity or Von-Karman nonlinearity, results from the stretching force developed along the beam due to large transverse deformations [1]. The transverse deformation causes the beam to elongate. However, when the beam has immovable ends, this elongation results in axial force due to the physical resistance to deformation at boundary conditions. This axial force is also called the stretching force and induces nonlinearity to the system. When the transverse deformations are low, this stretching force is small and does not significantly affect the beam behavior.

Nonetheless, if the transverse deformations are high, the effect of the stretching force on the beam's dynamic behavior becomes undeniable. This is the reason the nonlinearity is called large deformation nonlinearity. Therefore, when applied external forces are high and significant transverse deformations are present, the nonlinear forcing term must be added to the equation of motion. Additionally, this nonlinearity must be modeled carefully when the beam is rotating, and the Coriolis effect and centrifugal force fields are introduced to the system. These force fields lead to a strong coupling of the structural modes in axial, chordwise, and flapwise directions [2]–[4], and the stiffening and coupling effects need to be modeled properly to determine the nonlinear dynamics.

Composite beams and rotating composite beams that undergo large deformations are extensively used to analyze numerous engineering applications such as modeling airplane wings, helicopter propellers, wind turbines, etc. However, nonlinear modal features that are shaped with varying mechanical properties, large external loads, and rotating speeds have introduced additional design parameters to control and tune the modal characteristics of composite structures leading to reliable, economical, and optimal designs. Consequently, this study aims to develop a generic method to solve such crucial nonlinear vibration problems of stationary and rotating composite beams with cost-effective methods in the frequency domain.

CHAPTER 2

LITERATURE REVIEW

Materials that are composed of two or more different phases with distinct mechanical properties are specified as composite materials. Those phases are categorized into the matrix and dispersed phases. The matrix phase is the main continuous phase of the structure, whereas the dispersed phase is included in the matrix phase with a discontinuous distribution. When two phases are combined, a unique new material is formed with physical properties distinct from the properties of the two phases[5].

Composites can be categorized according to matrix constituent or reinforcement phases. The first category involves metal matrix, ceramic matrix, and organic matrix composites. Organic matrix composites are divided into polymer and carbon matrix composites. In the second category, the composites are classified as particulate, fiber-reinforced, and laminar composites. Particulate composites include particle form dispersed phases combined with a matrix phase. The particle inclusion can be random or with a preferred arrangement. When fibers are used in the dispersed phase, the composite structure is named fiber-reinforced or fibrous composites. Short fiber-reinforced composites include small discontinuous fiber as the dispersed phase, whereas long fiber-reinforced composites include continuous fiber orientation. Short fiber-reinforced composites are sub-categorized to random fiber orientations and preferred fiber orientations; meanwhile, long fiber-reinforced composites are sub-categorized to unidirectional and bidirectional fiber orientations. Lastly, when a composite comprises two or more distinct layers with different fiber orientations, it is called a laminate composite. Material properties in laminate composites also depend on the angles and stacking between the layers [5].

Apart from the categories mentioned above, the functionally graded composite materials should also be explained. A functionally graded material (FGM) is a type

of composite structure that consists of two or more phases to have preferred spatial variations of mechanical properties along its directions. Considering the categorization according to reinforcement phases, the FGM is not classified as a different category, and they are primarily associated with particulate composites and fiber-reinforced composites. There are many techniques to manufacture FGMs, such as electrophoretic deposition, chemical vapor deposition, spark plasma sintering and centrifugal casting. However, the design and manufacturing process of FGMs create new challenges that drew many researchers' attention [6].

When vibration studies in the literature are considered, several approaches are found to model the material properties of such described composite structures. One approach is predicting an overall material property using techniques such as the rule of mixture, Mori-Tanaka, and Halpin-Tsai methods. In those approaches, the problem has two stages. The first one is property estimation with those mentioned methods, and the second stage is the solution of the beam vibrations. However, since overall properties are estimated, the beam equation is similar to the uniform beam. This method is commonly preferred for laminated composite beams and FG beams that are graded along the thickness.

Another approach is based on inserting material variation profiles into the derivation of the equation of motion. Material property distributions of composite beams can either be assumed or found with experimental data as spatial functions. Inserting them into the derivation makes the differential equation of motion more complicated and challenging. Therefore, these types of studies are more focused on solving complicated beam equations efficiently than estimating the material properties correctly. This method is best applied for FG materials since they are designed to exhibit specific spatial material property variations.

2.1 Composite Beam Vibrations in Literature

2.1.1 Linear Composite Beam Vibrations in Literature

In many works, the mechanical properties of the composite beams are estimated with various methods, and free vibration analyses are done concerning those estimated properties without any nonlinearities. Alshorbagy et al. [7] worked on the dynamic characteristics of functionally graded (FG) Bernoulli Beams, graded along the thickness direction with a power law distribution. They modeled the beam as combinations of axially and transversely uniform beams. Sina et al. [8] considered the same type of FG beams but solved the problem with analytical methods. Vo-Duy et al. [9] worked on a 2-phase; laminated FG beam with a variation in the thickness direction, which involves carbon-nanotube(CNT) reinforcement. An extended rule of mixture is used to estimate the material properties, and first-order shear deformation theory is utilized to formulate the equations. They also investigated the effect of the CNTs volume fraction on the natural frequencies and mode shapes. Hesmati and Yas [10] also studied CNT-reinforced FG beams in the thickness direction but with an Eshelby-Mori-Tanaka approach to estimate the material properties. The above studies [9], [10], employed the finite element method to obtain free vibration solutions.

Some studies considered the material variation of the composite beams along the longitudinal direction. Liu et al.[11] suggested a new method called Spline Finite Point Method (SFPM) to solve the vibrations of axially tapered FG Bernoulli beams subjected to various boundary conditions. By SFPM, the researchers discretized the beam with scattered nodes instead of using meshes, unlike finite element methods, and approximated the transverse displacement using interpolation functions. Zhao et al.[12] also considered tapered axially FG beams but solved it for Bernoulli and Timoshenko beams using Spectral Chebyshev Technique (SCT). This technique is presented by Yagci et al. [13] to solve linear and nonlinear beam problems. In this method, Chebyshev polynomials are used as basis functions with the application of

Galerkin Method to get the discretized equations of motion, which a simple eigen-value problem can solve.

Vibrations of 2D-FG materials have also been studied by researchers. Wang et al. [14] studied the Euler-Bernoulli beams with material distribution along length according to power law and thickness according to exponential gradation. They solved the system by combining analytical methods and numerical methods, then found that the material property variation along with both directions strongly affects the beam's natural frequency. Researchers concluded that this strong effect could be used in the design of structures to make them vibrate at specific frequencies. Hao end Wei [15] utilized Hamilton's principle to find the equations of a 2D-FG Timoshenko beam and proposed a new dynamic stiffness method combined with Wittrick-William algorithm to calculate the natural frequencies. Şimşek [16] considered forced vibrations in the time domain in addition to free vibration according to both Bernoulli and Timoshenko models. He considered trial functions in both directions as simple polynomials and solved the equation of motion by using an implicit time integration method, Newmark-β.

In some research, simple laminated composites, in which mechanical properties depend on the ply angles and stacking sequence rather than a specific direction, are practiced. Hodges et al. [17] used both the finite element method and analytical methods to obtain the mechanical properties of the thin laminated composite beams. They solved the arising equations with analytical methods and finite element methods, then compared the results with the various experimental studies from the literature. They concluded that the finite element method is more effective than the analytical method since the analytical method requires a good estimation of natural frequency. Wu and colleagues [18] studied the thin laminated composites with the help of finite element methods, but they expanded the scope of the work by including the various beam shapes, including open and closed sections.

2.1.2 Nonlinear Composite Beam Vibrations with Large Deformations in Literature

Nonlinear free vibrations have drawn the attention of many researchers in recent years. Ghasemi and Mohandes [19] worked on the laminated composite Bernoulli beams by using Hamilton's principle and embedding Green-Langrange strain tensor. They obtained the governing equations and employed the generalized differential quadrature method (GDQM) to solve for mode shapes and natural frequencies. They also investigated the effect of lay-up sequences on modes and natural frequencies. Bangera and Chandrashekhara [20] developed a finite element method for the nonlinear vibrations of thick laminated beams. They considered a higher-order beam theory whose nonlinear equations are solved with the direct iterative method. They investigated the effect of boundary conditions, beam geometries, and ply orientation on the nonlinear mode shapes.

Ke, et al.[21] investigated the problem for the FG single-walled carbon nanotube (SWCNT) reinforced Timoshenko beams. In the study, material properties are assumed to be graded in the thickness direction of the beam. The rule of mixture is utilized for the estimation of properties. The direct iterative method is employed to solve the eigenvalue equations which are obtained via Ritz Method. In another work of theirs [22], they investigated the functionally graded Bernoulli Beams. This time they used the Galerkin method to obtain second-order nonlinear ordinary equations, which consist of cubic and quadratic nonlinear terms. With the Runge-Kutta method, the direct iterative method is used to obtain the natural frequencies and mode shapes for different end support. Raffie et al. [23] also worked CNTs reinforced FG-Bernoulli beams with surface bonded piezo-electric layers controlled via applied voltage. They used the Galerkin method; nevertheless, they considered only cubic nonlinear terms. They used the multiple time scales method to obtain the nonlinear vibration characteristics of the beam. Another nonlinear free vibration research oriented around FGM beams with material property variation in the thickness direction is conducted by Feng et al. [24] in which they focused on multilayer

polymer nanocomposite Timoshenko beams reinforced randomly with graphene platelets (GPLs). In their work, effective material properties are estimated by Halphin-Tsai micromechanics model. Natural frequencies and mode shapes are calculated by using the Ritz Method.

Tang et al. [25] studied the nonlinear free vibrations of 2D FG-Bernoulli beams. They applied Hamilton's Principle to derive the nonlinear equations and used GDQM to predict the modes. For the closed-form solutions, they practiced the homotopy analysis method. They concluded that the nonlinear dynamics of FG beams are highly dependent on material property distribution.

Multiple researchers practiced nonlinear forced vibrations of composite beams in the frequency domain. Chakrapani et al. [26] studied the forced vibrations for fiber-reinforced composites with various fiber orientations. They devised a nonlinear viscoelastic beam model using von Karman strains and Kelvin-Voigt stress-strain relationship. They benefitted from the classical plate theory, including the effect of composite fiber orientations on material properties. They used the method of multiple time scales for solving derived equations. Finally, they compared their results with the experimental ones and concluded to have a good agreement between them. Youzera et al. [27] practiced the same problem for three-layered, symmetric laminated composite beams. For the analytical formulation of the problem, they considered higher-order zig-zag theories that account for both shear and normal deformations. They applied the Galerkin method to equations and used the harmonic balance method (HBM) to solve the frequency response of a simply-supported system. Lastly, Sınır et al. [28] worked on FG-Bernoulli beams with varying cross-sections. They assumed that material properties varied along the beam length and used the multiple time scales method and DQM to find an approximate solution in the frequency domain.

In addition to those works, Ciğeroğlu and Samandari [29], [30] studied the nonlinear vibrations of regular and curved double-walled carbon nanotubes (DWCNT) embedded in an elastic medium by considering the nonlinear van der Waals force

combined with geometric nonlinearity. In their first work [30], they derived the equation of motion by using the Bernoulli beam model and represented the motion of DWCNT by multiple eigenfunctions of the linear system. Then, they employed the describing function method (DFM) to represent the nonlinear forces as external forces, which enabled identifying when multiple trial functions needed to be considered. By utilizing multiple trial functions, they found that detecting distinctive vibration modes at a particular frequency was possible. In the latter work [29], they advanced to curved DWCNTs. The equation of motion is discretized and obtained by DQM, which yields a set of nonlinear algebraic equations. They solved those equations by Newton's method with arc-length continuation. Apart from the findings of their previous study, they also observed that the boundary conditions had a powerful effect on the natural frequencies.

In conclusion, since this study aims to find an effective and accurate nonlinear vibration solution for beams, the focus is on nonlinear modeling rather than material property estimation. In this case, the modeling of axially functionally graded Euler-Bernoulli beams is studied as this study's primary composite beam structure. If nonlinear vibrations of distributed parameter beam equations can be solved, combining them with any property estimation method without changing the modeling and solution method is possible.

Regarding the discretization and solution of the problem, researchers have utilized many methods to solve linear and nonlinear equations. Finite element-based approaches result in accurate results for the system; however, they are computationally more expensive than the other methods due to the need for a large degree of freedom and proper meshing. Numerical methods such as DQM, GDQM, and direct iteration method provide faster solutions; however, they have convergence problems for frequency-domain approaches of nonlinear vibration systems. Approximate solutions such as Galerkin, Rayleigh-Ritz, and assumed modes are more efficient than the finite element methods; however, they require trial functions to be satisfied with respect to boundary conditions. When the equations and the

boundary conditions become more complex, it gets harder to identify those boundary trial functions.

A more recent method, Spectral Chebyshev Technique, has been developed as a meshless approximate method [13]. In this method, exponentially convergent Chebyshev polynomials are utilized as the basis to discretize the governing equations in either the weak or strong form. In the weak form, the motion equations are obtained implicitly in the form of algebraic equations. In this condition, the solution can be obtained easier when compared to solving the partial differential equations directly. The boundary conditions are incorporated into the solution by applying the projection matrix approach. Therefore, a different set of basis/trial functions for each boundary condition are no longer required.

After spatial domain discretization, the algebraic nonlinear governing differential equations can be solved in the frequency domain. The most popular techniques to solve such equations are, namely, the perturbation methods [31]–[38], describing function method (DFM) [39], and the harmonic balance method (HBM) [40]–[42]. Among these, HBM is capable of treating numerous kinds of nonlinearities with high accuracy and is applicable to large-scale models [40]. In this method, the periodic steady-state response of the system is expanded by the Fourier series, whose coefficients need to be determined. By inserting this expansion into the nonlinear equations governing the system's dynamics and balancing the identical harmonic terms, one can obtain and solve a set of nonlinear algebraic equations to obtain the unknown Fourier coefficients. Those nonlinear algebraic equations can be solved with path-following methods. Newton’s method with arc-length continuation is preferred in this study due to its accuracy and good convergence.

2.2 Nonlinear Uniform and Composite Rotating Beam Vibrations in Literature

As discussed in the previous section, functionally graded beam problems are more complicated than the property estimated laminated composites and uniformly CNT-reinforced ones. Therefore in this section, the literature search is more focused on the modeling-solution of the uniform and FG rotating beams.

One of the most critical topics in modeling rotating beams is including the centrifugal force field to model the stiffening effects appropriately. According to the literature, methods of including this force field in the model can be classified into three categories.

The first approach simplifies the model by introducing a stretch variable instead of axial deformation [4], [43]–[49]. Some researchers considered the effect of Coriolis force on the rotating beams and the coupling between the axial and flapwise motion. Nevertheless, they neglected the coupling of chordwise motion. Lin and Hsiao [2] studied the Timoshenko beams with this approach, derived the equations with the d'Alembert principle, and applied a power series-based solution. A similar study was conducted by Cai et al. [45] for cantilever beams in which they utilized the finite element method for solution. Younesian and Esmailzadeh [46] also had the same approach to the problem in modeling; however, they employed the Galerkin method for approximation and the multiple scales method for solution. Chung and Yoo [44] considered the coupling of all chordwise, flapwise, and stretching(axial) motions; however, they neglected the Coriolis effects on the beam motion and performed a finite element analysis. The above studies and some others [50], [51] have used simplified models and neglected either the gyroscopic terms caused by the Coriolis force field or considered only single or second-order deformations and neglected the couplings. Such studies improved computational efficiency; however, they are lacking in terms of meeting the desired accuracy.

Another aspect of the studies discussed in the previous paragraph was that they all considered uniform beams. Nevertheless, some studies utilize the stretching variable approach without neglecting coupling or gyroscopic effects and consider FG beams [43], [47]–[49], [52]–[54]. Li et al. [47] studied the free vibrations of rotating FG beams using the assumed modes method, whereas Arvin et al. [49] conducted a similar study using multiple scales. Oh and Yoo [43] extended the stretch variable approach to the pre-twisted functionally graded beams. Zhang and Li [48] considered tapered FG beams and employed a new dynamic method in which slope angle and stretch variable are combined to define the beam motion with the help of the B-spline method. They solved the forced vibrations in the time domain.

In the second approach, equivalent centrifugal force components are used, and direct integration of centrifugal forces (DICFs) is performed to calculate the work done by this force field [50], [52]–[70]. Adair and Jaeger [50] studied the non-uniform rotating Bernoulli beams by this approach; however, they neglected the chordwise coupling. Many researchers studied uniform rotating beams considering all coupling motions. Yang et al. [58] derived the Bernoulli beam equations containing centrifugal stiffening effects with Hamilton Principle and employed a finite element method for the solution. Mei [61] used a new approach called differential transformation to obtain equations and mode shapes of centrifugally stiffened Bernoulli Beams. Banerjee and Kennedy [63] derived the equations with Hamilton's principle and dynamic stiffness method and utilized the Frobenius method of power series solution. Yao et al. [62] studied the pre-twisted beams by using numerical simulations with the help of the multiple scales method. Zhang and Li [64] worked on the forced vibrations of pre-twisted rotating beams in the frequency domain by considering the external force of harmonic gas pressure.

Some researchers used DCIFs for rotating functionally graded beams. Zhu and Mote [55] considered the non-uniform Bernoulli beams with a mass attached to the endpoint. They observed that the high rotational speeds substantially affect the natural frequencies, whereas the effects of relatively low speeds can be neglected. Zarrinzadeh et al.[70] employed the finite element method to solve the free

vibrations of tapered FG beams. Banerjee [56] derived a dynamic stiffness matrix with the Frobenius method for uniform Bernoulli beams. However, he included an axial force at the end of the beam, which enabled assembling the stiffness matrix from different elements. As a result, he analyzed the non-uniform beams by assembling many uniform beams. In another study [57], he applied a similar technique for Timoshenko beams. Chen et al. [52] considered the 2D(in the axial and thickness direction) FG Timoshenko beams and used a finite element formulation with NURBS function. Additionally, various researchers practiced DCIFs of rotating beams with the differential transform method [59], [60], [71].

Many studies solving the rotations of FG beams with DCIFs regarded cases containing supersonic/subsonic airflow, thermal gradients, and pre-deformations(pre-twist). Fazelzadeh et al. [69] investigated the case with supersonic gas flow and utilized DQM for the solution. Subsonic air flow excitation case for the laminated pre-twisted thin-walled beams is practiced by Zhang et al. [66]. In the study, they applied the Chebyshev-Ritz method to obtain natural frequencies. Oh et al. [68] considered the thermal effects on the turbomachinery blades by modeling them as thin-walled beams graded in the thickness direction.

Rotating beams undergo steady-state equilibrium deformations (SSEDs), which are not considered in both of the mentioned categories. The methods of the third category are introduced to determine the SSEDs in the model by static analysis under centrifugal forces (SACF). Accordingly, these methods use nonlinear strain relations to obtain the stiffening effects [31], [72]–[78] . By using nonlinear strain relations, pre-stressed analysis is performed to achieve SACF, results in (**i**) linear stiffening term in equations governing the system's dynamics and (**ii**) nonlinear terms representing the couplings and large deformations. The results obtained with this method manifested that the predicted natural frequencies are different from the ones obtained with the first two categories.

Arvin and Nejad studied the free vibrations with Galerkin discretization and the multiple scales method. Huang et al. [73] found the natural frequencies by dividing

the beam into multiple equal segments and solving those divided equations with power series solution. Pesheck et al. [72] used a reduced order model and invariant manifold approach to find the solution in time domain. Kim et al [75] practised Galerkin method with numerical simulations to obtain mode shapes. Additionally, they investigated the forced response with a time-domain approach. Thomas et al. [77] employed discretized appropriate mode method with a path following numerical solution to get free vibrations and forced vibrations in both frequency and time domain. Afterward, they worked on the same case based on a finite element approach and compared the results.

The above studies regarded uniform rotating beams. Tian, Zhang, and Hua [76] studied the FG beams with double tapered cross-sections and uneven porosity phase distribution. They used the rule of mixture to describe material properties. The researchers modified the variational method based on the Ritz method for equation derivation of the beam divided into several free-free segments and then combined those equations with compatibility relations to solve with the weighted residuals method. Lotfan et al. [31] conducted a comprehensive study on both time and frequency responses of axially FG beams. They also added a time-dependent rotation speed variation into their study. They utilized the Spectral Chebyshev Method to discretize the problem and employed the method of multiple scales to study nonlinear behavior.

According to the discussion above, modeling the rotation effects appropriately and taking into account possible complexities arising from the geometry and/or material bring about convoluted models. In the past decades, these models with/without the above-discussed simplifications have been solved via several approaches, such as finite element [44], [51], [58], Galerkin [46], [62] , Rayleigh Ritz [4], [78], dynamic stiffness matrix (DSM) [63], power series [56], [57], [73], differential transform method (DTM), [59]–[61], [71], and differential quadrature method [32], [33], [53]. Like the case in the previous section, finite element based solutions provide precise predictions for the dynamic behavior of the system, however, they necessitate the use of a large number of degrees of freedom (DOFs) and, as a result, increase the

computational cost [34]. Approximate methods such as Galerkin, Rayleigh-Ritz or DSM are computationally efficient when compared to FE; however, a new set of basis/trial functions are required to satisfy each different boundary condition [35].

In the past decades, researchers have utilized power series method to investigate the dynamics of rotating beams. This method has proved accurate and efficient in both single-segment discretization of the beam [79], and multi-segment discretization with the application for cases with high rotating speed [73]. However, according to this approach, the boundary conditions must be homogeneous, which can be considered as a disadvantage of this approach [36]–[38]. Moreover, based on DTM and DQM, the derivative and integral operators are calculated numerically, and the basis functions highly affect the convergence and accuracy of the solution.

To study the nonlinear dynamics of rotating FG beams, again, SCT is applied, combining with HBM and Newton's method with arc-length continuation. The SCT has been used to model the dynamics of linear systems. However, few studies have included nonlinearity in the models [13]. Nevertheless, in the current work of rotating beams, the SCT can be advanced further to model the nonlinear vibrations of the system based on weak-form formulation. That is, by the aid of the element-wise multiplication definition, the strain and kinematic relations in the presence of couplings and large amplitude vibrations can be expressed by matrix form equations. The model of the rotating FG beam can be developed by including stiffening effects, SSEDs, structural mode couplings, and complexities coming from the material properties together. The developed model based on the nonlinear integral boundary value problem (IBVP) presents the internal nonlinear forcing functions in the matrix form such that HBM can be easily applied to obtain the forced nonlinear response about the SSEDs.

CHAPTER 3

METHODOLOGY

3.1 Harmonic Balance Method

Any periodic function can be represented by the summation of sines and cosines by Fourier Series. Additionally, periodic solutions of ordinary differential equations can be represented by Fourier Series. When we are dealing with vibration problems of periodically excited single or multi-degree of freedom systems, we can assume the solution by Fourier Series expansion.

For nonlinear vibration problems, HBM can be applied to obtain the nonlinear algebraic equations from the equations of motion of the system. In HBM, the nonlinear internal forces in the system can be written as a direct forcing vector. Then an assumed form of a periodic solution is embedded into the nonlinear equation to be expressed in Fourier Series. Finally, coefficients of similar terms can be balanced to determine unknown coefficients.

3.1.1 Case Study: Nonlinear Response of a SDOF system with Cubic Stiffness

A case study was performed in this section for a better explanation of the HBM. This study investigates a simple, single degree of freedom mass-spring problem with a cubic stiffness added. A free body diagram for the system is given in Figure 3.1.

The equation of motion for the system with mass(m), damping(c), linear and nonlinear springs with stiffnesses (k, k_c), and force amplitude F_0 at a frequency of w is given below.

$$m\ddot{x}+c\dot{x}+kx+k_c x^3 = F_0 \sin(wt) \tag{3.1}$$

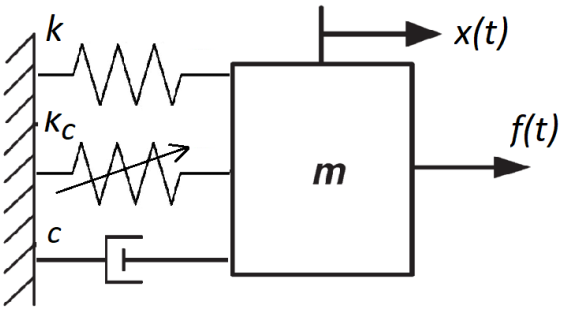

Figure 3.1. Free body diagram of the SDOF system

A single harmonic solution can be assumed to the problem.

$$x(t) = x_s \sin(wt) + x_c \cos(wt) \tag{3.2}$$

Derivatives of the assumed solution are,

$$\dot{x}(t) = wx_s \cos(wt) - wx_c \sin(wt) \tag{3.3}$$

$$\ddot{x}(t) = -w^2 x_s \sin(wt) - w^2 x_c \cos(wt) \tag{3.4}$$

The terms in the equation of motion can be expressed as:

$$\begin{aligned}(-w^2 m + k)(x_s \sin(wt) + x_c \cos(wt)) + (cw)(x_s \cos(wt) - x_c \sin(wt)) \\ + k_c (x_s \sin(wt) + x_c \cos(wt))^3 = F_0 \sin(wt)\end{aligned} \tag{3.5}$$

The cubic expression can be expanded and rewritten with the help of trigonometric relations.

$$\begin{aligned}(x_s \sin(wt) + x_c \cos(wt))^3 = x_c{}^3 \cos^3(wt) + 3x_c{}^2 x_s \cos^2(wt)\sin(wt) \\ + 3x_c x_s{}^2 \cos(wt)\sin^2(wt) + x_s{}^3 \sin^3(wt)\end{aligned} \tag{3.6}$$

$$\begin{aligned}(x_s \sin(wt) + x_c \cos(wt))^3 = \frac{3}{4}(x_s x_c{}^2 + x_s{}^3)\sin(wt) + \frac{3}{4}(x_c{}^3 + x_c x_s{}^2)\cos(wt) \\ + \frac{1}{4}(x_c{}^3 - 3x_c x_s{}^2)\cos(3wt) + \frac{1}{4}(3x_s x_c{}^2 - x_s{}^3)\sin(3wt)\end{aligned} \tag{3.7}$$

By considering the sine and cosine terms' equality and balancing the terms, two nonlinear algebraic equations can be obtained as:

$$\left(-mw^2+k\right)x_s - cwx_c + \frac{3}{4}k_c\left({x_s}^2+{x_c}^2\right)x_s = F_0 \tag{3.8}$$

$$\left(-mw^2+k\right)x_c + cwx_s + \frac{3}{4}k_c\left({x_s}^2+{x_c}^2\right)x_c = 0 \tag{3.9}$$

Since a single harmonic solution is assumed, higher-order terms, sin(3*wt*) and cos(3*wt*) are neglected. If a multi-harmonic solution was assumed, it would be necessary to consider the higher-order terms. The force and the solution could be assumed in the summation form given below for the multi-harmonic solution scenario.

$$x(t) = x_0 + \sum_{k=1}^{n}\left(x_{s_k}\sin(wt) + x_{c_k}\cos(wt)\right) \tag{3.10}$$

$$F(t) = F_0 + \sum_{k=1}^{n}\left(F_{s_k}\sin(wt) + F_{c_k}\cos(wt)\right) \tag{3.11}$$

Here the term x_0 is called the bias term. It is essential to consider the bias term even if there is no constant force since the bias term can occur anyways, depending on the nonlinearity type.

For the multi-harmonic case, unknown coefficients of the nonlinear forces are obtained in terms of sines and cosines with the help of the Fourier Transformation equations given below.

$$fn_0 = \frac{1}{2\pi}\int_0^{2\pi} f_{nl}\,d\theta \tag{3.12}$$

$$fn_{s_k} = \frac{1}{\pi}\int_0^{2\pi} f_{nl}\,\sin(k\theta)\,d\theta \tag{3.13}$$

$$fn_{c_k} = \frac{1}{\pi}\int_0^{2\pi} f_{nl}\,\cos(k\theta)\,d\theta \tag{3.14}$$

In the above equations, f_{nl} is the nonlinear internal force, and θ is the *wt* multiplication.

3.2 Frequency Response Functions of Nonlinear Systems with Newton's Method and Arc-Length Continuation

A frequency response function is used for the quantification of the system response to the excitation level, magnitudewise in the frequency domain. For linear systems, the equation of motion is written in the frequency domain, and response magnitude can be solved analytically for each frequency. Nevertheless, for a nonlinear system, an analytical solution is not possible. Therefore, numerical methods are utilized to get nonlinear frequency response functions.

In this study, Newton's method with arch-length continuation is preferred. Newton's method is not enough on his own to solve these nonlinear frequency responses due to some reasons. First of all, it is possible to get multiple solutions for a specific frequency which requires a good path following method to identify all of them. Additionally, at the turning of the frequency curve, there are local points whose Jacobian's are zero, making Newton's method unsolvable. By adding a new path following parameter called arch-length, the Jacobian is made non-zero at those points. What is more, this arc-length searches for the following solution in an arch and hence becomes very effective in identifying the next solution point; even the path starts to turn around.

With the addition of a new parameter to the system, the vector of unknowns can be written as

$$q = \begin{Bmatrix} \mathbf{x} \\ w \end{Bmatrix} \tag{3.15}$$

where **x** represents the vector with unknowns and *w* represents frequency. However, frequency becomes unknown too, and a new equation is required to be added into the system, which is the equation of a hypothetical sphere centered on the previous solution point and has a radius Δs.

$$\left(\mathbf{x}_k - \mathbf{x}_{k-1}\right)^2 + \left(w_k - w_{k-1}\right)^2 = \left(s_k - s_{k-1}\right)^2 \tag{3.16}$$

where, $\Delta x = x_k - x_{k-1}, \Delta w = w_k - w_{k-1}$ *and* $\Delta s = s_k - s_{k-1}$.

As a result, a new equation is obtained.

$$h(\mathbf{x}_k, w_k) = (\mathbf{x}_k - \mathbf{x}_{k-1})^{\mathrm{T}} (\mathbf{x}_k - \mathbf{x}_{k-1}) - (s_k - s_{k-1})^2 \tag{3.17}$$

With the addition of this new equation, the equation set of Newton's method is written.

$$\mathbf{q}_{k+1} = \mathbf{q}_k - \begin{bmatrix} \dfrac{\partial R(\mathbf{x}, w)}{\partial \mathbf{x}} & \dfrac{\partial R(\mathbf{x}, w)}{\partial w} \\ \dfrac{\partial h(\mathbf{x}, w)}{\partial \mathbf{x}} & \dfrac{\partial h(\mathbf{x}, w)}{\partial w} \end{bmatrix}^{-1} \begin{Bmatrix} R(\mathbf{x}, w) \\ h(\mathbf{x}, w) \end{Bmatrix} \tag{3.18}$$

An example nonlinear frequency response curve is given in Figure 3.2 for the cubic stiffness case described in Chapter 3.1.1 for different excitation levels. (Parameters are taken as k=10000 N/m, m=10 kg, k_c=1000000 N/m^3, μ=0.03, c=$k\mu$ and f=15,20,25N).

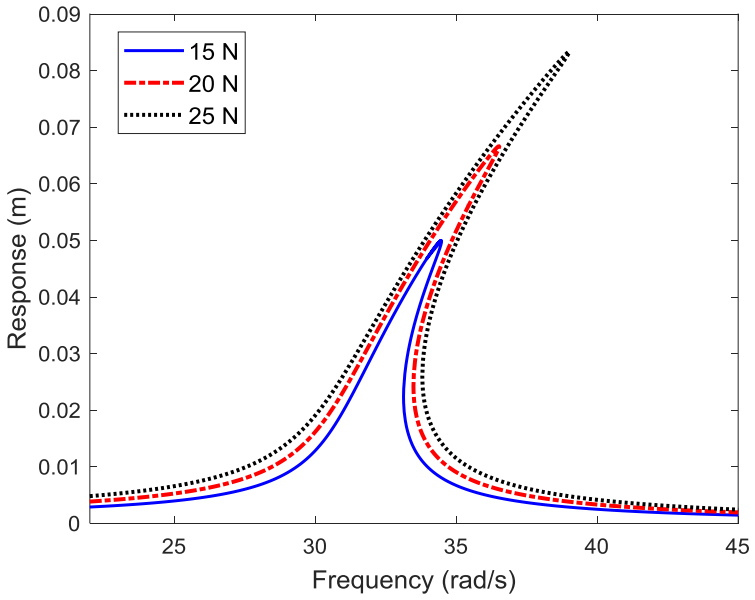

Figure 3.2. Frequency response of the SDOF system described in Chapter 3.1.1

3.3 Spectral Chebyshev Technique

In the SCT, Chebyshev polynomials are used for obtaining system matricies for the boundary value problemof beam vibrations. A function of the problem can be expressed by a Chebyshev series expansion as

$$y(x)=\sum_{k=0}^{\infty}\alpha_k T_k(x) \tag{3.19}$$

Where $T_k(x)$ is Chebyshev polynomials of the first kind which can be given as follows

$$T_k(x)=\cos(k\cos^{-1}(x)) \quad \text{for } k=0,1,2,.... \tag{3.20}$$

Chebyshev polynomial representation of a function is valid for (-1,1) interval since the cosine function is defined between those intervals. Consequently, there arises a need for mapping between the (-1,1) interval and the function boundaries. For instance, if a beam problem is considered with borders (l_1, l_2), then mapping should be done between $x \in (l_1, l_2)$ and $\zeta \in (-1, 1)$ to satisfy the equations below

$$x(\xi)=\xi\frac{l_2-l_1}{2}+\frac{l_2+l_1}{2} \tag{3.21}$$

$$\xi(x)=x\frac{2}{l_2-l_1}-\frac{l_2+l_1}{l_2-l_1} \tag{3.22}$$

Sampled points can represent the displacement function of the beam at specific increments for numerical calculations. If the sampling point number is selected the same as the number of Chebyshev polynomials, a one-to-one mapping occurs between the sampled points and Chebyshev coefficients α_k. For N number of Chebyshev polynomials, N number of Gauss-Lobatto points are used for sampling spatial domain, which is defined as

$$p_k=\cos\left(\frac{(k-1)\pi}{N-1}\right) \quad \text{for } k=1,2,...,N \tag{3.23}$$

The relation between sampled displacement function of the beam and the Chebyshev expansion coefficients can be written as

$$\mathbf{a} = \mathbf{\Gamma}_{\mathbf{F}}\,\mathbf{y} \tag{3.24}$$

where $\mathbf{\Gamma}_F$ is a N x N forward transformation matrix which can be expressed by Chebyshev polynomials.. Additionally, the backward transformation matrix can be defined which is the inverse of the forward transformation matrix.

Exact derivative and integral of any function and vector that is constructed by Chebyshev polynomials can be obtained as

$$\mathbf{y}^{(n)} = \mathbf{Q}_n\mathbf{y} \tag{3.25}$$

$$\int_{l_1}^{l_2} y(x)\,dx = \mathbf{v}^{\mathrm{T}}\mathbf{a} \tag{3.26}$$

Here $\mathbf{Q}_{\mathrm{n}}$ is the derivative matrix with respect to order n. $\mathbf{v}$ is the definite integral vector. Derivation of the $\mathbf{Q}_{\mathrm{n}}$ and $\mathbf{v}$ is given in Appendix A. Additionally, the inner product of two functions can be written in the form given below with the help of SCT.

$$\int_{l_1}^{l_2} f(x)\,g(x)\,dx = \mathbf{f}^{\mathrm{T}}\mathbf{V}\mathbf{g} \tag{3.27}$$

$\mathbf{V}$ is called the inner product matrix, and its calculation is also given in Appendix A.

For a wave equation (with boundaries l_1 and l_2) given in Eq. 3.28, the boundary conditions can be written in a generic way such as,

$$\ddot{y} = \lambda y + f \tag{3.28}$$

$$\sum_{k=0}^{1}\sum_{i=1}^{2}\left(\beta_{k_{ij}}{}^{(k)}\right) = \alpha_j(t) \tag{3.29}$$

Here β's are the constants of the spatial part of the boundary condition, whereas α's are the constants of the temporal part. Both can be written in vector form. The i and j indices correspond to the boundary location (l_1 and l_2, i=1,2) and the number of the boundary condition (j=1,2), and k is the derivative order. When boundary conditions change, the derivation of the equation does not change; only these matrices change.

By considering the Chebyshev expansion sampled at N points and the derivation, integration, and inner product matrices, the wave equation can be rewritten in the Chebyshev domain.

$$\ddot{\mathbf{y}} = \lambda \mathbf{Q}_2 \mathbf{y} + \mathbf{f} \tag{3.30}$$

A vital step in imposing boundary conditions to the equation in the Chebyshev domain is expressing **y** with the help of projection matrices **P** and **R** which are obtained by the singular value decomposition of β. This procedure makes it possible to solve the system for **z** that only satisfies the homogeneous boundary conditions, whereas **y** satisfies all boundary conditions. This stage is also named basis recombination.

$$\mathbf{y} = \mathbf{P}\mathbf{z} + \mathbf{R}\boldsymbol{\alpha} \tag{3.31}$$

After the projection matrices are involved, Eq. 3.30 can be expressed in the form given in Eq. 3.32, and the residual can be defined as given in Eq. 3.33.

$$\mathbf{P}\ddot{\mathbf{z}} + \mathbf{R}\ddot{\boldsymbol{\alpha}} = \lambda \mathbf{Q}_2 \left(\mathbf{P}\mathbf{z} + \mathbf{R}\boldsymbol{\alpha} \right) + \mathbf{f} \tag{3.32}$$

$$\phi = \mathbf{P}\ddot{\mathbf{z}} + \mathbf{R}\ddot{\boldsymbol{\alpha}} - \lambda \mathbf{Q}_2 \left(\mathbf{P}\mathbf{z} + \mathbf{R}\boldsymbol{\alpha} \right) - \mathbf{f} \tag{3.33}$$

The Galerkin method is applied to the system to obtain the approximate solution. By this method, the residual error is minimized by making its inner product with weighting functions go zero.

$$\int_{l_1}^{l_2} \theta(x)\phi(x)\,dx = \boldsymbol{\theta}^{\mathrm{T}} \mathbf{V} \boldsymbol{\phi} = 0 \tag{3.34}$$

Here θ(x) is the weighting function, which must satisfy the homogeneous boundary condition. A simple weighting function, such as $\theta = \mathbf{P}\bar{\theta}$, can be considered. That transforms Eq. 3.34 into the form given in Eq. 3.35.

$$\bar{\theta} \left\{ \mathbf{P}^{\mathrm{T}} \mathbf{V} \left(\left(\mathbf{P}\ddot{\mathbf{z}} - \lambda \mathbf{Q}_2 \mathbf{P}\mathbf{z} \right) - \left(\mathbf{f} + \lambda \mathbf{Q}_2 \mathbf{R}\boldsymbol{\alpha} - \mathbf{R}\ddot{\boldsymbol{\alpha}} \right) \right) \right\} = 0 \tag{3.35}$$

The equation above must be satisfied for arbitrary $\bar{\theta}$; therefore, the terms inside the brackets must be also zero. The resulting equation can be written as the following and can be easily expressed in mass-stiffness and force form.

$$\mathbf{P^T V P \ddot{z}} - \lambda \mathbf{P^T V Q_2 P z} = \mathbf{P^T V f} - \mathbf{P^T V R \ddot{\alpha}} + \lambda \mathbf{P^T V Q_2 R \alpha} \qquad 3.36$$

$$\mathbf{M \ddot{z}} + \mathbf{K z} = \mathbf{f}^* \qquad 3.37$$

where

$$\mathbf{M} = \mathbf{P^T V P \ddot{z}}, \quad \mathbf{K} = -\lambda \mathbf{P^T V Q_2 P z} \qquad 3.38$$

$$\mathbf{f}^* = \mathbf{P^T V f} - \mathbf{P^T V R \ddot{\alpha}} + \lambda \mathbf{P^T V Q_2 R \alpha}$$

CHAPTER 4

LINEAR AND NONLINEAR VIBRATIONS OF UNIFORM AND FUNCTIONALLY GRADED BEAMS

4.1 Mathematical Model

4.1.1 Uniform Beams

The equation of a Bernoulli Beam with uniform material properties is given below.

$$EI\frac{\partial^4 y(x,t)}{\partial x^4}+\rho A\frac{\partial^2 y(x,t)}{\partial t^2}=f(x,t) \tag{4.1}$$

Boundary conditions for this beam can be written in a generic way such that,

$$\beta_{3_{ij}}y'''+\beta_{2_{ij}}y''+\beta_{1_{ij}}y'+\beta_{0_{ij}}y=\alpha_{ij}(t) \tag{4.2}$$

For example, if a simply supported beam is considered, then the moment (related to the second derivative of deformation) and the deformation at the boundaries should be zero. Consequently, boundary conditions can be written as vectors with the SCT.

$$\boldsymbol{\beta}_{2_{01}}\mathbf{e}_1^{\mathrm{T}}\mathbf{Q_2}+\boldsymbol{\beta}_{0_{02}}\mathbf{e}_1^{\mathrm{T}}=\boldsymbol{\alpha}_{01}(\mathrm{t}) \tag{4.3}$$

$$\boldsymbol{\beta}_{2_{L1}}\mathbf{e}_1^{\mathrm{T}}\mathbf{Q_2}+\boldsymbol{\beta}_{0_{L2}}\mathbf{e}_1^{\mathrm{T}}=\boldsymbol{\alpha}_{L1}(\mathrm{t}) \tag{4.4}$$

Boundary projection matrices are imposed on the system, as it was described in Chapter 3.3. Then the residual is obtained given in the form below.

$$\phi=\rho A(\mathbf{P}\ddot{\mathbf{z}}+\mathbf{R}\ddot{\boldsymbol{\alpha}})-EI(\mathbf{Q_4}(\mathbf{Pz}+\mathbf{R}\boldsymbol{\alpha}))-\mathbf{f} \tag{4.5}$$

As the next step, Galerkin method is applied to the system, and the equation of motion is acquired in Chebyshev domain.

$$\rho A\mathbf{P^T V P}\ddot{\mathbf{z}}+EI\mathbf{P^T V Q_4 Pz}=\mathbf{P^T Vf}-\rho A\mathbf{P^T V R}\ddot{\boldsymbol{\alpha}}+EI\mathbf{P^T VQ_2 R}\boldsymbol{\alpha} \tag{4.6}$$

When the basic boundary conditions with no temporal dependencies are considered, which is the case for this study, the α, $\dot{\alpha}$ and $\ddot{\alpha}$ becomes zero. As a result, equivalent mass, stiffness, and forcing matrices are written.

$$\mathbf{M} = \rho A \mathbf{P}^{\mathrm{T}} \mathbf{V} \mathbf{P} \ddot{\mathbf{z}},\ \mathbf{K} = EI \mathbf{P}^{\mathrm{T}} \mathbf{V} \mathbf{Q}_4 \mathbf{P} \mathbf{z}\ ,\ \mathbf{f}^{*} = \mathbf{P}^{\mathrm{T}} \mathbf{V} \mathbf{f} \tag{4.7}$$

A simple eigenvalue problem solution can be handled by using **M** and **K** matrices to get the natural frequencies and mode shapes. To obtain the frequency response, a periodic force can be assumed to the system and Eq. 4.6 can be solved in the frequency domain.

If large deformation nonlinearity is also considered, then a new term comes for the equation of motion which is the stretching force developed in the beam due to the large deformations.Bernoulli beam equation for uniform beam, in the presence of an axial force, is given in the following equation [80].

$$EI \frac{\partial^4 y}{\partial x^4} + \rho A \frac{\partial^2 y}{\partial t^2} = -\frac{\partial}{\partial x}\left(P \frac{\partial w}{\partial x}\right) + f\left(x,t\right) \tag{4.8}$$

To explain the nonlinear force term, firstly, the nonlinear axial strain of a beam can be written as

$$\varepsilon_{xx} = \frac{\partial u_x}{\partial x} + \frac{1}{2}\left(\frac{\partial u_y}{\partial x}\right)^2 \tag{4.9}$$

The first term gives the axial strain developed along the beam due to the axial elongation. When modeling the large deformation nonlinearity of Bernoulli beams the first term is neglected and the problem is solved for immovable boundary conditions such as fixed-fixed and pinned-pinned. For the stress-free edges, the nonlinearity disappears since axial deformation is a function of transverse deformation already.

In the large deformation theory, nonlinear force occurs due to the total stretch developed along the beam. Therefore, the spatial dependence of strain should be removed from the equation by integration over length. Axial force developed along the beam can be written as

$$N_x = EA\varepsilon_{xx} \tag{4.10}$$

Integrating both sides yields,

$$\int_{l_1}^{l_2} N_x = \int_{l_1}^{l_2} \frac{EA}{2}\left(\frac{\partial u_y}{\partial x}\right)^2 dx \tag{4.11}$$

$$N_x = \frac{EA}{2L}\int_{l_1}^{l_2}\left(\frac{\partial u_y}{\partial x}\right)^2 dx$$

For the uniform case the beam equation is simplified as,

$$EI\frac{\partial^4 y}{\partial x^4} + \rho A\frac{\partial^2 y}{\partial t^2} = \left[\frac{EA}{2L}\int_{l_1}^{l_2}\left(\frac{\partial y}{\partial x}\right)^2 dx\right]\frac{\partial^2 y}{\partial x^2} + f\left(x,t\right) \tag{4.12}$$

The nonlinear term of this equation can be rewritten in the Chebyshev domain,

$$\left[\frac{EA}{2L}\int_{l_1}^{l_2}\left(\frac{\partial y}{\partial x}\right)^2 dx\right]\frac{\partial^2 y}{\partial x^2} = \frac{EA}{2L}\mathbf{v}^{\mathbf{T}}\boldsymbol{\Gamma}_{\mathbf{F}}\left(\mathbf{Q_1 P z}\right)^2\mathbf{Q_2 P z} \tag{4.13}$$

Afterwards, the above equation can be solved in the frequency domain using HBM and Newton's Method with arc-length continuation.

4.1.2 Functionally Graded Beams

The method for the non-uniform beams is the same as the uniform beam case; however, the equations become different. When a parameter or some parameters vary along the beam length, they are functions of the length rather than constants. Hence, inner product multiplication is defined in Eq. 3.34 changes form. New functions of parameter distribution involve multiplication. Therefore, the order of the multiplication increases, and a new higher-order inner product matrix is defined. The calculation of the higher-order inner product matrix is given in Appendix A.

$$\int_{l_1}^{l_2} f\left(x\right)h\left(x\right)g\left(x\right)dx = \mathbf{f}^{\mathrm{T}}\mathbf{V_h}\mathbf{g} \tag{4.14}$$

With the addition of a new inner product matrix, the equation of motion for a beam with varying Young Modulus along its length is written as an example.

$$\frac{\partial^2}{\partial x^2}\left[\ E(x)I\frac{\partial^2 y}{\partial x^2}\right]+\rho A\frac{\partial^2 y}{\partial t^2}=f(x,t) \tag{4.15}$$

The equation is expanded and written in the Chebyshev domain using the chain rule.

$$I\left[E(x)\frac{\partial^4 y}{\partial x^4}+2\frac{\partial E(x)}{\partial x}\frac{\partial^3 y}{\partial x^3}+\frac{\partial^2 E(x)}{\partial x^2}\frac{\partial^2 y}{\partial x^2}\right]+\rho A\frac{\partial^2 y}{\partial t^2}=f(x,t) \tag{4.16}$$

$$\rho A\mathbf{P^T V P\ddot{z}}+I\left[\mathbf{P^T}\left[\mathbf{V_E Q_4 Pz}+\mathbf{2V_E}'\mathbf{Q_3 Pz}+\mathbf{V_E}''\mathbf{Q_2 Pz}\right]\right]=\mathbf{P^T V f} \tag{4.17}$$

Here $\mathbf{V_E}'$ and $\mathbf{V_E}''$, are the inner product matrices calculated according to derivatives of sampled Young Modulus distribution functions. That means *h*(x) given in Eq. 4.14, is replaced with $\frac{\partial E(x)}{\partial x}$ and $\frac{\partial^2 E(x)}{\partial x^2}$.

If the beam had all of its properties varying along the beam length, then a helpful approach would be the group the various functions such that they can be written as a single function for the inner product multiplication, such as

$$a(x)=E(x)I(x) \tag{4.18}$$

$$b(x)=A(x)\rho(x) \tag{4.19}$$

$$d(x)=A(x)E(x) \tag{4.20}$$

which resolves the equation of motion in Chebyshev domain as

$$\mathbf{P^T V_b P\ddot{z}}+\mathbf{P^T}\left[\mathbf{V}_a\mathbf{Q_4 Pz}+\mathbf{2V}_a^{''}\mathbf{Q_3 Pz}+\mathbf{V}_a^{''}\mathbf{Q_2 Pz}\right]=\mathbf{P^T V f} \tag{4.21}$$

For the nonlinear case, the equation can be expressed with the form given below, which makes applying HBM and SCT easier.

$$\left[\frac{1}{2L}\int_{l_1}^{l_2}E(x)A(x)\left(\frac{\partial y}{\partial x}\right)^2 dx\right]\frac{\partial^2 y}{\partial x^2}=\left[\frac{1}{2L}\int_{l_1}^{l_2}\left(\frac{\partial y}{\partial x}\right)d(x)\left(\frac{\partial y}{\partial x}\right)dx\right]\frac{\partial^2 y}{\partial x^2} \tag{4.22}$$

Afterwards, this nonlinear phrase can be adapted to SCT, such as

$$\left[\frac{1}{2L}\int_{l_1}^{l_2}\left(\frac{\partial y}{\partial x}\right)d(x)\left(\frac{\partial y}{\partial x}\right)dx\right]\frac{\partial^2 y}{\partial x^2}=\frac{\mathbf{P}^T\mathbf{V}}{2L}\left[\left(\mathbf{Q_1 Pz}\right)^{\mathrm{T}}\mathbf{V_d}\left(\mathbf{Q_1 Pz}\right)\right]\mathbf{Q_2 Pz} \tag{4.23}$$

Considering the property variations between Eqs. 4.18-4.20 and by adding the nonlinear large deformation force obtained above equation to the Eq. 4.17, the nonlinear equation in the Chebyshev domain is obtained.

$$\mathbf{P^T V_b P\ddot{z} + P^T\left[V_a Q_4 Pz + 2V_a\,'Q_3 Pz + V_a\,''Q_2 Pz\right] =} \\ \frac{\mathbf{P^T V}}{2L}\left[\left(\mathbf{Q_1 Pz}\right)^T \mathbf{V_d}\left(\mathbf{Q_1 Pz}\right)\right]\mathbf{Q_2 Pz + P^T Vf} \tag{4.24}$$

Single or multi-harmonic solutions can be assumed for the system, and equations can be solved in the frequency domain. In this study, the application and formulation of HBM to the system are handled by computer programs since the nonlinear term given in Eq. 4.23 yields too many terms due to the multi-harmonics and different matrix multiplications.

4.2 Results and Discussion

4.2.1 Natural Frequencies and Convergence Analysis

First, natural frequencies of the uniform beam without nonlinearities are found with various numbers of used Chebyshev polynomials. In the process, different boundary conditions are regarded. The results are compared with the exact solution which is present for the linear vibrations of the uniform Bernoulli beam [80]. The comparison is given in Table 4.1.

Table 4.1. Natural frequencies of pinned-pinned uniform beam

	Natural Frequencies (rad/s)		
	Exact Solution	SCT with 9 Polynomials	SCT with 13 Polynomials
1st	144.244	144.244	144.244
2nd	576.977	576.994	576.977
3rd	1298.198	1298.677	1298.198

Table 4.1 (cont'd)

4th	2307.908	2452.392	2307.957
5th	3606.105	4012.955	3606.596

Table 4.2. Natutal frequencies of fixed-fixed uniform beam

	Natural Frequencies (rad/s)		
	Exact Solution	SCT with 9 Polynomials	SCT with 13 Polynomials
1st	326.980	326.986	326.986
2nd	901.347	901.647	901.348
3rd	1766.9999	1770.323	1767.003
4th	2920.959	3242.881	2921.322
5th	4363.408	5165.420	4365.938

Table 4.3. Natural frequencies of pinned- fixed uniform beam

	Natural Frequencies (rad/s)		
	Exact Solution	SCT with 9 Polynomials	SCT with 13 Polynomials
1st	225.337	225.337	225.337
2nd	730.240	730.309	730.236
3rd	1523.587	1525.877	1523.580
4th	2605.423	2811.163	2605.539
5th	3975.750	4601.434	3977.551

The natural frequencies are calculated according to the parameters (E=71 GPa, w_t=0.03 m, h_t=0.01 m, ρ=2770 kg/m^3). Additionally, in the study, beam cross-section is considered to be symmetric with respect to its axes for all scenarios. As a result, it is observed that the desired results are achieved for the first natural frequencies with an error smaller than %0.01. Nonetheless, as solutions are sought for the higher natural frequencies, distinguishable errors up to %15 start to occur with 9 polynomials. When the number of Chebyshev polynomials is increased again to 13, errors start to decrease below %0.05. That proves a direct correlation between the required number of Chebyshev polynomials and the number of natural frequencies that need to be found with the slightest error. A convergence analysis is conducted to observe the correlation between the error and the number of polynomials used. Initially, the first 5 mode shapes are regarded in this analysis. For three boundary conditions that are considered, natural frequency results are plotted with respect to different polynomial numbers used. A desired error percent is selected to be %0.1.

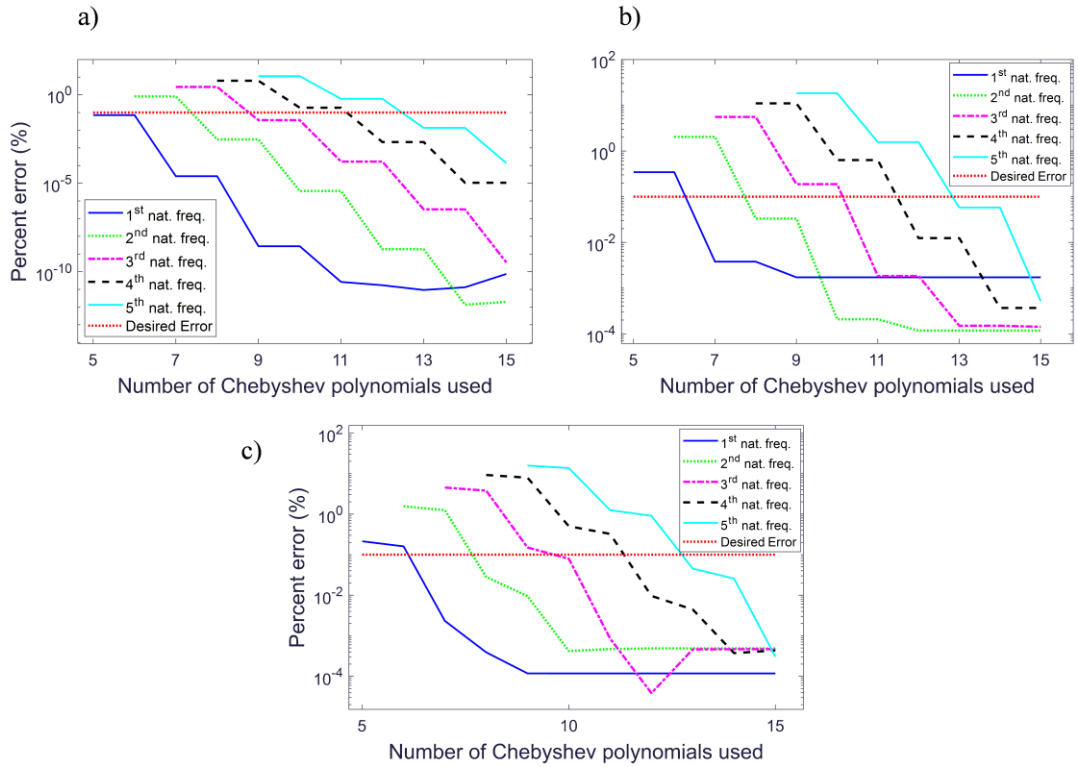

Figure 4.1. Errors of first five natural frequencies depending on the number of Chebyshev polynomials used(BCs: a)pinned-pinned, b)fixed-fixed, c)pinned-fixed)

Here it should be noted that to find *n* numbers of natural frequency, there is a need to use *n*+4 Chebyshev polynomials. This happens due to the singular value decomposition of the boundary projection matrices, which reflects the system with four boundary conditions. Results show that the error ratio increases as the natural frequencies increase (pinned-pinned to fixed-fixed). However, as seen in the previous figure, an increase in the used polynomial number results in a fast convergence to the exact values with negligible errors. As expected, more polynomials are required to obtain precise results for higher natural frequencies.

Secondly, natural frequencies and mode shapes for the functionally graded tapered beam are found. Since there is no exact solution is available for the case, the results are compared with the work in the literature. Liu et al. [11] considered the problem and provided the first two natural frequencies according to chosen material property distributions. Additionally, they compared their results with another study conducted by Shahba and Rajasekaran [81]. In their studies, property distributions are taken as below.

$$A(x) = A_0\left(1-\frac{c_b x}{L}\right)\left(1-\frac{c_h x}{L}\right) \tag{4.25}$$

$$I(x) = I_0\left(1-\frac{c_b x}{L}\right)\left(1-\frac{c_h x}{L}\right)^3 \tag{4.26}$$

$$\rho(x) = \rho_0\left(1+\frac{x}{L}+\left(\frac{x}{L}\right)^2\right) \tag{4.27}$$

$$E(x) = E_0\left(1+\frac{x}{L}\right) \tag{4.28}$$

By considering the above distributions, the eigenvalue problem derived by SCT is solved. The results are compared to the studies mentioned above with four scenarios of different property variations along with two boundary conditions, fixed-fixed (F-F) and pinned-pinned (P-P). In the Table 4.4 and Table 4.5, results were given by using 13 Chebyshev polynomials (the polynomial number is correlated according to

convergence analysis which will be described later). Material properties are taken as (E_0 =210 GPa, w_t =0.01 m, h_t =0.03 m, $A_0 = w_t\, h_t$, ρ_0 =7900 kg/m^3).

Natural frequencies are nondimensionalized in the table according to the below equation.

$$w^* = w\sqrt{\frac{\rho_0 A_0 L^4}{E_0 I_0}} \qquad 4.29$$

Table 4.4 Comparison of the normalized natural frequencies of varying parameter FG beam between the calculated ones and references found/ pinned-pinned

	c_b	0		0.2		0.4		0.6	
c_h		w_1	w_2	w_1	w_2	w_1	w_2	w_1	w_2
0	SCT	9.029	36.372	9.060	36.342	9.087	36.315	9.099	36.297
	R1	9.029	36.372	9.060	36.342	9.087	36.315	9.099	36.297
	R2	9.029	36.372	9.060	36.342	9.087	36.315	9.099	36.297
0.2	SCT	8.134	32.523	8.146	32.512	8.150	32.508	8.134	32.516
	R1	8.134	32.524	8.146	32.512	8.150	32.508	8.134	32.516
	R2	8.134	32.523	8.146	32.512	8.150	32.508	8.134	32.516
0.4	SCT	7.153	28.474	6.008	24.137	7.125	28.500	7.079	28.537
	R1	7.153	28.475	7.146	28.482	7.125	28.500	7.079	28.537
	R2	7.153	28.474	7.146	28.482	7.125	28.500	7.079	28.537
0.6	SCT	6.036	24.110	6.008	24.137	5.964	24.179	5.887	24.247
	R1	6.036	24.110	6.008	24.137	5.964	24.179	5.887	24.247
	R2	6.036	24.110	6.008	24.137	5.964	24.179	5.887	24.247

In the table R1 corresponds to Liu's work whereas R2 corresponds to Shahba's. It is observed that the results have an excellent agreement with Shahba's study. Additionally, the results suggest that the c_h dominates the outcome rather than the c_b value. Those parameters affect the area and moment of inertia distributions which are plotted in Appendix D. The first natural frequency distributions for 2 cases are given in Figure 4.2, the first has the c_h is fixed whereas is c_b varying, and the other is vice versa.

Table 4.5. Comparison of the normalized natural frequencies of varying parameter FG beam between the calculated ones and references found / fixed-fixed

	c_b	0		0.2		0.4		0.6	
c_h		w_1	w_2	w_1	w_2	w_1	w_2	w_1	w_2
0	SCT	20.472	56.548	20.415	56.471	20.288	56.297	20.019	55.920
	R1	20.472	56.549	20.415	56.472	20.288	56.298	20.019	55.921
	R2	20.472	56.548	20.415	56.471	20.288	56.297	20.019	55.920
0.2	SCT	18.217	50.479	18.200	50.456	18.129	50.359	17.944	50.101
	R1	18.217	50.480	18.200	50.456	18.129	50.359	17.944	50.101
	R2	18.217	50.479	18.200	50.456	18.129	50.359	17.944	50.101
0.4	SCT	15.828	44.024	15.850	44.054	15.835	44.036	15.737	43.901
	R1	15.828	44.025	15.850	44.055	15.835	44.037	15.737	43.903
	R2	15.828	44.024	15.850	44.054	15.835	44.036	15.737	43.901
0.6	SCT	13.229	36.964	13.289	37.049	13.332	37.112	13.323	37.108
	R1	13.229	36.965	13.290	37.051	13.332	37.114	13.324	37.111
	R2	13.229	36.964	13.289	37.049	13.332	37.112	13.323	37.108

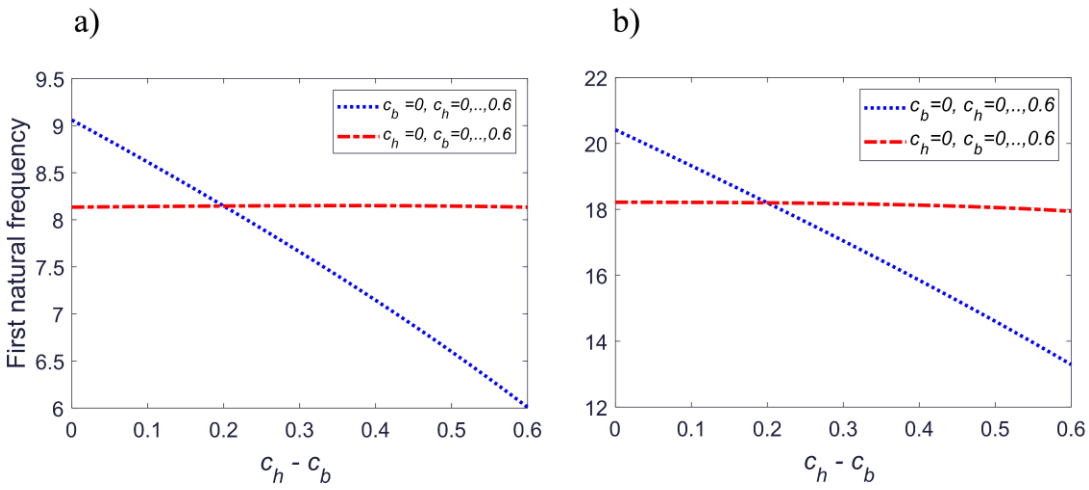

Figure 4.2. Non-dimensionalized natural frequency distributions with one of the parameters is fixed whereas the other varies (BCs: **a)**pinned-pinned, **b)**fixed-fixed)

As given in the Figure 4.2, variation of c_h affected the first natural frequencies dramatically, whereas variation of c_b didn't have such an effect. That is, the cubic term in the inertia distribution has a powerful effect on the natural frequency. As the next step, mode shapes for the first 5 natural frequencies of two scenarios with two

BCs (with distributions c_h=0.6 and c_b=0.6 and c_h=0.2 and c_b=0.2) are plotted in Figure 4.3 and Figure 4.4.

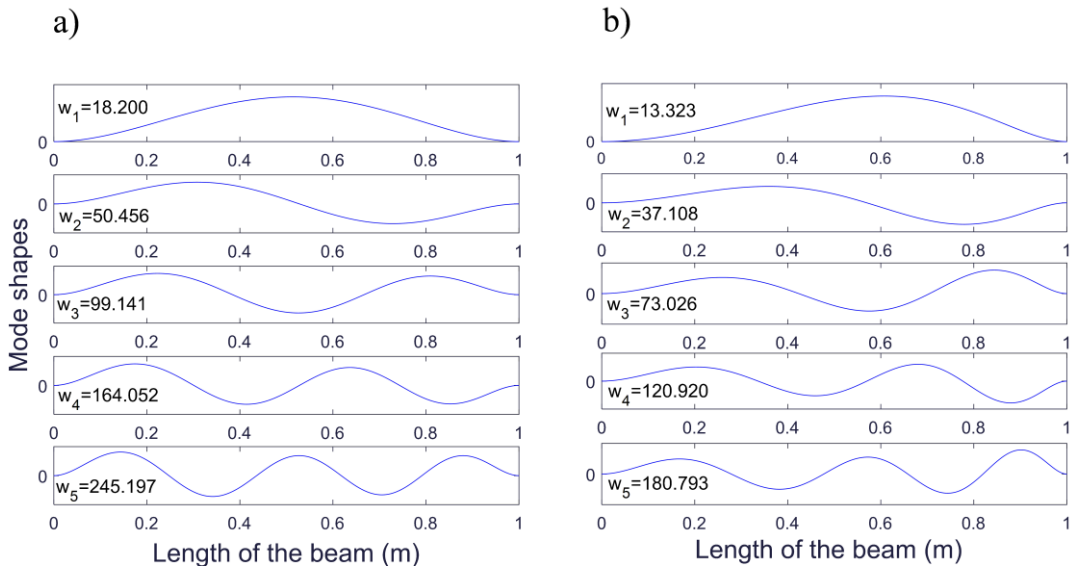

Figure 4.3. Mode shapes of non-uniform fixed-fixed beam (with distributions **a)**c_h=0.2\$c_b$=0.2 and **b)**$c_h$=0.6\$c_b$=0.6)

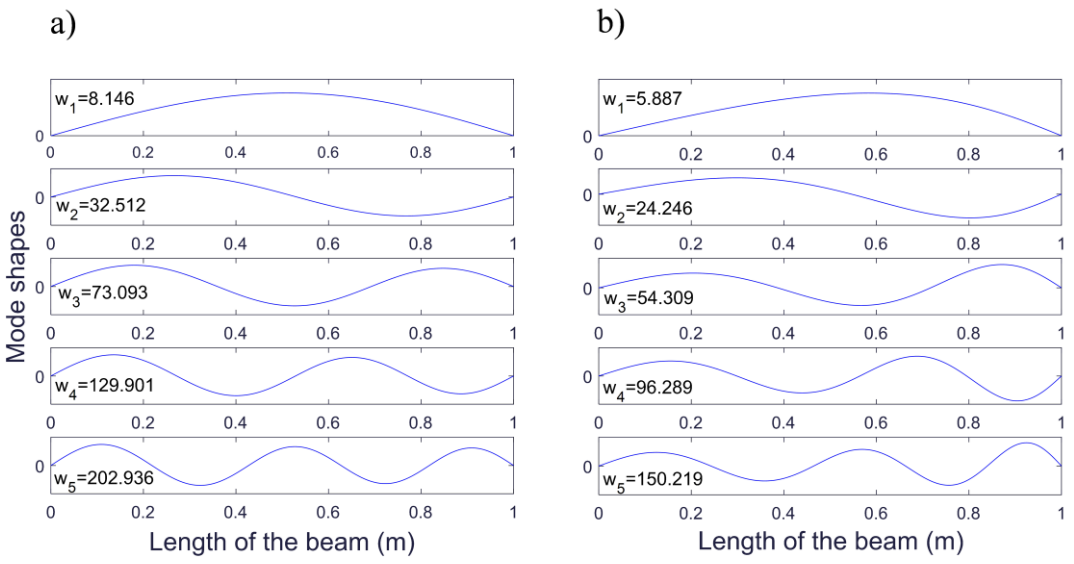

Figure 4.4. Mode shapes of non-uniform pinned-pinned beam (with distribution **a)**c_h=0.2\$c_b$=0.2 and **b)**$c_h$=0.6\$c_b$=0.6)

The mode shape of the uniform beam is not given here since it is very basic and present in many works (can be accessed for all boundary conditions from [80]). It was observed that when c_h and c_b are small, the mode shape is closer to the uniform

beam's symmetric mode shapes. However, when c_h and c_b increase, the beam becomes more functionally graded, resulting in more asymmetric mode shapes.

A convergence analysis was made similar to the previous case. Since now there are also property variation parameters c_h and c_b considered, the cases were not investigated separately according to natural frequencies. Instead, a relative logarithmic assessment is preferred which is given with the following equation

$$LCV_{N_\xi} = \log\left(\frac{1}{M}\sum_{i=1}^{M}\frac{\left|w_i^{N_\xi} - w_i^{N_{\xi ref}}\right|}{w_i^{N_{\xi ref}}}\right) \qquad 4.30$$

LCV is the logarithmic convergence value, $w_i^{N_\xi}$ denotes the natural frequency of the i^{th} vibration mode obtained by N_ξ number of polynomials, and *M* is the number of modes within the frequency bandwidth of interest. To determine the sufficient number of polynomials, $LCV \le \varepsilon$ should be satisfied (where ε is the threshold value selected by the user). In this case ε is selected to be 0.1% ($\varepsilon = -3$) and first 5 natural frequencies are considered. Since there is no exact solution available, it is necessary to find a reference case whose natural frequency is denoted $w_i^{N_{\xi ref}}$. To determine the reference case, the fifth natural frequencies were plotted for two boundary condition scenarios in Figure 4.5, since it is the last converging one among the first five natural frequencies.

In Figure 4.5, it can be seen that after 13 polynomials, natural frequencies do not change and converge to a specific value. It is also observed that as the variation parameters increase, the convergence occurs with more Chebyshev polynomials. $N_{\varepsilon_{ref}}$ is selected to be 21, which is a much bigger value than 13 to guarantee the convergence. The logarithmic convergence values are given in Figure 4.6.

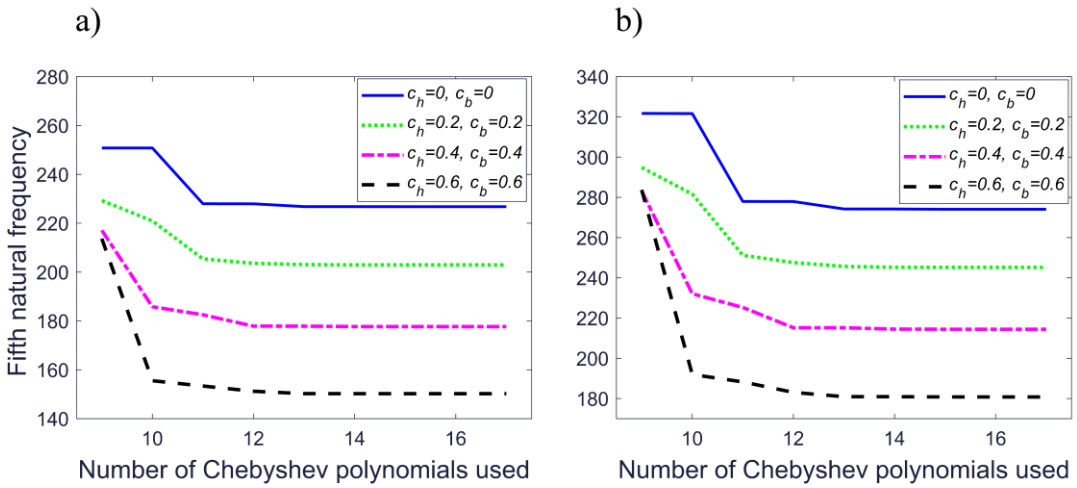

Figure 4.5. Non-dimensionalized fifth natural frequency with respect to the number of polynomials used (BCs: **a)**pinned-pinned, **b)**fixed-fixed)

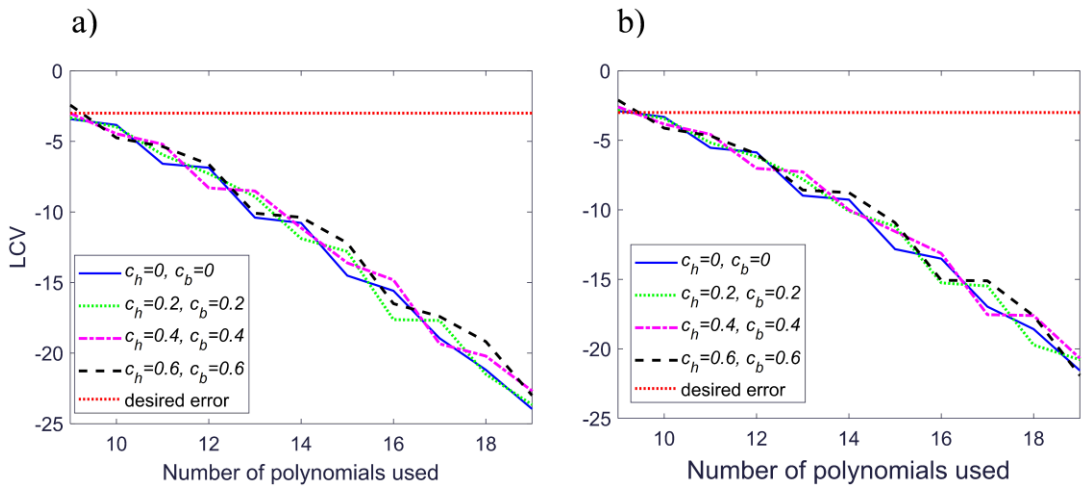

Figure 4.6. Convergence results with respect to logarithmic convergence value (BCs: **a)**pinned-pinned, **b)**fixed-fixed)

To obtain precise results for overall of 5 natural frequencsies, 10 polynomials are found to be adequate.

4.2.2 Frequency Responses

The nonlinear frequency responses of the uniform and non-uniform beams are discussed with respect to different boundary conditions and various amplitudes of

forces. The properties of the beam are taken the same as in the previous case. The study is performed by considering three harmonics. The damping is considered as

$$\mathbf{C} = \mu \mathbf{M} \tag{4.31}$$

Two boundary conditions, pinned-pinned and fixed-fixed, are considered. A point force is applied at the mid point of the beam structures for both cases. The fixed boundary condition implies that the assigned surface cannot deform or rotate. On the other hand, pinned boundary condition allows rotation but no translation at the point applied. For the fixed boundary, transverse deflection and the slope is zero. For the pinned boundary, the transverse deflection and the bending moment must be zero.

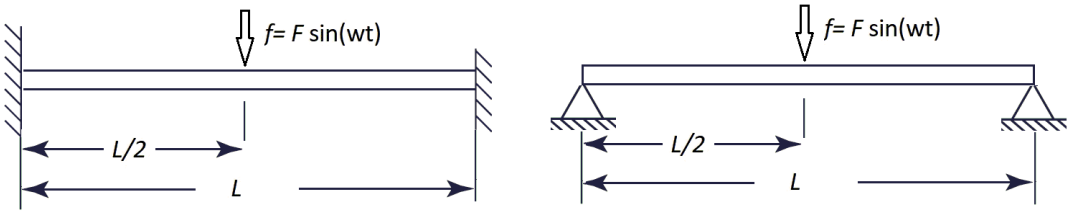

Figure 4.7. Fixed-fixed and pinned-pinned beams with a point force applied at the mid point

Firstly, frequency response plots for uniform beams are plotted. In all of the upcoming frequency response plots, the beam is excited at the middle point where also response is taken from. The first two plots give the first harmonic response (normalized with respect to the force applied) of the system subjected to different excitation levels concerning fixed-fixed and pinned-pinned boundary conditions. The linear response is also given for a single force value since the force normalized responses are the same for all force values for the linear system.

The upcoming frequency response studies are performed by using 7 Chebyshev polynomials. The responses are plotted around the first natural frequency. The previous convergence analysis found that 7 polynomials generate precise results for the first natural frequency. As of the initial step, the first harmonic responses of the beams with respect to different excitation levels and two BCs are given in Figure 4.8 and Figure 4.9. (μ taken as 0.05 for the rest of the cases in Chapter 4)

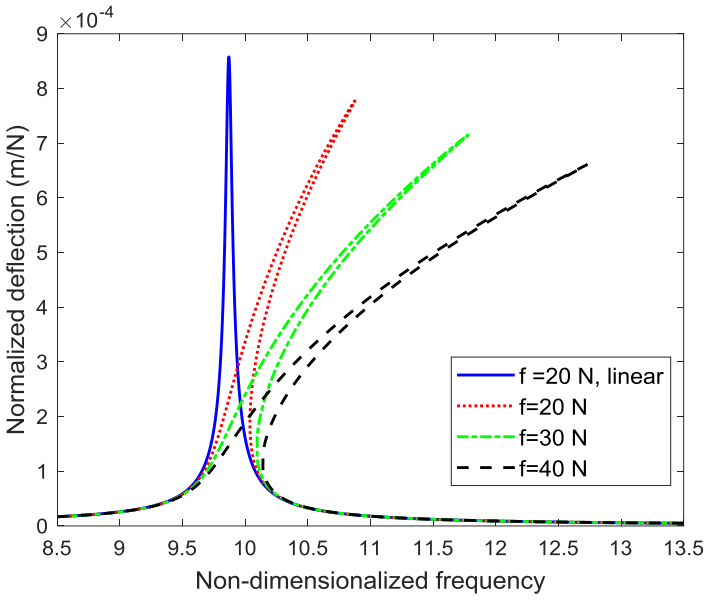

Figure 4.8. Force normalized, first harmonic nonlinear frequency response for uniform beam with pinned-pinned boundary conditions

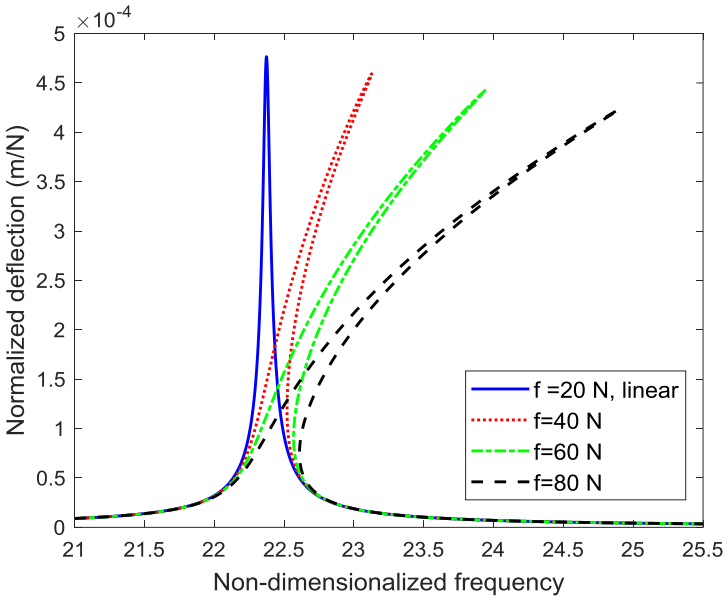

Figure 4.9. Force normalized, first harmonic nonlinear frequency response for uniform beam with fixed-fixed boundary conditions

In the nonlinear study, it is observed that as the force increases, the nonlinear effect (which can be reasoned with the shift of frequency curve) on the beam increases too. Higher forces result in higher stretching forces, raising the nonlinear behavior but

decreasing the transverse deflection. Additionally, it is observed that a third harmonic response occurs, whereas there isn't a second harmonic response or bias term. The reason is that the nonlinear force of large deformation has a cubic form that generates odd harmonics responses. If there was a quadratic force, it would be expected to have a second harmonic response and bias term. In Figure 4.10 and Figure 4.11, third harmonic responses are given.

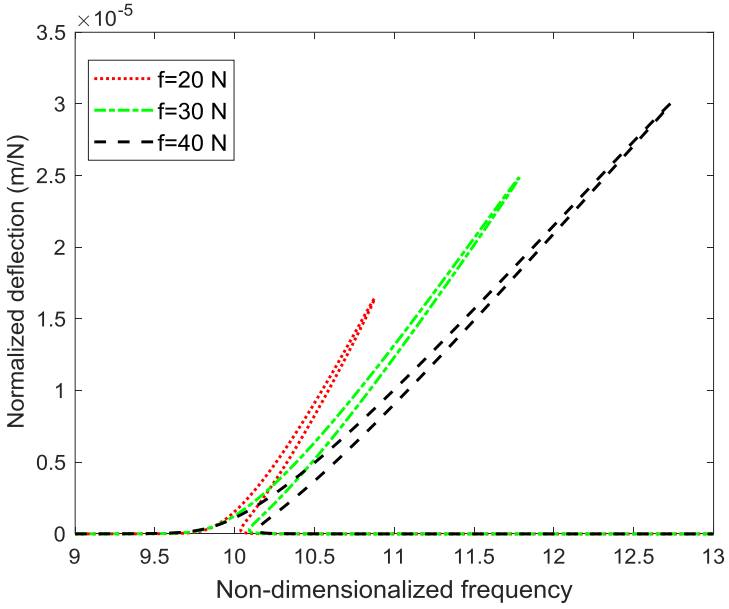

Figure 4.10. Force normalized, third harmonic nonlinear frequency response for uniform beam with pinned-pinned boundary conditions

The third harmonic response is much smaller compared to the first harmonic response. As the applied force increases, the nonlinear effect increases too. However, when applied force increases, the deflection caused by the third harmonic doesn't decrease like it was in the first harmonic. Figure 4.12 is given for comparison of the first and third harmonic responses for the pinned-pinned case.

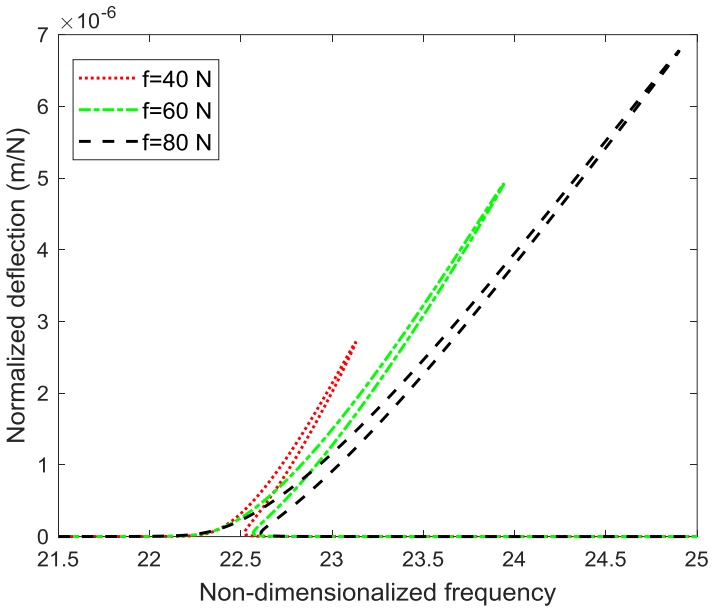

Figure 4.11. Force normalized, the third harmonic nonlinear frequency response for the uniform beam with fixed-fixed boundary conditions

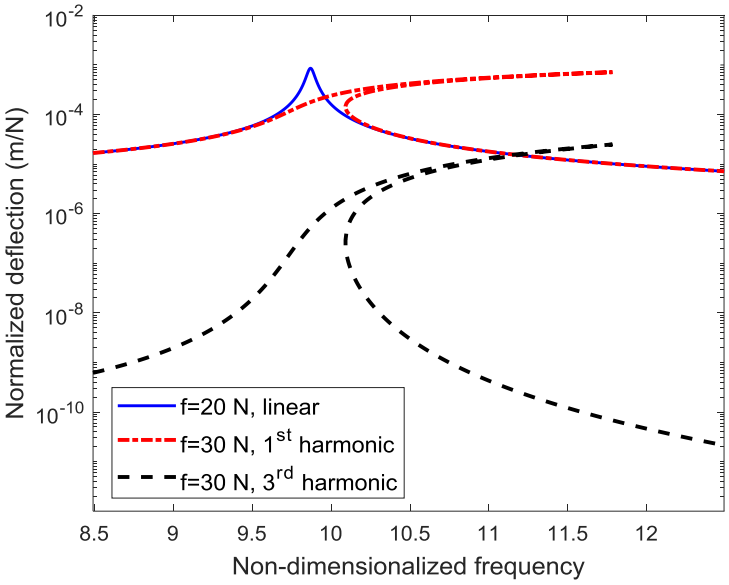

Figure 4.12. Force normalized, first harmonic and third harmonic nonlinear frequency response for uniform beam with pinned-pinned boundary conditions

As it can be seen from Figure 4.12, the third harmonic response is smaller than the first one. Nonetheless, it is not negligible for considering the total response since that response occurs in higher frequencies at which smaller deflections are expected.

Subsequently, the same study is performed for functionally graded tapered beams. As it was given in Figure 4.2, c_b distributions didn't affect the results significantly. Thus, the cases where c_h=c_b and c_h are varying, are considered in the upcoming scenarios (such as c_h=c_b=0, c_h=c_b=0.2, c_h=c_b=0.4, c_h=c_b=0.6). The first and third harmonic responses of two FG beams (c_h=c_b=0.2, pinned-pinned, and c_h=c_b=0.4 fixed-fixed) are given with different excitation levels in Figure 4.13 and Figure 4.14.

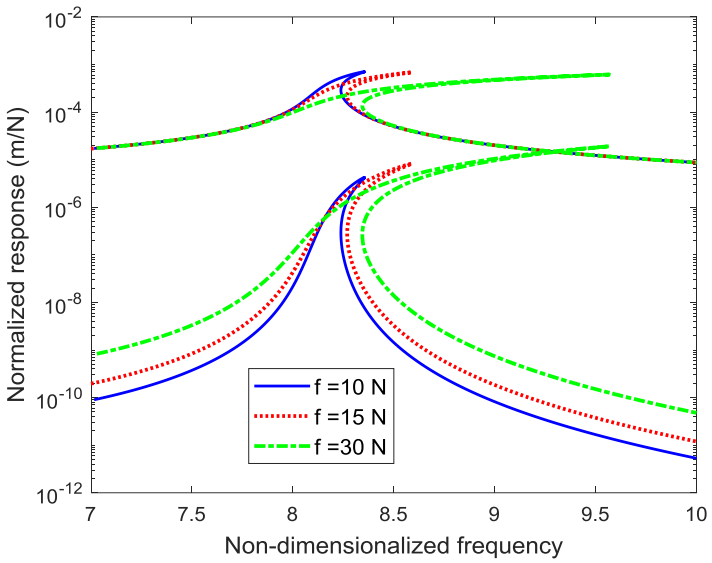

Figure 4.13. Force normalized, first harmonic, and third harmonic nonlinear frequency response for the FG beam with pinned-pinned boundary conditions (c_h=c_b=0.2)

Nonlinearity created a similar effect on the FG beam deformation to uniform beam deformation. However, the variation of parameters made the beam less stiff, resulting in larger deformations and higher stretching forces, creating a more significant nonlinear effect.

Nonetheless, the third harmonic response exhibited a different behavior by having 2 response peak regions for the fixed case. This is explained by modal coupling phenomena (or internal resonance). The different modes of the system can excite each other and the energy exchange between those different modes results in mixed frequency responses. The frequency at the first peak of the third harmonic response corresponds to the second natural frequency. This phenomenon does not only occur

for c_h=c_b=0.4 and BCs fixed-fixed case. If the frequency range of the case given in Figure 4.13 (c_h=c_b=0.4 and BCs pinned-pinned) is expanded, those internal resonances can also be identified.

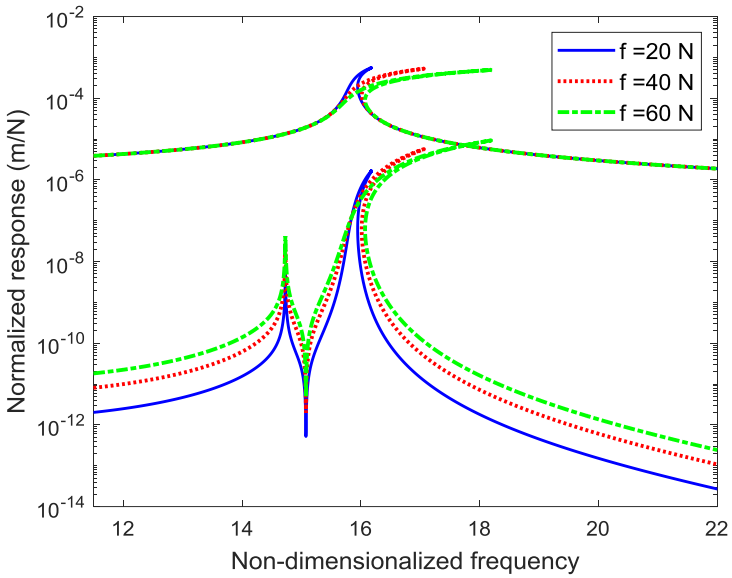

Figure 4.14. Force normalized, first harmonic and third harmonic nonlinear frequency response for the FG beam with pinned-pinned boundary conditions (c_h=c_b=0.4)

In Figure 4.15, modal couplings can be observed better. The multiplied frequency of the third harmonic response (with 3x due to the third harmonic) of the first frequency peak around the normalized frequency of 2.7 corresponds to the first natural frequency. The third peak around the normalized frequency of 10.9 corresponds to the second natural frequency. The coupling of the first mode is more powerful compared to the one with the second mode. Additionally, the coupling results to a linear response in both cases due to the low amplitude.

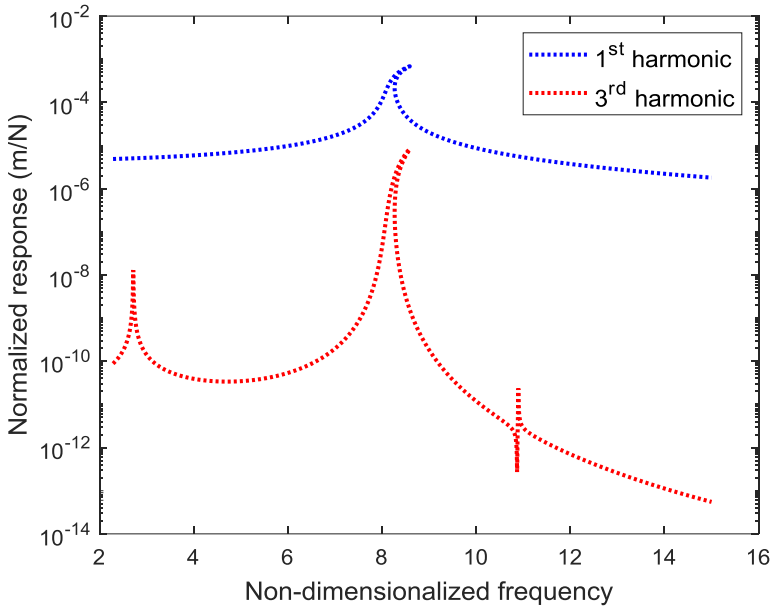

Figure 4.15. Force normalized, first harmonic and third harmonic nonlinear response for FG beam with pinned-pinned boundary conditions (c_h=c_b=0.4, f=15N)

As the next step in the study, the first harmonic responses of all considered FG beams are investigated in the same plot. Responses regarding different material property distributions are given in Figure 4.16 and Figure 4.17. Afterward, those responses are plotted with respect to normalized frequency (to their natural frequency) to obtain the effect of material distribution on nonlinear behavior.

When the response is normalized with respect to natural frequencies, the nonlinear effect can be observed better. From Figures 4.18 and 4.19, it can be clearly observed that, as the parameter variation increases and makes the beam less stiff, the nonlinear effect on the beam response increases too.

In Figures 4.20 and 4.21, linear frequency responses of uniform and FG beams are given together with nonlinear frequency responses of uniform and FG beams so as to show the effects of both nonlinearity and FG property distributions.

Interestingly, it is observed that the values of the case c_h=c_b=*0.8* give rise to the different behavior of the first harmonic frequency response with fixed-fixed boundary conditions.

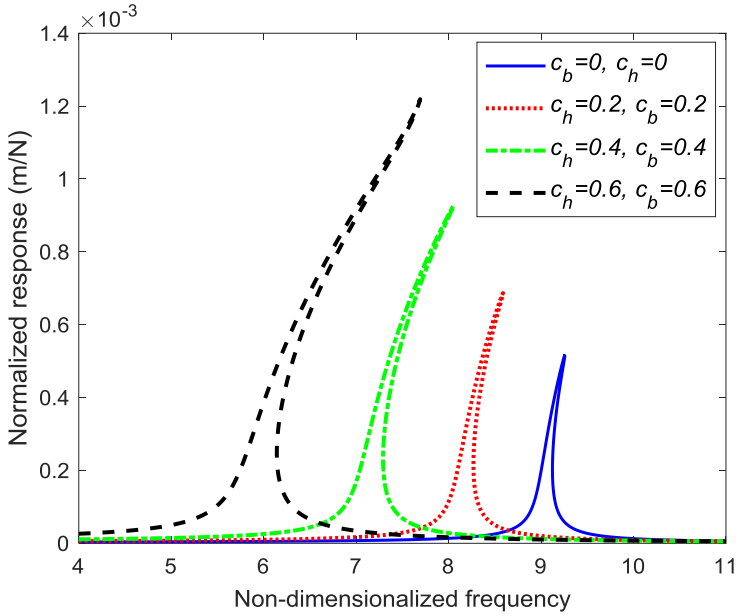

Figure 4.16. Force normalized, the first harmonic nonlinear frequency response for FG beams with pinned-pinned boundary conditions (f=15N)

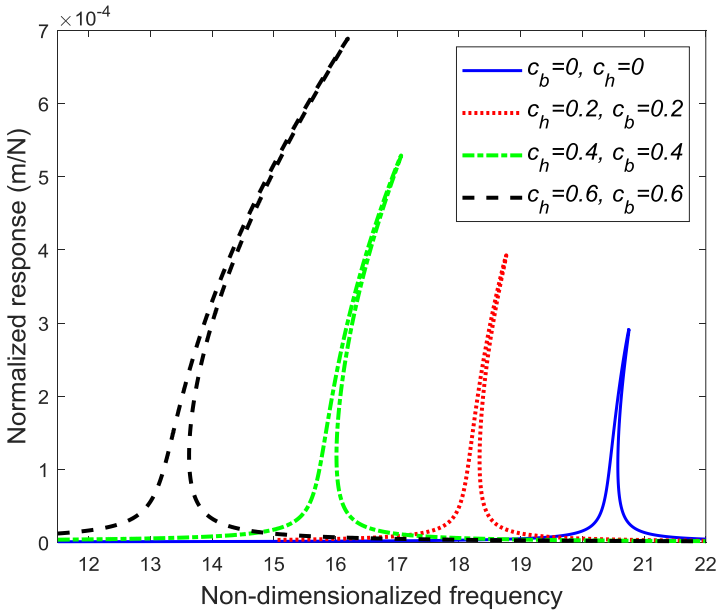

Figure 4.17. Force normalized, the first harmonic nonlinear frequency response for FG beams with fixed-fixed boundary conditions (f=40N)

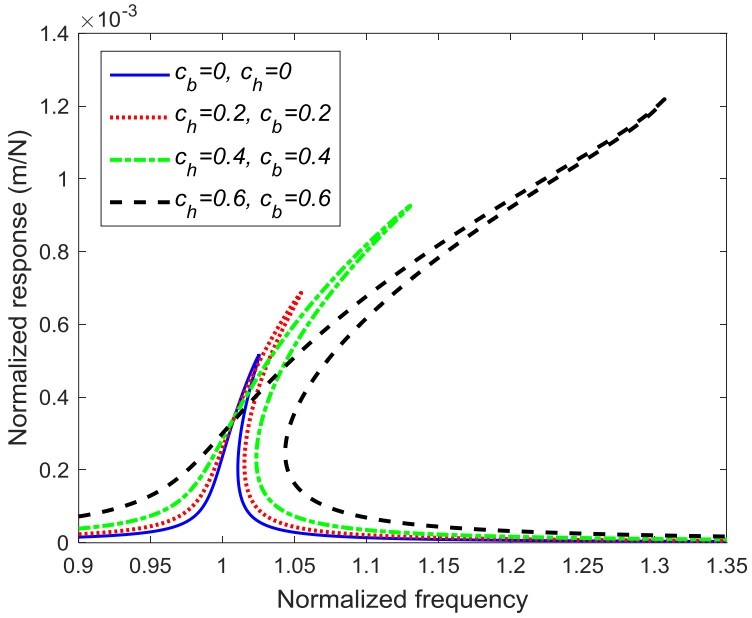

Figure 4.18. Force and frequency normalized, first harmonic nonlinear response for non-uniform beams with pinned-pinned boundary conditions (f=15N)

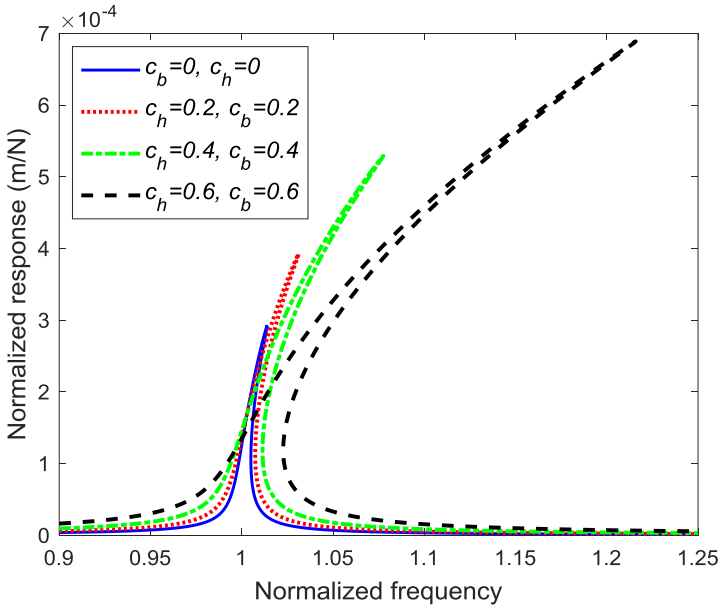

Figure 4.19. Force and frequency normalized, first harmonic nonlinear response for FG beams with fixed-fixed boundary conditions (f=40N)

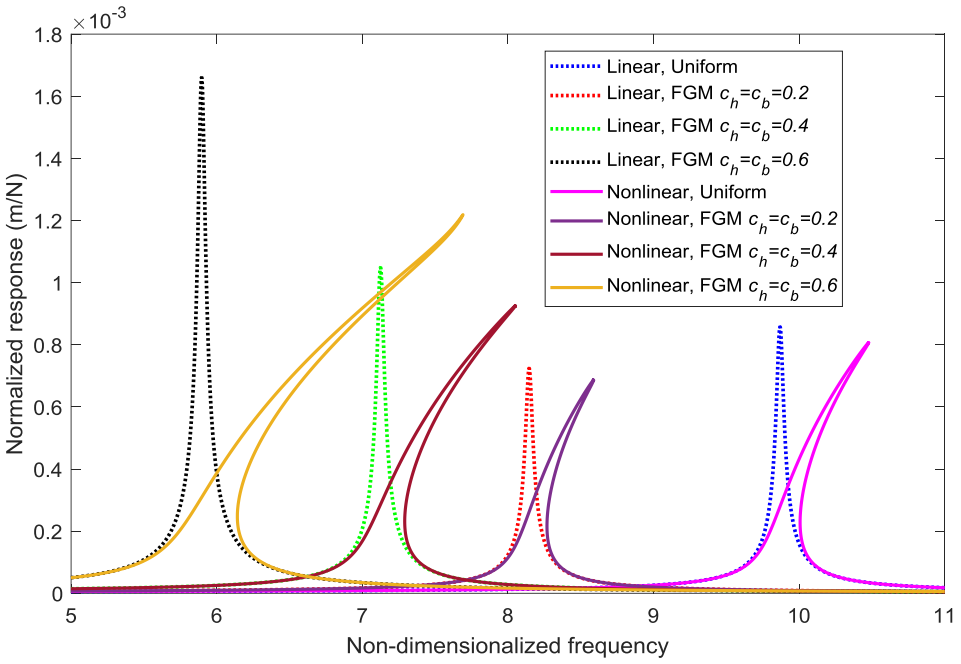

Figure 4.20. Force normalized, first harmonic linear/nonlinear responses of uniform and FG beams with 7 polynomials and pinned pinned BCs (*f*=15N)

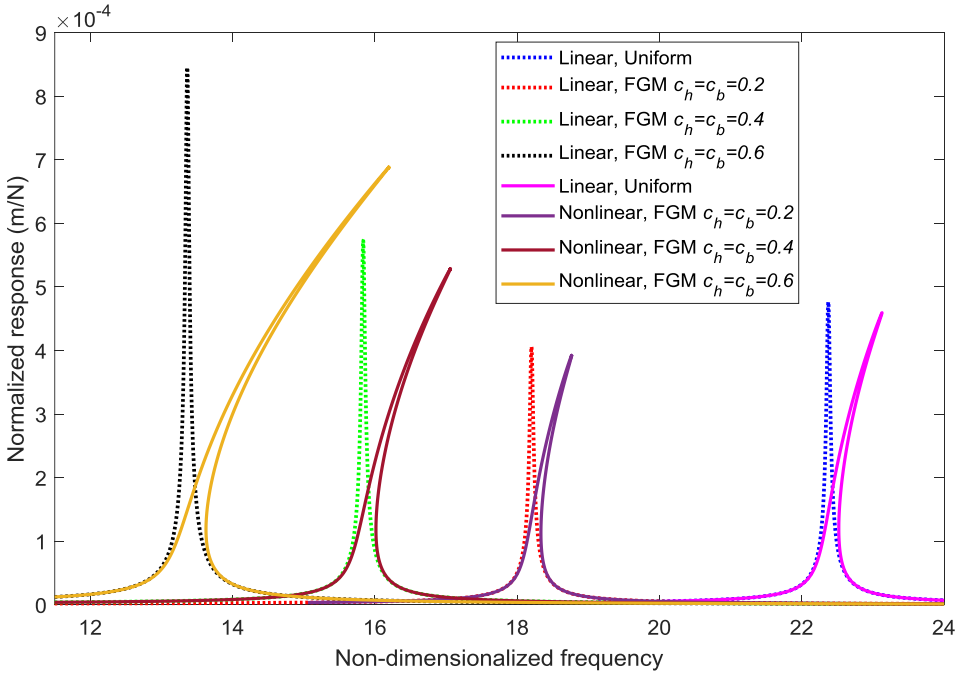

Figure 4.21. Force normalized, first harmonic linear/nonlinear responses of uniform and FG beams with 7 polynomials and fixed-fixed BCs (*f*=40N)

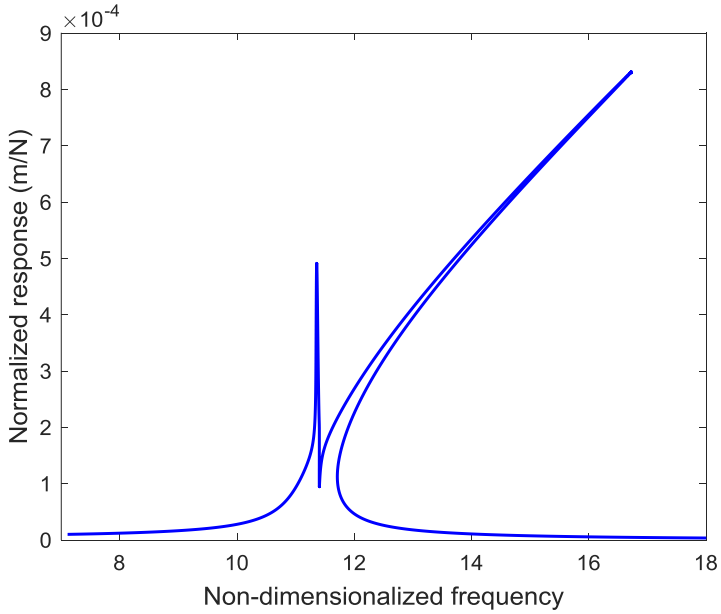

Figure 4.22. Force normalized, first harmonic nonlinear response of non-uniform beam(c_h=c_b=*0.8*) with 7 polynomials and fixed-fixed boundary conditions (f=15N)

In the Figure 4.22, it seems that there occurs an unexpected result that can not be explained with modal coupling. This happens due to the substantial variation of parameters along the beam length. In Figure D.2, it can be observed that values of c_h=c_b=*0.8* create a drastic change in the material properties along beam length. Although seven polynomials are sufficient to obtain the precise frequency response, it is not enough to discretize the beam. Due to one-to-one mapping of SCT, the beam is discretized into the number of points equal to the number of polynomials. However, it is found that the small number of discretization points is not useful for obtaining the response of the beams that have a highly-varied distribution of material properties. Therefore the same case is solved by using eleven polynomials, and the results are given in Figure 4.23.

Significant differences between the two plots are observed. The form of the curve is corrected, and the response appears to be smaller when a higher number of polynomials are considered. Additionally, the case is solved with 15 polynomials and found that the response is very close to the one with 11 polynomials, which

generated a convergence. It is concluded that, even though a specific number of polynomials are enough to obtain the first natural frequency precisely, it may not yield the correct frequency responses depending on the material property variation.

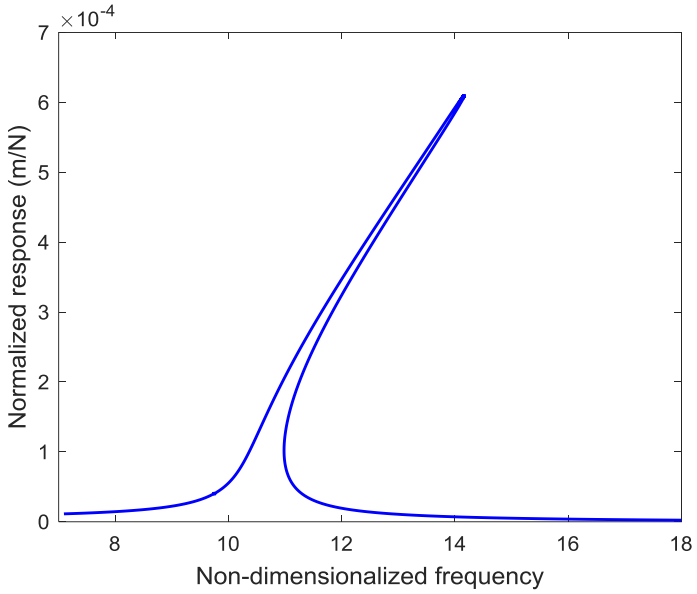

Figure 4.23. Force normalized, first harmonic nonlinear response of non-uniform beam(c_h=c_b=*0.8*) with 11 polynomials and fixed-fixed boundary conditions (*f*=15N)

CHAPTER 5

NONLINEAR VIBRATIONS OF FUNCTIONALLY GRADED BEAMS WITH SCT

5.1 Mathematical Model

The rotating axially FG beam geometry is depicted in Figure 5.1. Schematic of the rotating FG(axially) beam with coordinate systems. The beam is mounted to a rigid hub of radius r_h, which is rotating about its axis with constant velocity Ω. The beam has length L, thickness h_t, width h_w, and is assumed to be under an external harmonic force per unit length, f. Four Cartesian coordinate systems are considered to formulate the problem. The first is the fixed inertial coordinate system, O_1XYZ, the Z axis, which coincides with the rotation axis. Second is the rotating coordinate system, O_Rxyz, where O_R is placed at the root of the beam, and the z axis is parallel to the rotation axis. The third and fourth are local coordinate systems $O_Ux_1y_1z_1$ and $O_Dx_2y_2z_2$, which are located at the undeformed and deformed beam cross-section, respectively.

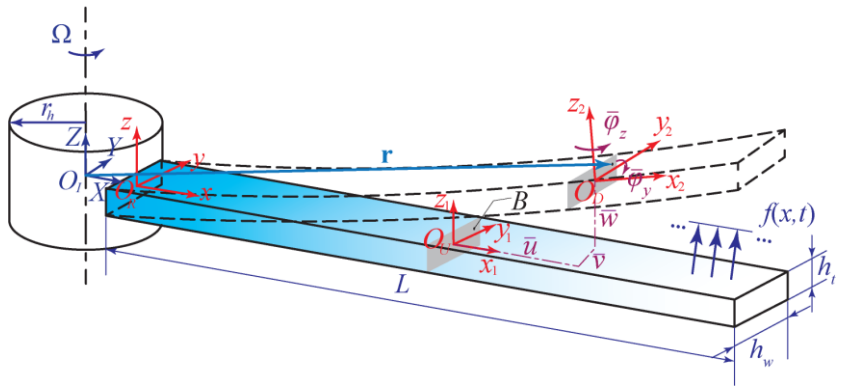

Figure 5.1. Schematic of the rotating FG(axially) beam with coordinate systems

The beam considered in this research is an axially FGM, and the material properties are functions of volume fractions of the constituents that are changing continuously

along the beam length. The effective material property, P, is calculated by the rule of mixtures, where P_A and P_B denote the material properties of the matrix, with A and B inclusions.

$$P = P_A V_A + P_B V_B \tag{5.1}$$

V_A and V_B are the corresponding volume fractions of the constituents, satisfying $V_A + V_B = 1$ at each cross-section. In this study, V_B is considered as a four-parameter variation profile given by

$$V_B = \left[1 - a(\frac{x}{l}) + b(\frac{x}{l})^c\right]^p \tag{5.2}$$

With this formulation, by changing the parameters a, b, c, and the volume fraction index $p(0 \leq p \leq \infty)$, it is possible to construct symmetric/asymmetric volume fraction distributions along the beam. Note that for p is zero or p goes to infinity, one can obtain homogeneous isotropic material as a special case of the FGM [82].

5.1.1 Strain-Displacement and Kinematic Relations

According to Figure 5.1, deformations of a generic point on the mid-plane of the beam along x_1, y_1, and z_1 axes, are denoted, respectively, by $\bar{u}$, $\bar{v}$, and $\bar{w}$, which sequentially represent the axial, the chordwise, and the flapwise deformations. Moreover, the bending rotations along y_2 and z_2 axes are shown by $\bar{\varphi}_y$ and $\bar{\varphi}_z$, respectively. Therefore, based on the first-order shear deformation theory, the position vector of a generic point B on the deformed beam cross-section can be obtained as

$$\mathbf{r} = \{u_1;\ u_2;\ u_3\} = \left\{r_h + x + \bar{u} - y_2\bar{\varphi}_z + z_2\bar{\varphi}_y;\ y_2 + \bar{v};\ z_2 + \bar{w}\right\} \tag{5.3}$$

Where (u_1, u_2, and u_3) is the displacement field of the beam along x, y, and z axes, respectively. According to Green's strain definition, and by supposing a slender geometry for the beam, the following strain-displacement relations are considered

$$\varepsilon_{xx} = u_{1,x} + \frac{1}{2}\left(u_{2,x}{}^2 + u_{3,x}{}^2\right) \tag{5.4}$$

$$\gamma_{xy} = u_{1,y} + u_{2,x} \tag{5.5}$$

$$\gamma_{xz} = u_{1,z} + u_{3,x} \tag{5.6}$$

Here, $u_{i,j}$ shows the derivation of u_i with respect to j.

To include the stiffening effects and the time-dependent axial, centrifugal force in the rotating beam, the SSEDs must be considered in the model [75]. The beam's deformations are considered a sum of the SSEDs, $\mathbf{q}_s$, and the disturbing deformations about the equilibrium position, **q,** in the following form.

$$\bar{\mathbf{q}} = \mathbf{q} + \mathbf{q}_s \tag{5.7}$$

$$\mathbf{q} = \left\{u;\ v;\ w;\ \varphi_y;\ \varphi_z\right\} \tag{5.8}$$

$$\mathbf{q}_s = \left\{u_s;\ v_s;\ w_s;\ \varphi_{y_s};\ \varphi_{z_s}\right\} \tag{5.9}$$

By using Eqs. 5.3-5.9, the strain in the beam is expressed as

$$\varepsilon = \mathbf{B}_{yz}\mathbf{q} + \mathbf{b}_{yz} + \sum_{i=1}^{2}\left[(\mathbf{B}_i^{nl}\mathbf{q}) \square (\mathbf{B}_i^{nl}\mathbf{q})\right] \tag{5.10}$$

Where $\mathbf{B}_{yz}$ is the differential operator matrix of the linear strains, $\mathbf{b}_{yz}$ is a vector resulting from steady-state equilibrium deformation terms, $\mathbf{B}_i^{nl}$'s are differential operator matrices of the nonlinear strains, and "$\square$" represents the element-wise multiplication. The details of the matrices and the vector in Eq. 5.10 are given in Appendix B.

To formulate the kinematics of deformations, the velocity of a generic point on the rotating beam is calculated by

$$\mathbf{v}_p = \dot{\mathbf{r}} + \boldsymbol{\Omega} \times \mathbf{r} \tag{5.11}$$

where Ω is expressed as below, and over-dot denotes derivation with respect to time. Similar to the strain in the beam, the velocity is given by Eq. 5.11, can be rewritten as

$$\mathbf{\Omega}_s = \{0;\ 0;\ \Omega\} \tag{5.12}$$

$$\mathbf{v}_p = \Lambda_{\mathrm{yz}_1}\dot{\mathbf{q}} + \Lambda_{\mathrm{yz}_2}(\mathbf{q}+\mathbf{q}_s)\times\mathbf{v}_{\mathrm{yz}} \tag{5.13}$$

The operator matrices Λ_{yz_i}'s, and the vector $\mathbf{v}_{\mathrm{yz}}$ are given in Appendix B.

5.1.2 Integral Boundary Value Problem

The IBVP governing the dynamics of the system can be derived using the extended Hamilton's principle. For this purpose, the variations of the kinetic energy is expressed as

$$\delta U_k = \int_0^L \int_A \rho(x)\delta\mathbf{v}_p^{\mathrm{T}}\mathbf{v}_p \mathrm{d}A\mathrm{d}x \tag{5.14}$$

where δ, ρ, and A are the variational parameter, mass density, and the cross-sectional area, respectively. According to the constitutive relation, the stress in the beam can be expressed as $\boldsymbol{\sigma} = \mathbf{C}\boldsymbol{\varepsilon}$, where $\mathbf{C}$ is the constitutive matrix defined as

$$\mathbf{C} = \begin{bmatrix} E(x) & 0 & 0 \\ 0 & G(x) & 0 \\ 0 & 0 & G(x) \end{bmatrix} \tag{5.15}$$

Here, E and G are Young's and shear modulus, respectively. Therefore, the variations of the elastic strain energy can be expressed as

$$\delta U_s = \int_0^L \int_A \delta\boldsymbol{\varepsilon}^{\mathrm{T}}\mathbf{C}^{\mathrm{T}}\boldsymbol{\varepsilon}\mathrm{d}A\mathrm{d}x \tag{5.16}$$

Moreover, by assuming the external force as $f = f_0 \sin(wt)$, variations of the work done by this (non-conservative) force can be defined by

$$\delta W_{nc} = \int_0^L \delta\mathbf{q}^{\mathrm{T}}\hat{\mathbf{f}}\mathrm{d}x \tag{5.17}$$

where forcing vector can be expressed as.

$$\hat{\mathbf{f}} = \{0;\ 0;\ f;\ 0;\ 0\} \tag{5.18}$$

Once the variations of the kinetic and elastic strain energies, and work done by the external force are calculated, by using Eqs. 5.10 and 5.13-5.18, the nonlinear IBVP, which models the problem based on weak-form governing equations, can be obtained as

$$\int_{t_1}^{t_2}\int_0^L \left\{ \begin{array}{l} \delta\mathbf{q}^{\mathrm{T}}\rho\left[\boldsymbol{\Lambda}_1^{\mathrm{T}}\boldsymbol{\Lambda}_2\ddot{\mathbf{q}} + (\boldsymbol{\Lambda}_1^{\mathrm{T}}\boldsymbol{\Lambda}_2 - \boldsymbol{\Lambda}_2^{\mathrm{T}}\boldsymbol{\Lambda}_1)\dot{\mathbf{q}} - \boldsymbol{\Lambda}_2^{\mathrm{T}}\boldsymbol{\Lambda}_2(\mathbf{q}+\mathbf{q}_s) - \boldsymbol{\Lambda}_2^{\mathrm{T}}\mathbf{v}\right] \\ +\delta\mathbf{q}^{\mathrm{T}}\left\{\mathbf{B}^{\mathrm{T}}\mathbf{C}^{\mathrm{T}}\mathbf{B}\mathbf{q} + \mathbf{B}^{\mathrm{T}}\mathbf{C}^{\mathrm{T}}\mathbf{b} + \mathbf{B}^{\mathrm{T}}\mathbf{C}^{\mathrm{T}}\sum_{i=1}^{2}\left[(\mathbf{B}_i^{nl}\mathbf{q})\circ(\mathbf{B}_i^{nl}\mathbf{q})\right]\right. \\ \left. +2\sum_{i=1}^{2}\mathbf{B}_i^{nl^{\mathrm{T}}}\left[(\mathbf{B}_i^{nl}\mathbf{q})\circ\left(\begin{array}{l}\mathbf{C}^{\mathrm{T}}\mathbf{B}\mathbf{q}+\mathbf{C}^{\mathrm{T}}\mathbf{b} \\ +A\mathbf{C}^{\mathrm{T}}\sum_{i=1}^{2}\left[(\mathbf{B}_j^{nl}\mathbf{q})\circ(\mathbf{B}_j^{nl}\mathbf{q})\right]\end{array}\right)\right] - \hat{\mathbf{f}}\right\} \end{array} \right\} \mathrm{d}x\mathrm{d}t = 0 \tag{5.19}$$

Where

$$\begin{aligned} \{\boldsymbol{\Lambda}_i^{\mathrm{T}}\boldsymbol{\Lambda}_i, \boldsymbol{\Lambda}_i^{\mathrm{T}}\boldsymbol{\Lambda}_j, \boldsymbol{\Lambda}_2^{\mathrm{T}}\mathbf{v}, \mathbf{B}^{\mathrm{T}}\mathbf{C}^{\mathrm{T}}\mathbf{B}, \mathbf{B}^{\mathrm{T}}\mathbf{C}^{\mathrm{T}}\mathbf{b}, \mathbf{B}, \mathbf{b}\} = \int_A \{&\boldsymbol{\Lambda}_{\mathrm{yz}_i}^{\mathrm{T}}\boldsymbol{\Lambda}_{\mathrm{yz}_i}, \\ &\boldsymbol{\Lambda}_{\mathrm{yz}_i}^{\mathrm{T}}\boldsymbol{\Lambda}_{\mathrm{yz}_j}, \boldsymbol{\Lambda}_{\mathrm{yz}_2}^{\mathrm{T}}\mathbf{v}_{\mathrm{yz}}, \mathbf{B}_{\mathrm{yz}}^{\mathrm{T}}\mathbf{C}^{\mathrm{T}}\mathbf{B}_{\mathrm{yz}}, \mathbf{B}_{\mathrm{yz}}^{\mathrm{T}}\mathbf{C}^{\mathrm{T}}\mathbf{b}_{\mathrm{yz}}, \mathbf{B}_{\mathrm{yz}}, \mathbf{b}_{\mathrm{yz}}\}\mathrm{d}A, \quad i, j = 1, 2 \end{aligned} \tag{5.20}$$

The discretization of the IBVP given by Eq. 5.19 via the spectral Chebyshev method is discussed in the next subsection. Accordingly, after applying the differential operators and integration over x domain, coefficients of the terms $\ddot{\mathbf{q}}$, $\dot{\mathbf{q}}$ and $\mathbf{q}$ respectively, contribute to the mass, Gyroscopic, and stiffness matrices. Moreover, the term $\rho\boldsymbol{\Lambda}_2^{\mathrm{T}}\mathbf{v}$ and those including $\mathbf{q}\circ\mathbf{q}$, and $\mathbf{q}\circ\mathbf{q}\circ\mathbf{q}$ sequentially, contribute to the steady-state equilibrium forcing, nonlinear quadratic forcing, and cubic nonlinear forcing functions. In addition, the stiffening effect is modeled by terms $(\mathbf{B}_i^{nl}\mathbf{q})\circ(\mathbf{C}^{\mathrm{T}}\mathbf{b})$'s. These terms are linear; however, they originate from nonlinear strains in the beam. It is also noteworthy that the following properties of the element-wise multiplication are used to obtain Eq. 5.19.

$$\mathbf{a}_1\circ(\mathbf{a}_2+\mathbf{a}_3) = \mathbf{a}_1\circ\mathbf{a}_2 + \mathbf{a}_1\circ\mathbf{a}_3 \tag{5.21}$$

$$(\mathbf{a}_1^{\mathrm{T}}\circ\mathbf{a}_2^{\mathrm{T}})\mathbf{a}_3 = \mathbf{a}_1^{\mathrm{T}}(\mathbf{a}_2\circ\mathbf{a}_3) \tag{5.22}$$

$$\mathbf{a}_1 \times \mathbf{a}_2 = \mathbf{a}_2 \times \mathbf{a}_1 \tag{5.23}$$

here $\mathbf{a}_i$'s are vectors of the same size.

5.1.3 The Spectral Chebyshev Technique for Nonlinear IBVP

The scaled Chebyshev polynomials of the first kind are used to discretize the IBVP given by Eq. 5.19. As discussed in Chapter 3.3, these recursive polynomials are orthogonal, exponentially convergent, and construct a complete set on the interval [-1,1]; thus, the spatial domain x is mapped to $\varepsilon \in [-1,1]$. Accordingly, each deformation q_i in the model, $(q_1 = u, q_2 = v, ...)$, needs to be presented with a Chebyshev series expansion as [13]

$$q_i = \sum_{k=1}^{N} a_{i_{k-1}} C_{k-1}(\xi) \tag{5.24}$$

Here C_{k-1}'s are the Chebyshev polynomials, and a_i's are the coefficients of the expansion, and N is the number of Gauss-Lobatto sampling points. Forward and backward transformation matrices, the derivative, and integral matrices can be defined as it is described in Chapter 3.3. Based on weighted inner product definition, definite integral of functions $\mathbf{g}_1$ and $\mathbf{g}_2$ can be expanded by Chebyshev polynomials,

$$\int_{\xi} r(\xi) g_1(\xi) g_2(\xi) \mathrm{d}\xi = \mathbf{g}_1^{\mathrm{T}} \mathbf{V}_r \mathbf{g}_2 \tag{5.25}$$

In which $\mathbf{V}_r$ is the weighted inner product matrix and r is the weighting function. $\mathbf{g}_1$ and $\mathbf{g}_2$ are vectors of the functions whose values are calculated in the sampled domain. After discretizing the IBVP given by Eq. 5.19, performing derivative and integral operations, and ignoring the nonlinear terms in the SSEDs, the equations of steady-state equilibrium condition, and the governing equations of motion about the equilibrium state for an unconstrained rotating beam are obtained as:

$$\mathbf{K}_s \mathbf{q}_s + \mathbf{f}_s = 0 \tag{5.26}$$

$$\mathbf{M}\ddot{\mathbf{q}} + \mathbf{G}\dot{\mathbf{q}} + (\mathbf{K}_0 + \mathbf{K}_s + \mathbf{K}_d)\mathbf{q} + \mathbf{f}_q^{nl}(\mathbf{q}) + \mathbf{f}_c^{nl}(\mathbf{q}) = \mathbf{f} \tag{5.27}$$

In Eq. 5.26, $\mathbf{K}_s$ the steady-state equilibrium stiffness matrix and force vector are, respectively. In Eq. 5.27, **M** is the mass matrix, **G** is the Gyroscopic matrix, $\mathbf{K}_0$ is the stiffness matrix of the non-rotating beam, $\mathbf{K}_d$ models the stiffening/softening effects, and **f** is the generalized external force vector, respectively. Moreover, $\mathbf{f}_q^{nl}$ and $\mathbf{f}_c^{nl}$ are sequentially internal quadratic nonlinear forcing and internal cubic nonlinear forcing functions, given by

$$\mathbf{f}_q^{nl}(\mathbf{q}) = \mathbf{N}_1(\mathbf{N}_2\mathbf{q}\,\mathbf{N}_2\mathbf{q} + \mathbf{N}_3\mathbf{q}\,\mathbf{N}_3\mathbf{q}) + 2\mathbf{N}_2^{\mathrm{T}}(\mathbf{N}_1^{\mathrm{T}}\mathbf{q}\,\mathbf{N}_2\mathbf{q}) + 2\mathbf{N}_3^{\mathrm{T}}(\mathbf{N}_1^{\mathrm{T}}\mathbf{q}\,\mathbf{N}_3\mathbf{q}) \tag{5.28}$$

$$\begin{aligned}\mathbf{f}_q^{nl}(\mathbf{q}) = {} & 2\mathbf{N}_2^{\mathrm{T}}(\mathbf{N}_4(\mathbf{N}_2\mathbf{q}\,\mathbf{N}_2\mathbf{q} + \mathbf{N}_3\mathbf{q}\,\mathbf{N}_3\mathbf{q})\,\mathbf{N}_2\mathbf{q}) \\ & + 2\mathbf{N}_3^{\mathrm{T}}(\mathbf{N}_4(\mathbf{N}_2\mathbf{q}\,\mathbf{N}_2\mathbf{q} + \mathbf{N}_3\mathbf{q}\,\mathbf{N}_3\mathbf{q})\,\mathbf{N}_3\mathbf{q})\end{aligned} \tag{5.29}$$

Where $\mathbf{N}_i$'s, the matrices and vectors in Eqs. 5.26-5.27 are given in Appendix C.

Like in the non-rotating beam case, basis recombination with projection matrices are used to impose the essential boundary conditions such as

$$\mathbf{q} = \mathbf{P}\hat{\mathbf{q}} \tag{5.30}$$

It is worth noting that the same boundary conditions are applied to the SSEDs, $\mathbf{q}_s$, and one can define $\mathbf{q}_s = \mathbf{P}\hat{\mathbf{q}}_s$. Accordingly, by using these transformations and pre-multiplying each term in Eqs. 5.26-5.27 by $\mathbf{P}^{\mathrm{T}}$, the governing equations of rotating an FG beam are obtained as

$$\bar{\mathbf{K}}_s\hat{\mathbf{q}}_s + \bar{\mathbf{f}}_s = 0 \tag{5.31}$$

$$\bar{\mathbf{M}}\ddot{\mathbf{q}} + (\bar{\mathbf{G}} + \bar{\mathbf{C}})\dot{\mathbf{q}} + (\bar{\mathbf{K}})\mathbf{q} + \bar{\mathbf{f}}_q^{nl}(\mathbf{q}) + \bar{\mathbf{f}}_c^{nl}(\mathbf{q}) = \bar{\mathbf{f}} \tag{5.32}$$

The damping effect is added to the model by inserting $\bar{\mathbf{C}}$ as a damping matrix proportional to the mass matrix with coefficient λ. The global matrices and vectors written above are defined as

$$\begin{aligned}&\bar{\mathbf{K}}_s = \mathbf{P}^{\mathrm{T}}\mathbf{K}_s\mathbf{P}, \quad \bar{\mathbf{f}} = \mathbf{P}^{\mathrm{T}}\mathbf{f}_s, \quad \bar{\mathbf{M}} = \mathbf{P}^{\mathrm{T}}\mathbf{M}\mathbf{P}, \\ &\bar{\mathbf{G}} = \mathbf{P}^{\mathrm{T}}\mathbf{G}\mathbf{P}, \quad \bar{\mathbf{K}} = \mathbf{P}^{\mathrm{T}}(\mathbf{K}_0 + \mathbf{K}_s + \mathbf{K}_d)\mathbf{P}, \\ &\bar{\mathbf{f}}_q^{nl} = \mathbf{P}^{\mathrm{T}}\mathbf{f}_q^{nl}(\mathbf{P}\hat{\mathbf{q}}), \ \bar{\mathbf{f}}_c^{nl} = \mathbf{P}^{\mathrm{T}}\mathbf{f}_c^{nl}(\mathbf{P}\hat{\mathbf{q}}), \quad \bar{\mathbf{f}} = \mathbf{P}^{\mathrm{T}}\mathbf{f}\end{aligned} \tag{5.33}$$

After solving the nonlinear algebraic equations given by Eq. 5.31 and obtaining the deformations $\hat{\mathbf{q}}_s$, one can investigate the nonlinear dynamics of the beam about the determined equilibrium condition via solving Eq. 5.32.

To solve the nonlinear equation of motion (given in Eq. 5.32) in the frequency domain, HBM is implemented. Displacement vector and nonlinear forces can be expressed in the form.

$$\hat{\mathbf{q}} = \mathbf{q}_0 + \sum_{k=1}^{H} \mathbf{q}_k^s \sin(k\theta) + \mathbf{q}_k^c \cos(k\theta), \qquad \theta = wt \tag{5.34}$$

where $\mathbf{q}_k^s$, and $\mathbf{q}_k^c$ are coefficient vectors and $\mathbf{q}_0$ is the bias vector representing the streaming/drifting caused by the quadratic nonlinearity, and H is the number of harmonics used in the solution. Similarly, the external force vector can be expressed as

$$\bar{\mathbf{f}} = \mathbf{f}_0 + \sum_{k=1}^{H} \mathbf{f}_k^s \sin(k\theta) + \mathbf{f}_k^c \cos(k\theta), \qquad \theta = wt \tag{5.35}$$

Fourier equations can be employed after placing the expressed forms into the equation of motion (Eqs. 3.12-3.14) to find the equivalent unknown coefficients resulting from HBM.

Based on the equality of trigonometric and bias terms, $2H+1$ number of nonlinear algebraic equations emerge for each degree of freedom. Those nonlinear algebraic equations can be solved by Newton's method with arc-length continuation.

5.2 Results and Discussion

This section investigates the nonlinear dynamic behavior of the rotating axially FG beam based on the developed model via several numerical examples. For more general results, the following dimensionless parameters are introduced.

$$\delta = \frac{r_h}{L}, \quad \alpha = \sqrt{\frac{AL^2}{I_z}}, \quad \zeta = T\lambda, \quad \hat{w}_n = Tw_n$$
$$\hat{\Omega} = T\Omega, \quad \hat{w} = Tw, \quad \gamma = \frac{f_0 L^3}{E_B I_z} \tag{5.36}$$

where δ, α, ζ, $\hat{w}_n$, $\hat{\Omega}$, $\hat{w}$ and γ denote hub radius ratio, slenderness ratio, damping ratio, n^{th} dimensionless natural frequency, dimensionless rotating speed, dimensionless excitation frequency, and dimensionless external force, respectively. Moreover, T is defined as

$$T = L^2 \sqrt{\frac{\rho_B A}{E_B I_z}} \tag{5.37}$$

The slenderness ratio, α, defines the geometrical property of the beam. It should also be mentioned that the beam's cross-section is considered square, *i.e.* $I_z = I_y$. The matrix and inclusions of the FGM are considered as aluminum (metal) and zirconia (ceramic), with $\rho_A = \rho_m = 2707$ kg\m^3, $E_A = E_m = 70$ GPa, $\rho_B = \rho_c = 5700$ kg\m^3, $E_B = E_c = 168$ GPa where subscripts m and c stand for metal and ceramic, respectively. Poisson's ratios are $v_A = v_m = 0.3$, and shear modulus is calculated by

$$G = E / 2(1+v) \tag{5.38}$$

In the study, two material property distributions are selected, which are given in Table 5.1. Those material variation profiles for parameters *a*,*b*,*c* and ρ are provided in Appendix D.

Table 5.1. Material property distributions of FG beams studied

	a	*b*	*c*	ρ
FGM A	1.5	0.8	2	1
FGM B	1.8	1.6	5	0.4

5.2.1 Convergence Analyses and Model Validation

A convergence analysis is performed similarly to the one in Chapter 4 in order to determine the required number of polynomials in solving the rotating beam natural frequencies with the spectral Chebyshev technique. Accordingly, to perform the convergence analysis N_ξ is gradually increased, and the predicted natural frequencies are compared to reference values calculated by a large value of N_ξ. To measure the level of convergence quantitatively, a relative logarithmic assessment given in Eq. 4.30 is carried out.

Convergence results are shown in Figure 5.2 for two sets of FGM distribution parameters as functions of dimensionless rotating speed. The *LCV* values are obtained based on the convergence of the first five natural frequencies of the rotating axially FG beam, *i.e. M*=5, and for the reference case, $N_{\xi_{ref}} = 20$ is assumed. Each colored contour represents a level of *LCV*, and the integer values of the *LCV* are provided on each contour. According to this figure, by considering the maximum convergence error to be 1% ($\varepsilon = -2$), the number of polynomials should be more than seven, as shown with horizontal lines. Accordingly, the discretization of the problem $N_\xi = 7$ is considered. Based on first-order shear deformation theory, the beam has five degrees of freedom at a point.

The proposed model based on IBVP formulation is validated by comparing the natural frequencies to those obtained by the FE modeling of the rotating blade in commercial software. The details regarding the model developed in this software are summarized in Table 5.2. The results of comparing the first four dimensionless natural frequencies for two different FGM parameter distributions are given in Table 5.3 and. The relative difference between the results is also given in these tables. It is observed that there is an excellent agreement between the presented results.

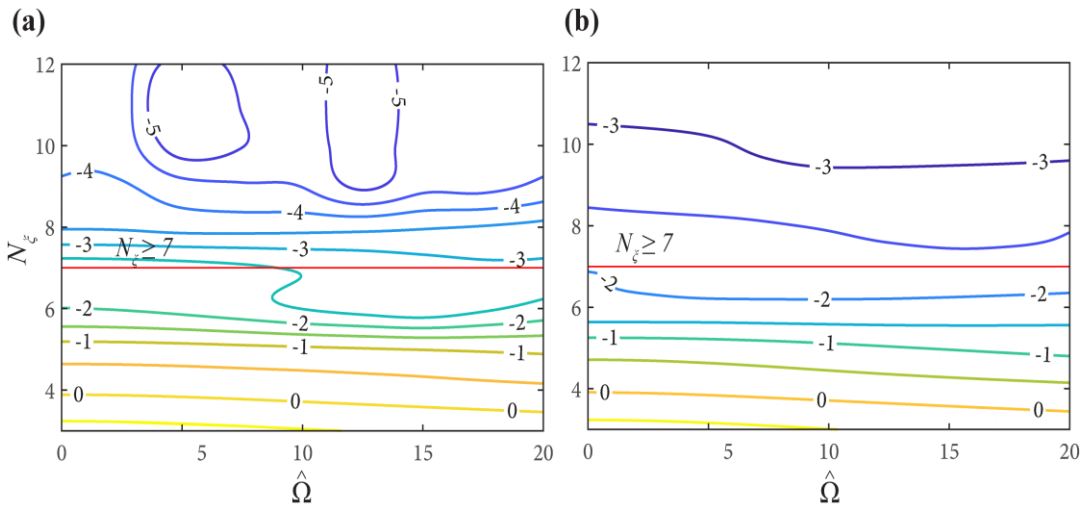

Figure 5.2. Convergence plots for dimensionless natural frequencies based on SCT as a function of dimensionless rotating speed for $\delta = 0,\ \alpha = 150$ and **a)**FGM A **b)**FGM B

Table 5.2. Details of the FE modeling

Software	COMSOL Multiphysics v5.6
Physics Type	3D solid mechanics under rotating frame volume forces
Study Type	Pre-stressed eigenfrequency analysis
Element Type	Tetrahedral
Number of elements	892
Number of DOFs	5595

Table 5.3. The comparison of dimensionless natural frequencies of the rotating FG beam, with the FE model $\delta = 0.1,\ \alpha = 150$ FGM A.

$\hat{\Omega} = 2$	**Mode**	**Present Model**	**FE Model**	**Relative difference (%)**
0	1	4.0216	4.0289	0.18
	2	4.0216	4.0289	0.18
	3	22.5376	22.5736	0.16

Table 5.3. (cont'd)

	4	22.5376	22.5736	0.16
5	1	5.0066	5.0193	0.25
	2	7.0779	7.0865	0.12
	3	25.5825	25.6222	0.15
	4	26.0691	26.1072	0.14
10	1	6.8743	6.9082	0.49
	2	12.1457	12.1642	0.16
	3	33.0580	33.1101	0.16
	4	34.5499	34.5974	0.14
15	1	8.8694	8.9513	0.91
	2	17.4553	17.4962	0.23
	3	42.6189	42.7093	0.21
	4	45.2176	45.2982	0.18

Table 5.4. The comparison of dimensionless natural frequencies of the rotating FG beam, with the FE model $\delta = 0.1,\ \alpha = 150$ FGM B.

$\hat{\Omega} = 2$	**Mode**	**Present Model**	**FE Model**	**Relative difference (%)**
0	1	3.8208	3.8162	0.12
	2	3.8208	3.8162	0.12
	3	21.3601	21.3094	0.24
	4	21.3601	21.3094	0.24
5	1	4.8253	4.8281	0.06
	2	6.9509	6.9523	0.02
	3	24.6624	24.7138	0.21
	4	25.1667	25.2161	0.20
10	1	6.6770	6.6891	0.18
	2	12.0352	12.0411	0.05

Table 5.4. (cont'd)

	3	32.6026	32.8498	0.75
	4	34.1151	34.4887	1.08
15	1	8.6374	8.6573	0.23
	2	17.3390	17.3478	0.05
	3	42.5911	43.0581	1.08
	4	45.1947	45.6303	0.61

For the case of the HBM, the harmonic truncation order, *H*, plays an important role in the accuracy and quality of the vibration response. For example, low values of *H* may omit the higher-order relevant components that significantly influence the response of the system. On the other hand, assuming high values for this parameter will increase the computational cost. Therefore, a convergence analysis is performed to determine a suitable value for *H*. Since the acceleration response is more affected by the contribution of higher harmonics, the acceleration responses of the axial, chordwise, and flapwise motions at the tip of the rotating beam generated by a high value of *H* are considered as the reference values to perform the convergence study. Accordingly, *H* is gradually increased, and the relative error of prediction with respect to the reference value, calculated by $H_{ref} = 10$, is considered as a quantitative criterion to assess the level of convergence.

The convergence errors are determined by calculating the maximum relative differences between the acceleration responses in a half-period time range at the nonlinear resonance frequency. Accordingly, in Table 5.5 the relative errors of prediction are reported for the axial, e_a, chordwise e_c, and flapwise e_f motions. Similar to the SCT convergence error, the maximum error is considered to be 1%, thus, $H = 2$ is assumed for the HBM. In this regard, for the 30 degrees-of-freedom rotating beam, 150 equations are solved to obtain the nonlinear frequency response of the system.

Table 5.5. Convergence results for HBM based on relative errors of acceleration prediction with respect to the reference case with H_{ref} =10 at the nonlinear frequency for $\delta = 0.1,\ \alpha = 150,\ \zeta = 0.005,\ \hat{\Omega} = 5,\ \gamma = 0.002$ and FGM A.

	H				
	1	2	3	4	5
e_{a} %	12.1754	0.6151	0.2841	0.0077	0.0080
e_{c} %	7.0015	0.5278	0.2657	0.0068	0.0099
e_{f} %	19.8558	0.7013	0.3169	0.0031	0.0122

5.2.2 Frequency Responses of Nonlinear Model

In the upcoming cases, the system is considered to be under a transverse force per unit length of the beam. The deflection at the tip of the beam is obtained, and the related frequency responses are plotted. The displacement at the tip is normalized by the beam thickness, and the frequencies are normalized around the first flapwise natural frequency of the system, meaning that the excitation frequency is close to the second natural frequency. The obtained responses include the zeroth harmonic, $\mathbf{q}_0$, and the first and second harmonics response of which is calculated as

$$\mathbf{q}_k = \sqrt{\mathbf{q}_k^{s2} + \mathbf{q}_k^{c2}}, \quad k = 1, 2 \tag{5.39}$$

The zeroth and second harmonics have vital importance on the beam's nonlinear behavior since they are directly related to the quadratic nonlinearity. In the case of cubic nonlinearity, the first harmonic plays the main role.

For a non-rotating beam, there occurs a coupling between the axial and flapwise motions, as shown in Figure 5.3, whereas the beam is excited just transversely. In this figure, all the obtained harmonics are provided for the axial, chordwise, and flapwise motions. For the chordwise motion, all the harmonics are zero, representing no coupling effect for this structural mode. However, due to the presence of quadratic

nonlinearity, there is a significant bias term affecting the response of the beam in the axial direction (Figure 5.3a). Therefore, including the bias term in the analysis is quite important to obtain correct results. Additionally, the effect of the second harmonic term in the axial response can be seen in Figure 5.3c. Hence, it is not possible to observe the dynamic coupling of the axial and flapwise motions unless the second harmonic is considered in the analysis. The coupling of structural modes here is due to the large deformation and subsequent axial tensile force in the beam. However, in the case of a rotating FG beam, the coupling occurs among all the structural motions. Figure 5.4 shows the frequency response plot for the beam rotating with the speed of $\hat{\Omega}=1$. In this case, the coupling is due to the large amplitude deflections, as well as time-dependent centrifugal force. Therefore, chordwise motion is also present in the frequency response.

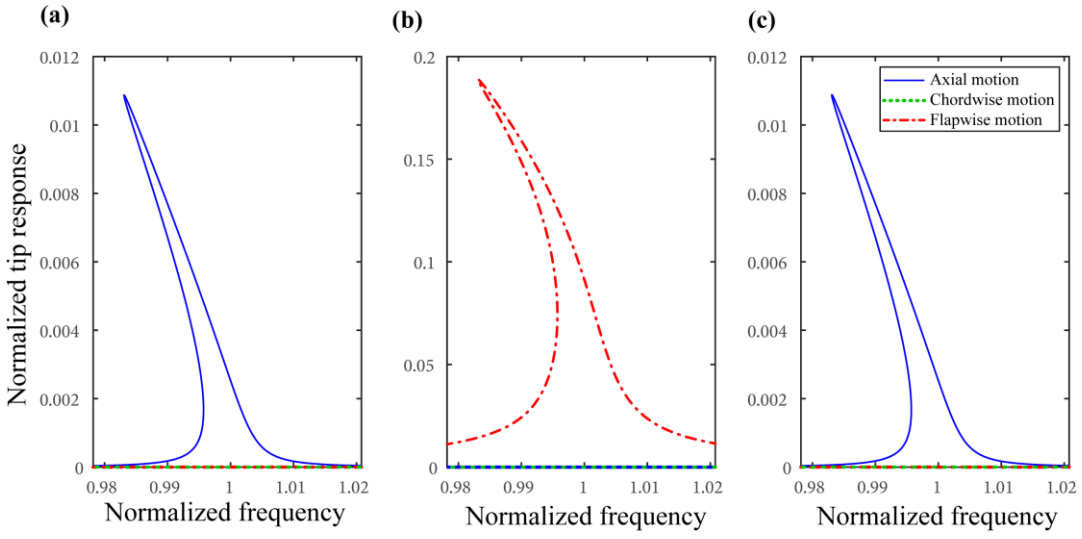

Figure 5.3. Frequency response based on the axial, chordwise, and flapwise tip response of the beam for $\delta=0,\ \alpha=150,\ \zeta=0.01,\ \hat{\Omega}=0,\ \gamma=0.003$, and FGM B, **a)**bias term (zeroth harmonic) **b)**first harmonic **c)**second harmonic

The FGM's parameters can be considered design parameters since they significantly affect the nonlinear behavior of the system. A case study is performed to investigate the effect of volume fraction index on the nonlinear behavior of the rotating FG beam. The frequency response plots are obtained for four different values of the volume fraction in FGM B, and shown in Figure 5.5. For the simplicity, response of

the only first harmonic flapwise motion is given since for the other harmonics and motions, the effect of ρ is similar. It is observed that different volume fractions can result in totally different nonlinear behaviors. Since ρ has a dramatic effect on the frequency response, it can be used as a design parameter to control the nonlinearity in the system.

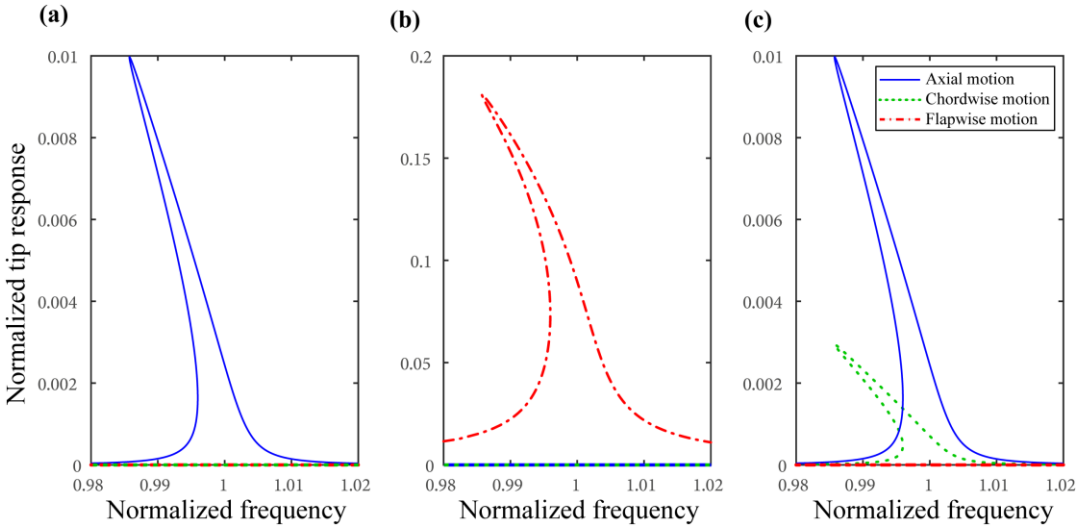

Figure 5.4. Frequency response based on the axial, chordwise, and flapwise tip response of the beam for $\delta = 0$, $\alpha = 150$, $\zeta = 0.01$, $\hat{\Omega} = 1$, $\gamma = 0.003$, and FGM A, **a)**bias term (zeroth harmonic) **b)**first harmonic **c)**second harmonic

To investigate the effect of rotation speed on the frequency response, results are obtained for four different dimensionless rotation speeds. Figure 5.6 to Figure 5.8 depict the nonzero harmonics of the axial, chordwise, and flapwise motions. Results are provided for two different values of the volume fraction index, which induce different effects on the nonlinear response, such as hardening or softening. It is observed that change in the rotation speed directly affects the axial and flapwise motions of the beam. As the rotation speed increases, the deformation of the beam and the nonlinear effect on the response decrease. However, for the chordwise motion, the rotation has not such a one-way effect on the response. As the rotation speed increases, the resonance amplitude in the chordwise direction increases to a maximum value and then decreases as the rotating speed increases. This observation

implies that there exists a rotating speed about $\hat{\Omega} = 2$ that plays a role of critical speed to maximize the chordwise deformation.

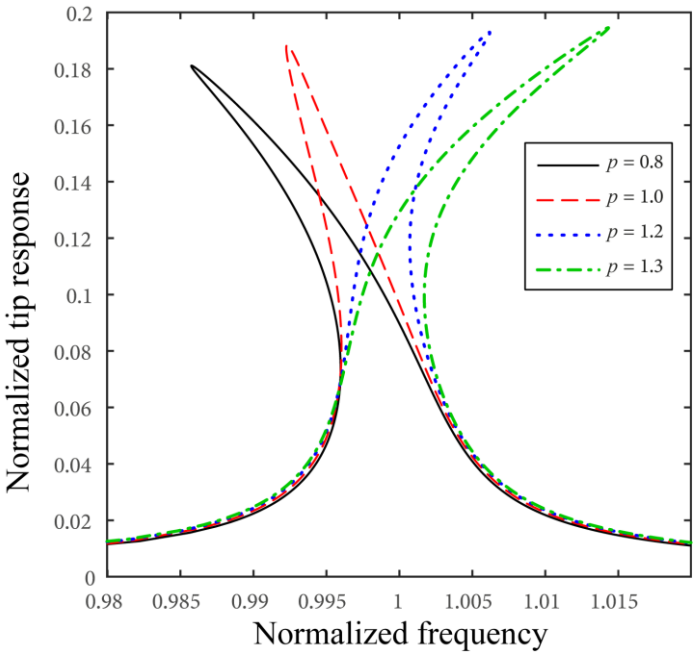

Figure 5.5 Frequency response based on the flapwise tip response of the beam for different values of volume fraction index with $\delta = 0,\ \alpha = 150,$ $\zeta = 0.01,\ \hat{\Omega} = 1,\ \gamma = 0.003$, and FGM B

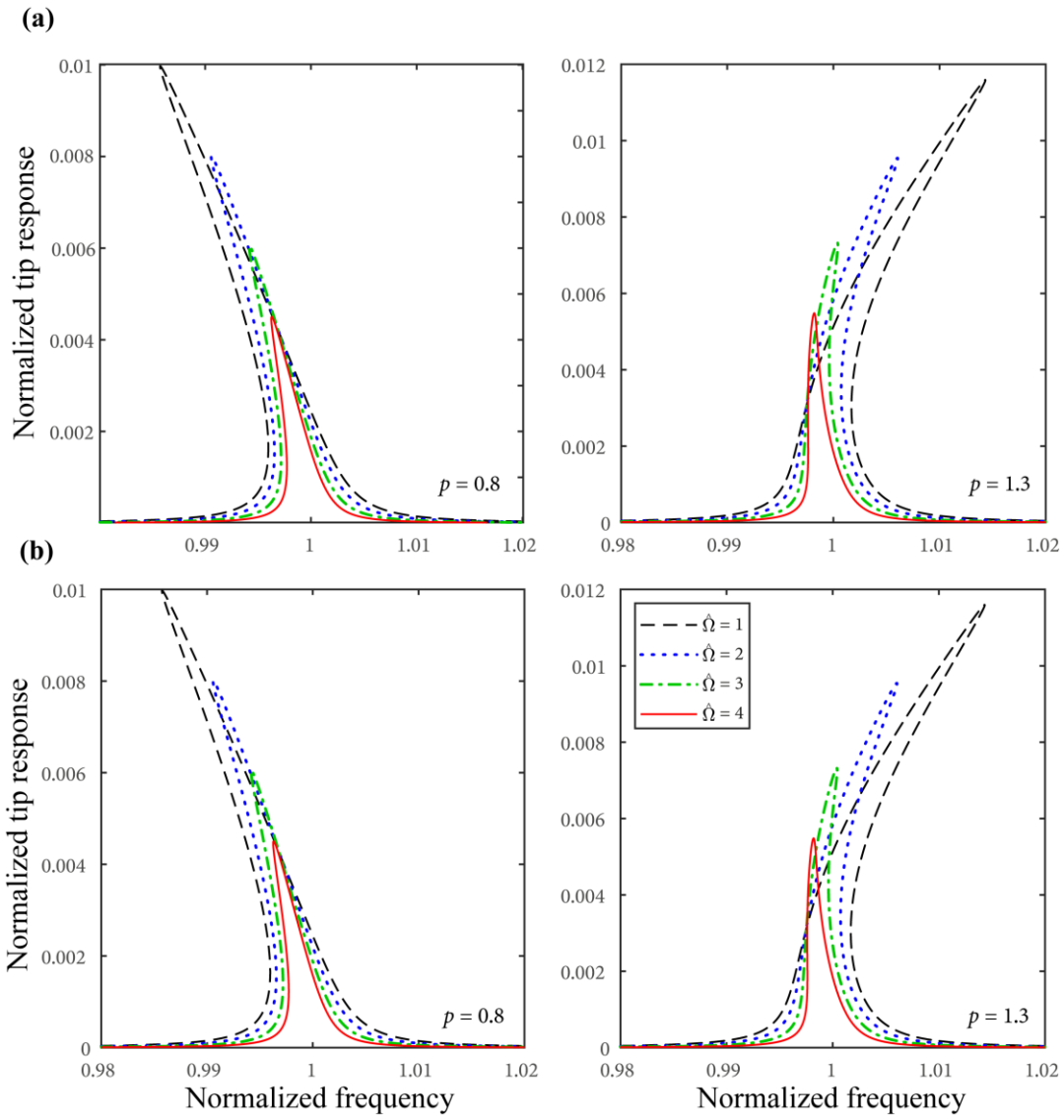

Figure 5.6 Nonzero harmonics of the frequency response based on the azial motion of the beam for different values of rotation speed and volume fraction index with $\delta = 0,\ \alpha = 150,\ \zeta = 0.01,\ \gamma = 0.003$ and FGM B, a)zeroth harmonic, b)second harmonic

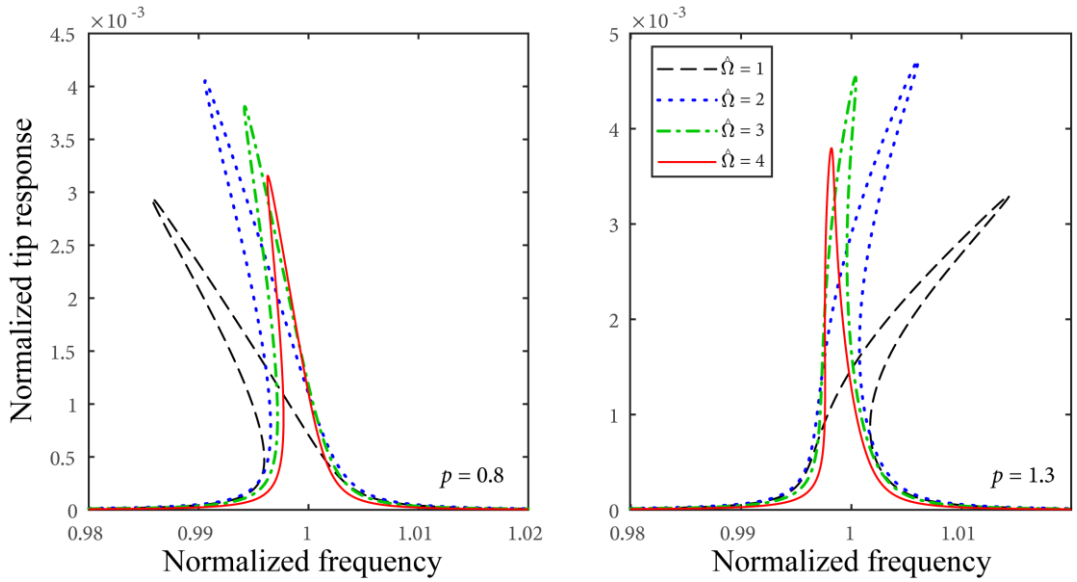

Figure 5.7 Second harmonics of the frequency response based on the chordwise motion of the beam for different values of rotation speed and volume fraction index with $\delta = 0,\ \alpha = 150,\ \zeta = 0.01,\ \gamma = 0.003$ and FGM B

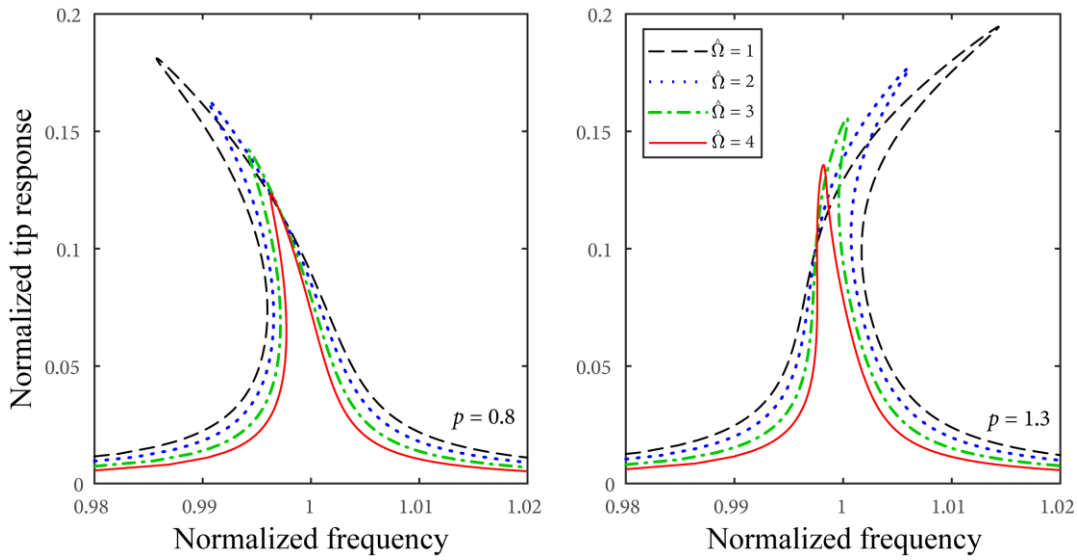

Figure 5.8 First harmonics of the frequenct response based on the flapwise motion of the beam for different values of rotation speed and volume fraction index with $\delta = 0,\ \alpha = 150,\ \zeta = 0.01,\ \gamma = 0.003$ and FGM B

CHAPTER 6

CONCLUSION

6.1 Overview of Results

In this study, nonlinear vibrations of the uniform and composite beam structures are studied. Functionally graded beams are selected as the composite structure type, and large deformation nonlinearity is considered. The spectral Chebyshev Technique is used for discretization and solution of the problem. The harmonic Balance Method with the arch-length continuation of Newton's method is employed to obtain nonlinear frequency responses. Responses consisting of multiple harmonics are considered. Many case scenarios based on the material property distribution, boundary conditions, and excitation levels are performed to observe the effects of nonlinearities. As a result, the main findings are listed as follows:

- The material distribution of FG beams directly affects the natural frequencies, mode shapes, and deformations of the beam; therefore, it can be optimized to control the vibration characteristics of structures in the design process.
- The first and third harmonic responses occur when a non-rotating beam is modeled with large deformation nonlinearity. The nonlinearity creates a hardening effect on the beam(due to the stretching force developed), and the frequency curve shifts towards higher frequencies.
- SCT generates accurate results without the need for a high number of polynomials. However, for studying higher natural frequencies, it is necessary to have more polynomials. Due to material property variations, a rule of thumb for determining required polynomial numbers could not be generated. In such scenarios, a convergence study of the natural frequencies should be performed.

- Depending on the material property distribution, a specific number of Chebyshev polynomials may not be adequate to obtain a precise frequency response, even though it is enough to determine natural frequencies. Due to one-to-one mapping of SCT, the number of polynomials may not generate enough discretization points to model the beam correctly.
- When a rotating beam is considered, bias terms, first harmonic, second harmonic, and third harmonic responses occur. However, the third harmonic response becomes negligible compared to other ones. Bias term and second harmonic response occur due to the nonlinear quadratic force, whereas cubic nonlinear force affects first and third harmonic responses.
- Due to the different types of nonlinear forces, the material property variations can result in hardening or softening behavior depending on FGM variables in the case of rotating beams. These variables can be utilized as design parameters to determine and optimize the structure's vibration characteristics. Additionally, it can be used to identify the points where nonlinear vibration behavior is close to linear behavior.
- The rotation speed of the beam has a significant effect on the nonlinear behavior. Increasing speed results in lower nonlinear effect and vibration responses.

6.2 Future Works

In this thesis study, nonlinear vibrations of the FG beams are studied. As future work, the study might be expanded for FG plate and shell structures which involve more complicated equations of motion. Additionally, more complex boundary conditions can be considered in the study. Furthermore, the method can be combined with material property estimation techniques to obtain more real-life case FG variations.

Another suggestion of future work would be the study to identify nonlinear behavior change for rotating beams. As given in Figure 5.5, the nonlinear behavior might be shaped by he variation parameters of the FG material. A study to determine the points

where the structure exhibits linear vibration characteristics would be important for advanced vibration technologies.

Additionally, a reverse study may be conducted for the identification of FG beam properties. In SCT, property variation of the FG material is embedded into the inner product matrix V, as described in Chapter 4.1.2. Experimental methods can be used to find the frequency response of an unidentified FG structure. Then SCT can be employed to find the matched frequency response with the experimental method and define the V matrix. From the V matrix, material property variations can be identified.

REFERENCES

[1] Marco Amabili, *Nonlinear Vibrations and Stability of Shells and Plates*. Cambrdige: Cambridge University Press, 2008.

[2] S. C. Lin and K. M. Hsiao, "Vibration analysis of a rotating Timoshenko beam," *J Sound Vib*, vol. 240, no. 2, pp. 303–322, Feb. 2001, doi: 10.1006/jsvi.2000.3234.

[3] S. Y. Lee and J. J. Sheu, "Free vibrations of a rotating inclined beam," *Journal of Applied Mechanics, Transactions ASME*, vol. 74, no. 3, pp. 406–414, May 2007, doi: 10.1115/1.2200657.

[4] H. H. Yoo and S. H. Shin, "Vibration Analysis Of Rotating Cantilever Beams," 1998.

[5] M. H. Saleh and M. M. Dawoud, *Characterizations of Some Composite Materials*. IntechOpen, 2019. doi: 10.5772/intechopen.73357.

[6] V. Birman and L. W. Byrd, "Modeling and analysis of functionally graded materials and structures," *Applied Mechanics Reviews*, vol. 60, no. 1–6. pp. 195–216, 2007. doi: 10.1115/1.2777164.

[7] A. E. Alshorbagy, M. A. Eltaher, and F. F. Mahmoud, "Free vibration characteristics of a functionally graded beam by finite element method," *Appl Math Model*, vol. 35, no. 1, pp. 412–425, Jan. 2011, doi: 10.1016/j.apm.2010.07.006.

[8] S. A. Sina, H. M. Navazi, and H. Haddadpour, "An analytical method for free vibration analysis of functionally graded beams," *Mater Des*, vol. 30, no. 3, pp. 741–747, Mar. 2009, doi: 10.1016/j.matdes.2008.05.015.

[9] T. Vo-Duy, V. Ho-Huu, and T. Nguyen-Thoi, "Free vibration analysis of laminated FG-CNT reinforced composite beams using finite element method," *Frontiers of Structural and Civil Engineering*, vol. 13, no. 2, pp. 324–336, Apr. 2019, doi: 10.1007/s11709-018-0466-6.

[10] M. Heshmati and M. H. Yas, “Free vibration analysis of functionally graded CNT-reinforced nanocomposite beam using Eshelby-Mori-Tanaka approach,” *Journal of Mechanical Science and Technology*, vol. 27, no. 11, pp. 3403–3408, Nov. 2013, doi: 10.1007/s12206-013-0862-8.

[11] P. Liu, K. Lin, H. Liu, and R. Qin, “Free Transverse Vibration Analysis of Axially Functionally Graded Tapered Euler-Bernoulli Beams through Spline Finite Point Method,” *Shock and Vibration*, vol. 2016, 2016, doi: 10.1155/2016/5891030.

[12] Y. Zhao, Y. Huang, and M. Guo, “A novel approach for free vibration of axially functionally graded beams with non-uniform cross-section based on Chebyshev polynomials theory,” *Compos Struct*, vol. 168, pp. 277–284, May 2017, doi: 10.1016/j.compstruct.2017.02.012.

[13] B. Yagci, S. Filiz, L. L. Romero, and O. B. Ozdoganlar, “A spectral-Tchebychev technique for solving linear and nonlinear beam equations,” *J Sound Vib*, vol. 321, no. 1–2, pp. 375–404, Mar. 2009, doi: 10.1016/j.jsv.2008.09.040.

[14] Z. hai Wang, X. hong Wang, G. dong Xu, S. Cheng, and T. Zeng, “Free vibration of two-directional functionally graded beams,” *Compos Struct*, vol. 135, pp. 191–198, Jan. 2016, doi: 10.1016/j.compstruct.2015.09.013.

[15] H. Deng and W. Cheng, “Dynamic characteristics analysis of bi-directional functionally graded Timoshenko beams,” *Compos Struct*, vol. 141, pp. 253–263, May 2016, doi: 10.1016/j.compstruct.2016.01.051.

[16] M. Şimşek, “Bi-directional functionally graded materials (BDFGMs) for free and forced vibration of Timoshenko beams with various boundary conditions,” *Compos Struct*, vol. 133, pp. 968–978, Dec. 2015, doi: 10.1016/j.compstruct.2015.08.021.

[17] D. H. Hodges, A. R. Atilgan, M. v. Fulton, and L. W. Rehfield, “Free-vibration analysis of composite beams,” *Journal of the American Helicopter Society*, vol. 36, no. 3, pp. 36–47, 1991, doi: 10.4050/jahs.36.36.

[18] X. X. Wu and C. T. Sun, “Vibration analysis of laminated composite thin-walled beams using finite elements,” *AIAA Journal*, vol. 29, no. 5, pp. 736–742, 1991, doi: 10.2514/3.10648.

[19] A. R. Ghasemi and M. Mohandes, “Nonlinear free vibration of laminated composite Euler-Bernoulli beams based on finite strain using generalized differential quadrature method,” *Mechanics of Advanced Materials and Structures*, vol. 24, no. 11, pp. 917–923, 2017, doi: 10.1080/15376494.2016.1196794.

[20] K. M. Bangera and K. Chandrashekhara, “Nonlinear vibration of moderately thick laminated beams using finite element method,” 1991.

[21] L. L. Ke, J. Yang, and S. Kitipornchai, “Nonlinear free vibration of functionally graded carbon nanotube-reinforced composite beams,” *Compos Struct*, vol. 92, no. 3, pp. 676–683, Feb. 2010, doi: 10.1016/j.compstruct.2009.09.024.

[22] L. L. Ke, J. Yang, and S. Kitipornchai, “An analytical study on the nonlinear vibration of functionally graded beams,” *Meccanica*, vol. 45, no. 6, pp. 743–752, Dec. 2010, doi: 10.1007/s11012-009-9276-1.

[23] M. Rafiee, J. Yang, and S. Kitipornchai, “Large amplitude vibration of carbon nanotube reinforced functionally graded composite beams with piezoelectric layers,” *Compos Struct*, vol. 96, pp. 716–725, Feb. 2013, doi: 10.1016/j.compstruct.2012.10.005.

[24] C. Feng, S. Kitipornchai, and J. Yang, “Nonlinear free vibration of functionally graded polymer composite beams reinforced with graphene nanoplatelets (GPLs),” *Eng Struct*, vol. 140, pp. 110–119, Jun. 2017, doi: 10.1016/j.engstruct.2017.02.052.

[25] Y. Tang, X. Lv, and T. Yang, “Bi-directional functionally graded beams: asymmetric modes and nonlinear free vibration,” *Compos B Eng*, vol. 156, pp. 319–331, Jan. 2019, doi: 10.1016/j.compositesb.2018.08.140.

[26] S. K. Chakrapani, D. J. Barnard, and V. Dayal, “Nonlinear forced vibration of carbon fiber/epoxy prepreg composite beams: Theory and experiment,” *Compos B Eng*, vol. 91, pp. 513–521, Apr. 2016, doi: 10.1016/j.compositesb.2016.02.009.

[27] H. Youzera, S. A. Meftah, N. Challamel, and A. Tounsi, “Nonlinear damping and forced vibration analysis of laminated composite beams,” *Compos B Eng*, vol. 43, no. 3, pp. 1147–1154, Apr. 2012, doi: 10.1016/j.compositesb.2012.01.008.

[28] S. Sınır, M. Çevik, and B. G. Sınır, “Nonlinear free and forced vibration analyses of axially functionally graded Euler-Bernoulli beams with non-uniform cross-section,” *Compos B Eng*, vol. 148, pp. 123–131, Sep. 2018, doi: 10.1016/j.compositesb.2018.04.061.

[29] E. Cigeroglu and H. Samandari, “Nonlinear free vibrations of curved double walled carbon nanotubes using differential quadrature method,” *Physica E Low Dimens Syst Nanostruct*, vol. 64, pp. 95–105, 2014, doi: 10.1016/j.physe.2014.07.010.

[30] E. Cigeroglu and H. Samandari, “Nonlinear free vibration of double walled carbon nanotubes by using describing function method with multiple trial functions,” *Physica E Low Dimens Syst Nanostruct*, vol. 46, pp. 160–173, Sep. 2012, doi: 10.1016/j.physe.2012.09.016.

[31] S. Lotfan, M. R. Anamagh, B. Bediz, and E. Cigeroglu, “Nonlinear resonances of axially functionally graded beams rotating with varying speed including Coriolis effects,” *Nonlinear Dyn*, vol. 107, no. 1, pp. 533–558, Jan. 2022, doi: 10.1007/s11071-021-07055-1.

[32] C. N. Chen, “Variational derivation of equilibrium equations of arbitrarily loaded pre-stressed shear deformable non-prismatic composite beams and solution by the DQEM buckling analysis,” *Commun Numer Methods Eng*, vol. 19, no. 2, pp. 137–154, Feb. 2003, doi: 10.1002/cnm.577.

[33] C. N. Chen, “DQEM analysis of out-of-plane deflection of non-prismatic curved beam structures considering the effect of shear deformation,” *Commun Numer Methods Eng*, vol. 24, no. 7, pp. 555–571, Jul. 2008, doi: 10.1002/cnm.976.

[34] K. M. Liew, X. Zhao, and A. J. M. Ferreira, “A review of meshless methods for laminated and functionally graded plates and shells,” *Compos Struct*, vol. 93, no. 8, pp. 2031–2041, 2011, doi: 10.1016/j.compstruct.2011.02.018.

[35] P. Khandar Shahabad, M. R. Anamagh, and B. Bediz, “Design of laminated conical shells using spectral Chebyshev method and lamination parameters,” *Compos Struct*, vol. 281, Feb. 2022, doi: 10.1016/j.compstruct.2021.114969.

[36] J. Tian, J. Su, K. Zhou, and H. Hua, “A modified variational method for nonlinear vibration analysis of rotating beams including Coriolis effects,” *J Sound Vib*, vol. 426, pp. 258–277, Jul. 2018, doi: 10.1016/j.jsv.2018.04.027.

[37] M. Rezaee and S. Lotfan, “Non-linear nonlocal vibration and stability analysis of axially moving nanoscale beams with time-dependent velocity,” *Int J Mech Sci*, vol. 96–97, pp. 36–46, Jun. 2015, doi: 10.1016/j.ijmecsci.2015.03.017.

[38] R. Farshbaf Zinati, M. Rezaee, and S. Lotfan, “Nonlinear Vibration and Stability Analysis of Viscoelastic Rayleigh Beams Axially Moving on a Flexible Intermediate Support,” *Iranian Journal of Science and Technology - Transactions of Mechanical Engineering*, vol. 44, no. 4, pp. 865–879, Dec. 2020, doi: 10.1007/s40997-019-00305-z.

[39] E. Ciğeroğlu and H. N. Özgüven, “Nonlinear vibration analysis of bladed disks with dry friction dampers,” *J Sound Vib*, vol. 295, no. 3–5, pp. 1028–1043, Aug. 2006, doi: 10.1016/j.jsv.2006.02.009.

[40] Y. B. Kim and S.-K. Choi, “A Multiple Harmonic Balance Method For The Internal Resonant Vibration Of A Non-Linear Jeffcott Rotor,” 1997.

[41] Z. K. Peng, G. Meng, Z. Q. Lang, W. M. Zhang, and F. L. Chu, “Study of the effects of cubic nonlinear damping on vibration isolations using Harmonic Balance Method,” in *International Journal of Non-Linear Mechanics*, Dec. 2012, vol. 47, no. 10, pp. 1073–1080. doi: 10.1016/j.ijnonlinmec.2011.09.013.

[42] S. D. Yavuz, Z. B. Saribay, and E. Cigeroglu, “Nonlinear time-varying dynamic analysis of a spiral bevel geared system,” *Nonlinear Dyn*, vol. 92, no. 4, pp. 1901–1919, Jun. 2018, doi: 10.1007/s11071-018-4170-9.

[43] Y. Oh and H. H. Yoo, “Vibration analysis of rotating pretwisted tapered blades made of functionally graded materials,” *Int J Mech Sci*, vol. 119, pp. 68–79, Dec. 2016, doi: 10.1016/j.ijmecsci.2016.10.002.

[44] J. Chung and H. H. Yoo, “Dynamic analysis of a rotating cantilever beam by using the finite element method,” *J Sound Vib*, vol. 249, no. 1, pp. 147–164, Jan. 2002, doi: 10.1006/jsvi.2001.3856.

[45] G. P. Cai, J. Z. Hong, and S. X. Yang, “Model study and active control of a rotating flexible cantilever beam,” *Int J Mech Sci*, vol. 46, no. 6, pp. 871–889, Jun. 2004, doi: 10.1016/j.ijmecsci.2004.06.001.

[46] D. Younesian and E. Esmailzadeh, “Non-linear vibration of variable speed rotating viscoelastic beams,” *Nonlinear Dyn*, vol. 60, no. 1–2, pp. 193–205, Apr. 2010, doi: 10.1007/s11071-009-9589-6.

[47] L. Li, D. G. Zhang, and W. D. Zhu, “Free vibration analysis of a rotating hub-functionally graded material beam system with the dynamic stiffening

effect," *J Sound Vib*, vol. 333, no. 5, pp. 1526–1541, Feb. 2014, doi: 10.1016/j.jsv.2013.11.001.

[48] L. Li and D. Zhang, "Dynamic analysis of rotating axially FG tapered beams based on a new rigid-flexible coupled dynamic model using the B-spline method," *Compos Struct*, vol. 124, pp. 357–367, Jun. 2015, doi: 10.1016/j.compstruct.2015.01.018.

[49] H. Arvin, A. Arena, and W. Lacarbonara, "Nonlinear vibration analysis of rotating beams undergoing parametric instability: Lagging-axial motion," *Mech Syst Signal Process*, vol. 144, Oct. 2020, doi: 10.1016/j.ymssp.2020.106892.

[50] D. Adair and M. Jaeger, "Simulation of tapered rotating beams with centrifugal stiffening using the Adomian decomposition method," *Appl Math Model*, vol. 40, no. 4, pp. 3230–3241, Feb. 2016, doi: 10.1016/j.apm.2015.09.097.

[51] J. Babu Gunda and R. Ganguli, "New rational interpolation functions for finite element analysis of rotating beams," *Int J Mech Sci*, vol. 50, no. 3, pp. 578–588, Mar. 2008, doi: 10.1016/j.ijmecsci.2007.07.014.

[52] D. Chen, S. Zheng, Y. Wang, L. Yang, and Z. Li, "Nonlinear free vibration analysis of a rotating two-dimensional functionally graded porous micro-beam using isogeometric analysis," *European Journal of Mechanics, A/Solids*, vol. 84, Nov. 2020, doi: 10.1016/j.euromechsol.2020.104083.

[53] M. Azimi, S. S. Mirjavadi, N. Shafiei, A. M. S. Hamouda, and E. Davari, "Vibration of rotating functionally graded Timoshenko nano-beams with nonlinear thermal distribution," *Mechanics of Advanced Materials and Structures*, vol. 25, no. 6, pp. 467–480, Apr. 2018, doi: 10.1080/15376494.2017.1285455.

[54] S. A. Fazelzadeh and M. Hosseini, "Aerothermoelastic behavior of supersonic rotating thin-walled beams made of functionally graded

materials," *J Fluids Struct*, vol. 23, no. 8, pp. 1251–1264, Nov. 2007, doi: 10.1016/j.jfluidstructs.2007.06.006.

[55] W. D. Zhu and C. D. Mote, "Dynamic Modeling and Optimal Control of Rotating Euler-Bernoulli Beams," 1997. [Online]. Available: http://asmedigitalcollection.asme.org/dynamicsystems/article-pdf/119/4/802/5651907/802_1.pdf

[56] J. R. Banerjee, "Free vibration of centrifugally stiffened uniform and tapered beams using the dynamic stiffness method," *J Sound Vib*, vol. 233, no. 5, pp. 857–875, Jun. 2000, doi: 10.1006/jsvi.1999.2855.

[57] J. R. Banerjee, "Dynamic stiffness formulation and free vibration analysis of centrifugally stiffened Timoshenko beams," *J Sound Vib*, vol. 247, no. 1, pp. 97–115, Oct. 2001, doi: 10.1006/jsvi.2001.3716.

[58] J. B. Yang, L. J. Jiang, and D. C. Chen, "Dynamic modelling and control of a rotating Euler-Bernoulli beam," *J Sound Vib*, vol. 274, no. 3–5, pp. 863–875, Jul. 2004, doi: 10.1016/S0022-460X(03)00611-4.

[59] Ö. Özdemir and M. O. Kaya, "Flapwise bending vibration analysis of a rotating tapered cantilever Bernoulli-Euler beam by differential transform method," *J Sound Vib*, vol. 289, no. 1–2, pp. 413–420, Jan. 2006, doi: 10.1016/j.jsv.2005.01.055.

[60] O. O. Ozgumus and M. O. Kaya, "Energy expressions and free vibration analysis of a rotating double tapered Timoshenko beam featuring bending-torsion coupling," *Int J Eng Sci*, vol. 45, no. 2–8, pp. 562–586, Feb. 2007, doi: 10.1016/j.ijengsci.2007.04.005.

[61] C. Mei, "Application of differential transformation technique to free vibration analysis of a centrifugally stiffened beam," *Comput Struct*, vol. 86, no. 11–12, pp. 1280–1284, Jun. 2008, doi: 10.1016/j.compstruc.2007.10.003.

[62] M. H. Yao, Y. P. Chen, and W. Zhang, “Nonlinear vibrations of blade with varying rotating speed,” *Nonlinear Dyn*, vol. 68, no. 4, pp. 487–504, Jun. 2012, doi: 10.1007/s11071-011-0231-z.

[63] J. R. Banerjee and D. Kennedy, “Dynamic stiffness method for inplane free vibration of rotating beams including Coriolis effects,” *J Sound Vib*, vol. 333, no. 26, pp. 7299–7312, Dec. 2014, doi: 10.1016/j.jsv.2014.08.019.

[64] B. Zhang and Y. Li, “Nonlinear vibration of rotating pre-deformed blade with thermal gradient,” *Nonlinear Dyn*, vol. 86, no. 1, pp. 459–478, Oct. 2016, doi: 10.1007/s11071-016-2900-4.

[65] B. Zhang, Y. L. Zhang, X. D. Yang, and L. Q. Chen, “Saturation and stability in internal resonance of a rotating blade under thermal gradient,” *J Sound Vib*, vol. 440, pp. 34–50, Feb. 2019, doi: 10.1016/j.jsv.2018.10.012.

[66] W. Zhang, G. Liu, and B. Siriguleng, “Saturation phenomena and nonlinear resonances of rotating pretwisted laminated composite blade under subsonic air flow excitation,” *J Sound Vib*, vol. 478, Jul. 2020, doi: 10.1016/j.jsv.2020.115353.

[67] B. Zhang, H. Ding, and L. Q. Chen, “Three to one internal resonances of a pre-deformed rotating beam with quadratic and cubic nonlinearities,” *Int J Non Linear Mech*, vol. 126, Nov. 2020, doi: 10.1016/j.ijnonlinmec.2020.103552.

[68] S. Y. Oh, L. Librescu, and O. Song, “Vibration of turbomachinery rotating blades made-up of functionally graded materials and operating in a high temperature field,” *Acta Mech*, vol. 166, no. 1–4, pp. 69–87, Dec. 2003, doi: 10.1007/s00707-003-0049-y.

[69] S. A. Fazelzadeh, P. Malekzadeh, P. Zahedinejad, and M. Hosseini, “Vibration analysis of functionally graded thin-walled rotating blades under high temperature supersonic flow using the differential quadrature method,”

J Sound Vib, vol. 306, no. 1–2, pp. 333–348, Sep. 2007, doi: 10.1016/j.jsv.2007.05.011.

[70] Hossein Zarrinzadeh, Reze Atternejad, and Ahmad Shahba, "Free vibration of rotating axially functionally graded tapered beams, Proceedings of the Institution of Mechanical Engineers," *Proc Inst Mech Eng G J Aerosp Eng*, vol. 226, no. 4, pp. 363–379, Dec. 2011.

[71] F. Ebrahimi and M. Mokhtari, "Transverse vibration analysis of rotating porous beam with functionally graded microstructure using the differential transform method," *Journal of the Brazilian Society of Mechanical Sciences and Engineering*, vol. 37, no. 4, pp. 1435–1444, Jul. 2015, doi: 10.1007/s40430-014-0255-7.

[72] E. Pesheck, C. Pierre, and S. W. Shaw, "Modal reduction of a nonlinear rotating beam through nonlinear normal modes," *Journal of Vibration and Acoustics, Transactions of the ASME*, vol. 124, no. 2, pp. 229–236, 2002, doi: 10.1115/1.1426071.

[73] C. L. Huang, W. Y. Lin, and K. M. Hsiao, "Free vibration analysis of rotating Euler beams at high angular velocity," *Comput Struct*, vol. 88, no. 17–18, pp. 991–1001, 2010, doi: 10.1016/j.compstruc.2010.06.001.

[74] H. Arvin and F. Bakhtiari-Nejad, "Non-linear modal analysis of a rotating beam," *Int J Non Linear Mech*, vol. 46, no. 6, pp. 877–897, Jul. 2011, doi: 10.1016/j.ijnonlinmec.2011.03.017.

[75] H. Kim, H. Hee Yoo, and J. Chung, "Dynamic model for free vibration and response analysis of rotating beams," *J Sound Vib*, vol. 332, no. 22, pp. 5917–5928, Oct. 2013, doi: 10.1016/j.jsv.2013.06.004.

[76] J. Tian, Z. Zhang, and H. Hua, "Free vibration analysis of rotating functionally graded double-tapered beam including porosities," *Int J Mech Sci*, vol. 150, pp. 526–538, Jan. 2019, doi: 10.1016/j.ijmecsci.2018.10.056.

[77] O. Thomas, A. Sénéchal, and J. F. Deü, “Hardening/softening behavior and reduced order modeling of nonlinear vibrations of rotating cantilever beams,” *Nonlinear Dyn*, vol. 86, no. 2, pp. 1293–1318, Oct. 2016, doi: 10.1007/s11071-016-2965-0.

[78] D. Invernizzi and L. Dozio, “A fully consistent linearized model for vibration analysis of rotating beams in the framework of geometrically exact theory,” *J Sound Vib*, vol. 370, pp. 351–371, May 2016, doi: 10.1016/j.jsv.2016.01.049.

[79] R. Attarnejad, A. Shahba, and M. A. Shahba, “Application of Differential Transform Method in Free Vibration Analysis of Rotating Non-Prismatic Beams Seismic Semi-Rigid Steel Frames View project Performance-based seismic design of soil-structure systems View project Application of Differential Transform Method in Free Vibration Analysis of Rotating Non-Prismatic Beams,” *World Appl Sci J*, vol. 5, no. 4, pp. 441–448, 2008, [Online]. Available: https://www.researchgate.net/publication/237448781

[80] Singiresu S.Rao, *Vibration of Continuous Systems*, 2nd ed. Wiley, 2019.

[81] A. Shahba and S. Rajasekaran, “Free vibration and stability of tapered Euler-Bernoulli beams made of axially functionally graded materials,” *Appl Math Model*, vol. 36, no. 7, pp. 3094–3111, Jul. 2012, doi: 10.1016/j.apm.2011.09.073.

[82] F. Tornabene and E. Viola, “2-D solution for free vibrations of parabolic shells using generalized differential quadrature method,” *European Journal of Mechanics, A/Solids*, vol. 27, no. 6, pp. 1001–1025, Nov. 2008, doi: 10.1016/j.euromechsol.2007.12.007.

APPENDICES

A. Calculation of Operation Matrices of SCT

Forward and Backward Transformation Matrix

Forward and backward transformation matrices can be written as

$$\mathbf{a} = \mathbf{\Gamma}_{\mathbf{F}}\,\mathbf{y} \qquad \text{A.1}$$

$$\mathbf{y} = \mathbf{\Gamma}_{\mathbf{B}}\mathbf{a} \qquad \text{A.2}$$

The relation given in A.2 can be opened in the form given below. And the $\mathbf{\Gamma}_{\mathbf{B}}$ matrix can be constructed according to Chebyshev expansion. $\mathbf{\Gamma}_{\mathbf{F}}$ can be written as the inverse of $\mathbf{\Gamma}_{\mathbf{B}}$.

$$\begin{Bmatrix} y_0 \\ : \\ y_N \end{Bmatrix} = \begin{bmatrix} T_0(x_0) & .. & T_N(x_0) \\ : & .. & : \\ T_0(x_n) & .. & T_N(x_n) \end{bmatrix} \begin{Bmatrix} a_0 \\ : \\ a_N \end{Bmatrix} \qquad \text{A.3}$$

Derivation Matrix

The derivatives of Chebyshev polynomials exhibit the relation shown below.

$$T_{n+1} = 2xT_n - T_{n-1} \qquad \text{A.4}$$

$$T_0 = 1, \qquad T_0^{'} = 0,$$

$$T_1 = x, \qquad T_1^{'} = 1 = T_0,$$

$$T_2 = 2x^2 - 1, \qquad T_2^{'} = 4x = 4T_1,$$

$$T_3 = 4x^3 - 3x, \quad T_3^{'} = 12x^3 - 3 = (6T_2 + 3T_0),$$

This can be written in the matrix form such as

$$\begin{Bmatrix} b_0 \\ b_1 \\ b_2 \\ b_3 \end{Bmatrix} = \begin{bmatrix} 0 & 1 & 0 & 3 \\ 0 & 0 & 4 & 0 \\ 0 & 0 & 0 & 6 \\ 0 & 0 & 0 & 0 \end{bmatrix} \begin{Bmatrix} a_0 \\ a_1 \\ b_2 \\ b_3 \end{Bmatrix} \quad \text{A.5}$$

The 4x4 matrix is the derivation matrix. This can be implemented in an algorithm for bigger systems. However, the derivative matrix should be divided by $\frac{l_2 - l_1}{2}$ in order to make it applicable to the beam system.

Definite Integral Vector

The definite integral of a function can be written with Chebyshev polynomials as

$$\int_{l_1}^{l_2} y(x)dx = a_0 \int_{l_1}^{l_2} T_0(x)dx + a_1 \int_{l_1}^{l_2} T_1(x)dx + ... = \mathbf{v}^{\mathrm{T}}\mathbf{a} \quad \text{A.6}$$

Here **v** is the definite integral vector and a is the coefficient vector of expanded polynomials. A relation for the elements of the vector can be written respectively,

$$v_{k+1} = \int_{l_1}^{l_2} T_k(x)dx \quad \text{A.7}$$

When the definite integrals are calculated with respect to *k* values, a recursive formula is derived such as

$$\int_{l_1}^{l_2} T_k(x)dx = \begin{Bmatrix} (\frac{l_2 - l_1}{1-k^2}) & \text{if k is even} \\ 0 & \text{if k is odd} \end{Bmatrix} \quad \text{A.8}$$

Inner Product Matrix

Inner product can be conscructed as stated in Eq. 3.27. According to this structure, the values of any two functions f(x) and g(x) at *N* Gauss-Lobatto points are written as $\mathbf{f}_N$ and $\mathbf{g}_N$. Product of interpolated functions has order of 2*N* and can be expressed as

$$\mathbf{f}_{2N} = \mathbf{S}_2\mathbf{f}_N \quad \text{A.9}$$

$\mathbf{S}_2$ can be constructed as

$$\mathbf{S}_2 = \mathbf{\Gamma}_{\mathrm{B}_{2N}} \left[\mathbf{I}_N ; \mathbf{O}_N \right] \mathbf{\Gamma}_{\mathrm{F}_N} \tag{A.10}$$

$\mathbf{\Gamma}_{\mathrm{B}_{2N}}$ is the 2*N* x 2*N* backward transformation matrix. $\mathbf{I}_N$ and $\mathbf{O}_N$ *N* x *N* identity and zero matrices. Consequently, the inner product of f(x) and g(x) functions can be written as,

$$\int_{l_1}^{l_2} f(x) g(x) dx = \mathbf{f}_N^{\mathrm{T}} \mathbf{V} \mathbf{g}_N = \mathbf{f}_{2N}^{\mathrm{T}} \mathbf{v}_{d,2N} \mathbf{g}_{2N} \tag{A.11}$$

In the above equation, $\mathbf{v}_{d,2N}$ is a matrix that has the elements of $\mathbf{v}_{2N}^{\mathrm{T}} \mathbf{\Gamma}_{\mathrm{F}_{2N}}$ multiplication on its diagonals. As a result, inner product matrix can be defined as given below.

$$\mathbf{V} = \mathbf{S}_2^{\mathrm{T}} \mathbf{v}_{d,2N} \mathbf{S}_2 \tag{A.12}$$

When more functions are involved in the inner product operation as described in Eq. 4.14, the multiplication order incerases to 3*N*. In this case, inner product operation can be written as

$$\int_{l_1}^{l_2} f(x) g(x) h(x) dx = \mathbf{f}_N^{\mathrm{T}} \mathbf{V}_h \mathbf{g}_N \tag{A.13}$$

Equations A.9, A.10 and A.12 are redifined accordingly such as.

$$\mathbf{f}_{3N} = \mathbf{S}_3 \mathbf{f}_N \tag{A.14}$$

$$\mathbf{S}_3 = \mathbf{\Gamma}_{\mathrm{B}_{3N}} \left[\mathbf{I}_N ; \mathbf{O}_N ; \mathbf{O}_N \right] \mathbf{\Gamma}_{\mathrm{F}_N} \tag{A.15}$$

$\mathbf{v}_{d,3N}$ has the elements of $\mathbf{v}_{3N}^{\mathrm{T}} \mathbf{\Gamma}_{\mathrm{F}_{3N}}$ on its diagonals whereas $\mathbf{h}_{d,3N}$ has the values of $\mathbf{h}_{3N}$. Finally, $\mathbf{V}_h$ is written such as

$$\mathbf{V}_h = \mathbf{S}_3^{\mathrm{T}} \mathbf{v}_{d,3N} \mathbf{h}_{d,3N} \mathbf{S}_3 \qquad \text{A.16}$$

B. Operator Matrices/Vectors Used in Chapter 5

In this part, the details of the differential operator matrices and vectors introduced in subsection 5.1 are given

$$\mathbf{B}_{yz} = \begin{bmatrix} \frac{\partial}{\partial x} & v_s' \frac{\partial}{\partial x} & w_s' \frac{\partial}{\partial x} & z_2 \frac{\partial}{\partial x} & y_2 \frac{\partial}{\partial x} \\ 0 & \frac{\partial}{\partial x} & 0 & 0 & -1 \\ 0 & 0 & \frac{\partial}{\partial x} & 1 & 0 \end{bmatrix} \qquad \text{B.17}$$

$$\mathbf{b}_{yz} = \left\{ u_s' + z_2 \varphi_{y_s}' + \frac{1}{2}(v_s'^2 + w_s'^2);\ v_s' - \varphi_{z_s};\ w_s' + \varphi_{y_s} \right\} \qquad \text{B.18}$$

$$\mathbf{B}_1^{nl} = \begin{bmatrix} 0 & \frac{1}{\sqrt{2}} \frac{\partial}{\partial x} & 0 & 0 & 0 \\ 0 & 0 & 0 & 0 & 0 \\ 0 & 0 & 0 & 0 & 0 \end{bmatrix} \quad \mathbf{B}_2^{nl} = \begin{bmatrix} 0 & \frac{1}{\sqrt{2}} \frac{\partial}{\partial x} & 0 & 0 & 0 \\ 0 & 0 & 0 & 0 & 0 \\ 0 & 0 & 0 & 0 & 0 \end{bmatrix} \qquad \text{B.19}$$

$$\mathbf{\Lambda}_{yz_1} = \begin{bmatrix} 1 & 0 & 0 & z_2 & -y_2 \\ 0 & 1 & 0 & 0 & 0 \\ 0 & 0 & 1 & 0 & 0 \end{bmatrix} \quad \mathbf{\Lambda}_{yz_2} = \begin{bmatrix} 0 & -\Omega & 0 & 0 & 0 \\ \Omega & 0 & 0 & \Omega z_2 & -\Omega y_2 \\ 0 & 0 & 0 & 0 & 0 \end{bmatrix} \qquad \text{B.20}$$

$$\mathbf{v}_{yz} = \left\{ -\Omega y_2;\ -\Omega(r_h + x);\ 0 \right\} \qquad \text{B.21}$$

C. Matrix/Vector Elements Used in Chapter 5

Following the SCT, the details of the system matrices developed in Chapter 5.1 are given below. For each matrix/vector, element representation is shown and subsequently, the nonzero elements are defined.

$$\mathbf{K}_s = [\mathbf{K}_{s_{ij}}], \quad \text{i,j=1,2,...,5} \tag{C.1}$$

$$\mathbf{K}_{s_{11}} = -A\Omega^2\mathbf{V}_\rho + A\mathbf{Q}^{\mathrm{T}}\mathbf{V}_E\mathbf{Q}, \quad \mathbf{K}_{s_{22}} = -A\Omega^2\mathbf{V}_\rho + A\mathbf{Q}^{\mathrm{T}}\mathbf{V}_G\mathbf{Q},$$
$$\mathbf{K}_{s_{25}} = -A\mathbf{Q}^{\mathrm{T}}\mathbf{V}_G, \ \mathbf{K}_{s_{33}} = A\mathbf{Q}^{\mathrm{T}}\mathbf{V}_G\mathbf{Q}, \quad \mathbf{K}_{s_{33}} = A\mathbf{Q}^{\mathrm{T}}\mathbf{V}_G,$$
$$\mathbf{K}_{s_{43}} = A\mathbf{Q}\mathbf{V}_G, \ \mathbf{K}_{s_{44}} = -I_y\Omega^2\mathbf{V}_\rho + I_y\mathbf{Q}^{\mathrm{T}}\mathbf{V}_E\mathbf{Q} + A\mathbf{V}_G,$$
$$\mathbf{K}_{s_{52}} = -A\mathbf{V}_G\mathbf{Q}, \quad \mathbf{K}_{s_{55}} = -I_z\Omega^2\mathbf{V}_\rho + I_z\mathbf{Q}^{\mathrm{T}}\mathbf{V}_E\mathbf{Q} + A\mathbf{V}_G,$$

$$\mathbf{f}_s = \left\{\mathbf{f}_{s_i}\right\}, \quad i=1,2,...,5 \tag{C.2}$$
$$\mathbf{f}_{s_1} = -Ar_h\Omega^2\mathbf{V}_\rho\mathbf{v}_\mathbf{I} - A\Omega^2\mathbf{V}_{\xi\rho}\mathbf{v}_\mathbf{I}$$

$$\mathbf{M} = [\mathbf{M}_{ij}], \quad \text{i,j=1,2,...,5} \tag{C.3}$$
$$\mathbf{M}_{11} = \mathbf{M}_{22} = \mathbf{M}_{33} = A\mathbf{V}_\rho, \ \mathbf{M}_{44} = I_y\mathbf{V}_\rho, \ \mathbf{M}_{55} = I_z\mathbf{V}_\rho,$$

$$\mathbf{M} = [\mathbf{M}_{ij}], \quad \text{i,j=1,2,...,5} \tag{C.4}$$
$$\mathbf{M}_{11} = \mathbf{M}_{22} = \mathbf{M}_{33} = A\mathbf{V}_\rho, \ \mathbf{M}_{44} = I_y\mathbf{V}_\rho, \ \mathbf{M}_{55} = I_z\mathbf{V}_\rho,$$

$$\mathbf{G} = [\mathbf{G}_{ij}], \quad \text{i,j=1,2,...,5} \tag{C.5}$$
$$\mathbf{G}_{21} = -\mathbf{G}_{12} = 2A\Omega\mathbf{V}_\rho,$$

$$\mathbf{K} = \mathbf{K}_0 + \mathbf{K}_s + \mathbf{K}_d = [\mathbf{K}_{ij}], \quad \text{i,j=1,2,...,5} \tag{C.6}$$

$$\mathbf{K}_{11} = -A\Omega^2\mathbf{V}_\rho + A\mathbf{Q}^{\mathrm{T}}\mathbf{V}_E\mathbf{Q}, \quad \mathbf{K}_{12} = \mathbf{K}_{21} = A\mathbf{Q}^{\mathrm{T}}\mathbf{V}_{Ev_s'}\mathbf{Q},$$

$$\mathbf{K}_{13} = \mathbf{K}_{31} = A\mathbf{Q}^{\mathrm{T}}\mathbf{V}_{Ew_s'}\mathbf{Q},$$

$$\mathbf{K}_{22} = -A\Omega^2\mathbf{V}_\rho + A\mathbf{Q}^{\mathrm{T}}\mathbf{V}_{Ev_s'^2}\mathbf{Q} + A\mathbf{Q}^{\mathrm{T}}\mathbf{V}_G\mathbf{Q} + A\mathbf{Q}^{\mathrm{T}}\mathbf{V}_{Eu_s'}$$

$$+ \mathbf{Q} + \frac{1}{2}A\mathbf{Q}^{\mathrm{T}}\mathbf{V}_{Ev_s'^2}\mathbf{Q} + \frac{1}{2}A\mathbf{Q}^{\mathrm{T}}\mathbf{V}_{Ew_s'^2}\mathbf{Q},$$

$$\mathbf{K}_{23} = \mathbf{K}_{32} = A\mathbf{Q}^{\mathrm{T}}\mathbf{V}_{Ev_s'w_s'^2}\mathbf{Q}, \quad \mathbf{K}_{25} = -A\mathbf{Q}^{\mathrm{T}}\mathbf{V}_G,$$

$$\mathbf{K}_{33} = A\mathbf{Q}^{\mathrm{T}}\mathbf{V}_{Ew_s'^2}\mathbf{Q} + A\mathbf{Q}^{\mathrm{T}}\mathbf{V}_G\mathbf{Q} + A\mathbf{Q}^{\mathrm{T}}\mathbf{V}_{Eu_s'}\mathbf{Q}$$

$$+ \frac{1}{2}A\mathbf{Q}^{\mathrm{T}}\mathbf{V}_{Ev_s'^2}\mathbf{Q} + \frac{1}{2}A\mathbf{Q}^{\mathrm{T}}\mathbf{V}_{Ew_s'^2}\mathbf{Q},$$

$$\mathbf{K}_{34} = A\mathbf{Q}^{\mathrm{T}}\mathbf{V}_G, \ \mathbf{K}_{43} = A\mathbf{V}_G\mathbf{Q}$$

$$\mathbf{K}_{44} = -I_y\Omega^2\mathbf{V}_\rho + I_y\mathbf{Q}^{\mathrm{T}}\mathbf{V}_E\mathbf{Q} + A\mathbf{V}_G,$$

$$\mathbf{K}_{52} = -A\mathbf{V}_G\mathbf{Q}, \quad \mathbf{K}_{s_{55}} = -I_z\Omega^2\mathbf{V}_\rho + I_z\mathbf{Q}^{\mathrm{T}}\mathbf{V}_E\mathbf{Q} + A\mathbf{V}_G$$

$$\mathbf{f} = \{\mathbf{f}_i\}, \quad i=1,2,...,5 \tag{C.7}$$

$$\mathbf{f}_3 = f\mathbf{V}^{\mathrm{T}}\mathbf{v}_\mathbf{I}$$

Where I_y and I_z are the second moment of cross-sectional area with respec to y_1 and z_1 axes, and $\mathbf{v}_\mathbf{I}$ is a vector of ones. Additionally, the matrices in the nonlinear forcing functions are expressed as given below

$$\mathbf{N}_1 = \begin{bmatrix} A\mathbf{Q}^{\mathrm{T}}\mathbf{V}_E & 0 & 0 \\ A\mathbf{Q}^{\mathrm{T}}\mathbf{V}_{Ev_s'} & A\mathbf{Q}^{\mathrm{T}}\mathbf{V}_G & 0 \\ A\mathbf{Q}^{\mathrm{T}}\mathbf{V}_{Ew_s'} & 0 & A\mathbf{Q}^{\mathrm{T}}\mathbf{V}_G \\ 0 & 0 & A\mathbf{V}_G \\ 0 & -A\mathbf{Q}^{\mathrm{T}}\mathbf{V}_G & 0 \end{bmatrix}, \quad \mathbf{N}_2 = \begin{bmatrix} 0 & \frac{1}{\sqrt{2}}\mathbf{Q} & 0 & 0 & 0 \\ 0 & 0 & 0 & 0 & 0 \\ 0 & 0 & 0 & 0 & 0 \end{bmatrix} \tag{C.8}$$

$$\mathbf{N}_3 = \begin{bmatrix} 0 & 0 & \frac{1}{\sqrt{2}}\mathbf{Q} & 0 & 0 \\ 0 & 0 & 0 & 0 & 0 \\ 0 & 0 & 0 & 0 & 0 \end{bmatrix}, \quad \mathbf{N}_4 = \begin{bmatrix} A\mathbf{V}_E & 0 & 0 \\ 0 & A\mathbf{V}_G & 0 \\ 0 & 0 & A\mathbf{V}_G \end{bmatrix}$$

D. Material Variation Profiles

The material distributions of FG beams considered in Chapter 4 and 5 are plotted in this section. The distributions considered in Chapter 4 (denoted by Equations 4.25-4.28) are plotted in Figure D.1 and Figure D.2.

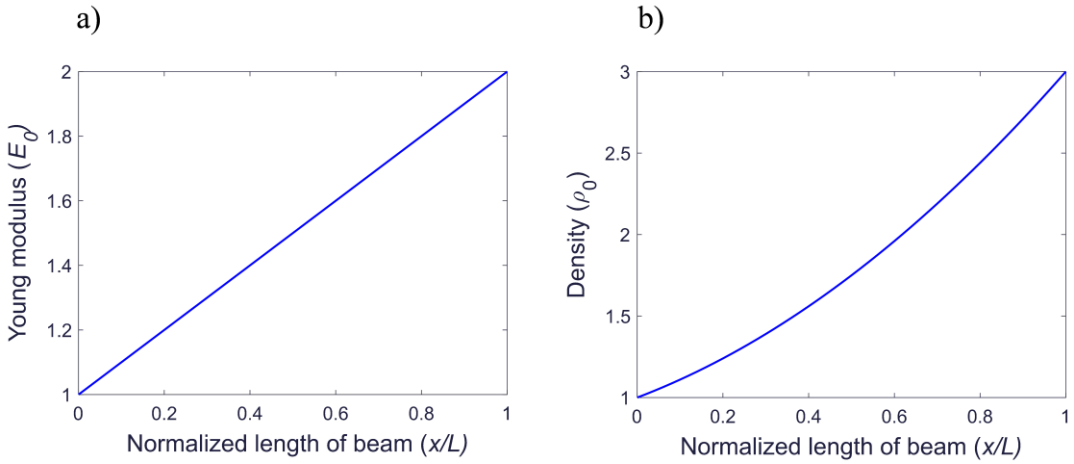

Figure D.1 Young modulus and density distributions of the FG beam used in Chapter 4

The area and moment of inertia distributions depend on c_h and c_b whereas density and young modulus distributions doesn't. Consequently, area and moment of inertia are plotted with respect to various c_h and c_b values.

For FGM parameters used in Chapter 5, including a,b,c and ρ, the obtained profiles are shown in Figure D.3 based on the variation of the volume fraction of the inclusions along the beam. In this figure, the volume fraction V_B are depicted for different sets of FGM parabeters along the beam.

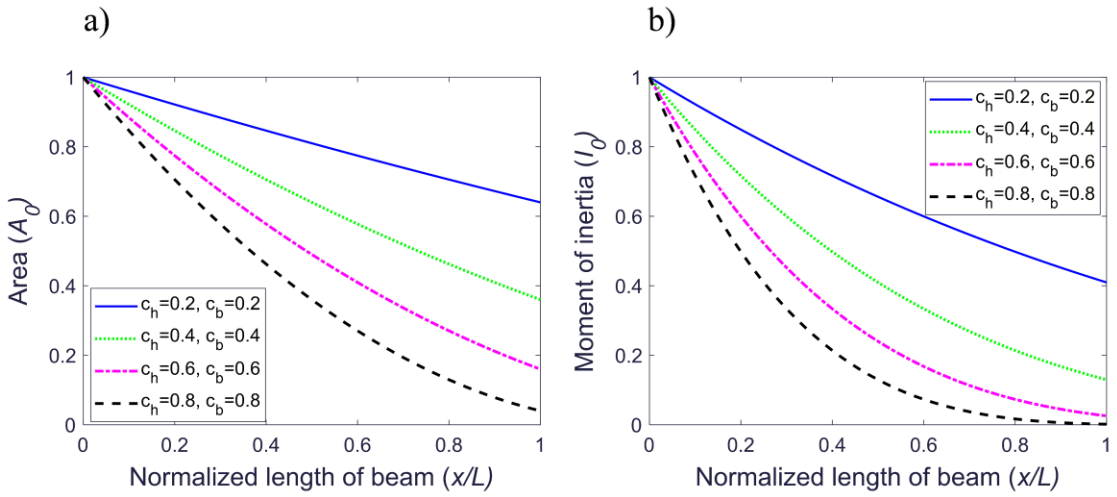

Figure D.2 Area and moment of inertia distributions of the FG beam used in Chapter 4

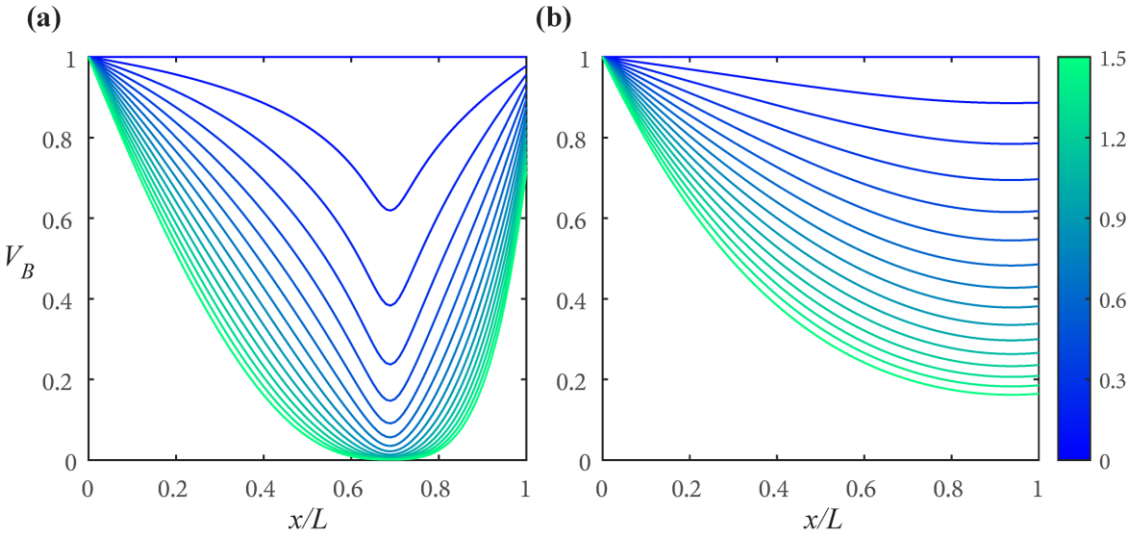

Figure D.3 The volüme fraction V_B along the beam as functions of FGM parameters *a*, *b*, *c* and *ρ*. **a)**FGM B **b)**FGM A